DR. 0414-6

Energy CONSERVATION

DOE/CE/40545-20
(DE88005025)

DIAGNOSIS OF SOURCES OF CURRENT INEFFICIENCY IN INDUSTRIAL MOLTEN SALT ELECTROLYSIS CELLS BY RAMAN SPECTROSCOPY— A TOPICAL REPORT ON CHLORIDES

Topical Report for the Period June 1982—June 1987

By
Donald R. Sadoway

June 1987

Work Performed Under Contract No. FG07-82CE40545

For
U. S. Department of Energy
Office of Industrial Programs
Washington, DC

By
Massachusetts Institute of Technology
Cambridge, Massachusetts

DISCLAIMER

DISCLAIMER

Available from the National Technical Information Service, U. S. Department of Commerce, Springfield, Virginia 22161.

Price: Printed Copy A09
Microfiche A01

Codes are used for pricing all publications. The code is determined by the number of pages in the publication. Information pertaining to the pricing codes can be found in the current issues of the following publications, which are generally available in most libraries: *Energy Research Abstracts (ERA); Government Reports Announcements* and Index *(GRA* and I); *Scientific and Technical Abstract Reports (STAR);* and publication NTIS-PR-360 available from NTIS at the above address.

Printed in the United States of America
USDOE Office of Scientific and Technical Information
Oak Ridge, Tennessee

DOE/CE/40545-20
(DE88005025)

DIAGNOSIS OF SOURCES OF CURRENT INEFFICIENCY IN INDUSTRIAL MOLTEN SALT ELECTROLYSIS CELLS BY RAMAN SPECTROSCOPY - A TOPICAL REPORT ON CHLORIDES

Topical Report
June 1982 - June 1987

by
Donald R. Sadoway

June 1987

Work Performed Under Grant No. DE-FG07-82CE40545

Prepared for
U.S. Department of Energy
Idaho Operations Office, Idaho Falls, Idaho
Sponsored by the Office of the Assistant Secretary for
Conservation and Renewable Energy
Office of Industrial Programs,
Washington, DC

Prepared by
Massachusetts Institute of Technology
Cambridge, Massachusetts 02139

THIS PAGE

WAS INTENTIONALLY

LEFT BLANK

Topical Report

on

Chloride Electrolysis

The attached dissertation "A Spectroelectrochemical Study of Aluminum and Magnesium Electrolysis in Molten Chlorides" describes the research performed under the Department of Energy Grant Number DE-FG07-82CE40545 "Diagnosis of Sources of Current Inefficiency in Industrial Molten Salt Electrolysis Cells by Raman Spectroscopy," at the Massachusetts Institute of Technology during the period of June 1982 through June 1987. The research was performed by S.-Y. Yoon, J. H. Flint, and G. J. Kipouros under the supervision of the principal investigator D. R. Sadoway.

A subsequent report will describe similar research being performed on fluoride electrolytes.

A SPECTROELECTROCHEMICAL STUDY OF ALUMINUM AND MAGNESIUM ELECTROLYSIS IN MOLTEN CHLORIDES

by

Seok-Yeol Yoon

B. S., Seoul National University, Seoul, Korea
(1979)

M. S., Seoul National University, Seoul, Korea
(1982)

Submitted to the
Department of Materials Science and Engineering
in partial fulfillment of the requirements
for the degree of

DOCTOR OF PHILOSOPHY

at the

Massachusetts Institute of Technology

June 1987

Signature of Author Seok-Yeol Yoon
Department of Materials Science and Engineering
May 1, 1987

Certified by D. R. Sadoway
Donald R. Sadoway
Thesis Supervisor

Accepted by
Samuel M. Allen, Chairman
Departmental Graduate Committee

A SPECTROELECTROCHEMICAL STUDY OF ALUMINUM AND MAGNESIUM ELECTROLYSIS IN MOLTEN CHLORIDES

by

Seok-Yeol Yoon

Submitted to Department of Materials Science and Engineering
on May 1, 1987 in partial fulfillment of the requirements
for the Degree of Doctor of Philosophy in
Metallurgy

ABSTRACT

Molten salt electrolysis, a very energy-intensive process, is used in the extraction of light metals. Aluminum production by the Hall process and magnesium production in the Dow and I.G. Farbenindustrie cells constitute the major commercial applications of metal electrowinning from molten-salt media at present. The energy input into the electrolysis cell is in the form of direct current, and the energy efficiencies in the magnesium or aluminum processes are only in the 30 to 40% range. Major energy reductions are achieved by reducing the cell voltage or by increasing the current efficiency.

The ultimate goal of the research is the identification of the sources of the current losses occurring in molten salt electrolysis, using a spectroelectrochemical technique which is the combination of spectroscopy and electrochemistry. However, this combined technique has been applied to the molten salt systems so recently that the available data or experimental techniques were quite few. With the intention of building experimental data and techniques, this research worked on the systems of I.G. magnesium chloride and Alcoa smelting aluminum chloride processes, which are industrially important and have been known to be relatively easy to handle. Raman spectroscopy was used in this research as a spectroscopic means, because it has been known as one of the most powerful tools for identifying complexes in molten salts.

Raman spectra were measured and analyzed for each component or their mixtures of the electrolyte for magnesium and aluminum reduction in chloride melts. Raman measurements were also conducted on the melts of industrial composition for aluminum and magnesium electrolysis. In laboratory-scale cells which imitated industrial practice, Raman spectra were measured in situ during electrolysis in attempts to identify the streamers, coloration of electrolyte, and any subvalent species. They were known to occur only during electrolysis, and they have been reported to be possible current losses. Cyclic voltammetry was conducted as an electroanalytical technique to obtain information about the generation of subvalent species which were not detected by Raman measurement. These were thought to be kinetic entities present only during electrolysis.

Results of Raman spectroscopy and electrochemistry of magnesium and aluminum reduction from molten chloride bath are presented. All the results would be of importance in themselves, but more importantly, the results and skills developed during this research would be useful to establish the basis for the study of the more complex, but industrially more significant process, electrolysis of aluminum from molten fluoride media.

Thesis Supervisor: Prof. Donald R. Sadoway

Title: Associate Professor of Materials Engineering

TABLE OF CONTENTS

LIST OF FIGURES

(c) Raman spectra of 25 mol.% $AlCl_3$ + 75 mol.% CsCl. T=700°C.

(d) Raman spectra of 33 mol.% $AlCl_3$ + 67 mol.% CsCl. T=700°C.

Fig. 4.38 Raman spectra of 11 wt.% $MgCl_2$ - 6 wt.% $CaCl_2$ - 18 wt.% KCl - 65 wt.% NaCl measured during pre-electrolysis at 1.6 V. T=750°C. (a) Before electrolysis; (b) After 1 hour; (c) After 5 hours; (d) After 10 hours.

Fig. 4.39 Raman spectra of 5 wt.% $AlCl_3$ - 42 wt.% LiCl - 53 wt.% NaCl measured during pre-electrolysis at 1.6 V. T=700°C. (a) Before electrolysis; (b) After 1 hour; (c) After 4.5 hours; (d) After 10 hours.

Fig. 4.40 Raman spectra of 11 wt.% $MgCl_2$ - 6 wt.% $CaCl_2$ - 18 wt.% KCl - 65 wt.% NaCl measured during electrolysis at different current densities. T=750°C. (a) No current; (b) 30 mA/cm^2; (c) 90 mA/cm^2; (d) 150 mA/cm^2.

Fig. 4.41 Raman spectra of 10 wt.% $AlCl_3$ - 40 wt.% LiCl - 50 wt.% NaCl measured during electrolysis at different current densities. T=700°C (a) No current; (b) 3 mA/cm^2; (c) 30 mA/cm^2; (d) 60 mA/cm^2; (e) 90 mA/cm^2.

Fig. 4.42 Photographs showing the smoke-like particle generation during electrolysis of 10 wt.% $AlCl_3$ - 40 wt.% LiCl - 50 wt.% NaCl at 1.9 V. T=700°C. (a) Before electrolysis; (b) After 1 min.; (c) After 2 min.; (d) After 5 min.

Fig. 4.43 Streamer development during $AlCl_3$ electrolysis. Electrolyte: 10 wt.% $AlCl_3$ - 40 wt.% LiCl - 50 wt.% NaCl. V = 2.30 V. T=700°C. (a) When electrolysis started; (b) After 10 sec; (c) After 30 sec; (d) After 10 min.

Fig. 4.44 Streamer development during $MgCl_2$ electrolysis. Electrolyte: 11 wt.% $MgCl_2$ - 6 wt.% $CaCl_2$ - 18 wt.% KCl - 65 wt.% NaCl. T=750°C. i = 100 mA/cm^2. (a) After 1 min. (b) After 2 min. (c) After 5 min. (d) After 10 min.

Fig. 4.45 Raman spectra of 1 wt.% $AlCl_3$ in the supporting electrolyte (NaCl:LiCl = 50:40 by weight). T=620°C. Total equivalent charge based on $AlCl_3$ content was 650 coulombs. (a) Before

electrolysis; (b) After 400 coulombs of charge passed; (c) At the cathode boundary layer after 30 coulombs of charge passed.

Fig. 5.1 A typical cyclic voltammogram of 2.2 wt.% $MgCl_2$ in $CaCl_2$-KCl-NaCl mixture melt in the weight ratio of 6:18:65. Working electrode: Silver. Area: 0.08 cm^2. T=800°C. v=0.2 V/s.

Fig. 5.2 Schematic of cell cap for the voltammetric study. The detached valve(1) is connected to the valve(2) after purging the connection tube with argon gas.

Fig. 5.3 Residual current in the $CaCl_2$-KCl-NaCl mixture melt in the weight ratio of 6:18:65. Working electrode: Tungsten. Area: 0.0242 cm^2. T=750°C. v=0.05 V/s.

Fig. 5.4 Voltammogram of 2.2 wt.% $MgCl_2$ in the molten $CaCl_2$-KCl-NaCl mixture in the weight ratio of 6:18:65. Working electrode: Silver. Area: 0.08 cm^2. T=750°C. v=0.4 V/s.

Fig. 5.5 A plot of $\log[(i_p-i)/i]$ vs V on the reduction wave for the Mg^{2+} reduction at silver working electrode. $MgCl_2$ content: 2.2 wt.% in the molten $CaCl_2$-KCl-NaCl mixture in the weight ratio of 6:18:65. Area: 0.08 cm^2. T=750°C. v=0.4 V/s.

Fig. 5.6 Cyclic voltammograms at different scan rates for 2.2 wt.% $MgCl_2$ in the molten $CaCl_2$-KCl-NaCl mixture in the weight ratio of 6:18:65. Working electrode: Silver. Area: 0.08 cm^2. T=750°C. (1) v=0.2 V/s. (2) v=0.4 V/s. (3) v=0.6 V/s. (4) v=1.0 V/s. (5) v=1.5 V/s.

Fig. 5.7 Cyclic voltammogram of 2.2 wt.% $MgCl_2$ in the molten $CaCl_2$-KCl-NaCl mixture in the weight ratio of 6:18:65. Working electrode: Platinum. Area: 0.08 cm^2. T=750°C. v=0.1 V/s.

Fig. 5.8 Cyclic voltammograms at different scan rates for 2.2 wt.% $MgCl_2$ in the molten $CaCl_2$-KCl-NaCl mixture in the weight ratio of 6:18:65. Working electrode: Platinum. Area: 0.08 cm^2. T=750°C.
(a) v=0.3 V/s.
(b) v=0.5 V/s.
(c) v=0.8 V/s.

Fig. 5.9 Cyclic voltammogram at glassy carbon electrode for 2.2 wt.%

$MgCl_2$ in the molten $CaCl_2$-KCl-NaCl mixture in the weight ratio of 6:18:65. Area: 0.542 cm^2. T=750°C. v=0.1 V/s.

Fig. 5.10 A plot of the cathodic peak current vs (scan rate)$^{1/2}$ for the reduction of Mg^{2+} at silver electrode. $MgCl_2$: 2.2 wt.% in the molten $CaCl_2$-KCl-NaCl mixture in the weight ratio of 6:18:65. T=750°C. Area: 0.08 cm^2.

Fig. 5.11 A plot of the cathodic peak current vs (scan rate)$^{1/2}$ for the reduction of Mg^{2+} at platinum electrode. $MgCl_2$: 2.2 wt.% in the molten $CaCl_2$-KCl-NaCl mixture in the weight ratio of 6:18:65. T=750°C. Area: 0.08 cm^2.

Fig. 5.12 A cyclic voltammogram for 1.5 wt.% $AlCl_3$ in the molten LiCl-NaCl mixture in the weight ratio of 40:50. Working electrode: Gold. Area: 0.173 cm^2. v=0.05 V/s. T=700°C.

Fig. 5.13 A plot of $\log[(i_p-i)/i]$ vs V on the cathodic wave for Al^{3+} reduction at gold working electrode. $AlCl_3$ content: 1.5 wt.% in the molten LiCl-NaCl mixture in the weight ratio of 40:50. Area: 0.173 cm^2. T=700°C. v=0.05 V/s.

Fig. 5.14 Cyclic voltammograms at different scan rates for 1.5 wt.% $AlCl_3$ in the molten LiCl-NaCl mixture in the weight ratio of 40:50. Working electrode: Gold. Area: 0.173 cm^2. T=700°C. (1) v=0.08 V/s. (2) v=0.15 V/s. (3) v=0.2 V/s. (4) v=0.5 V/s. (5) v=1.0 V/s.

Fig. 5.15 A cyclic voltammogram at 800°C for 1.5 wt.% $AlCl_3$ in the molten LiCl-NaCl mixture in the weight ratio of 40:50. Working electrode: Gold. Area: 0.173 cm^2. v=0.5 V/s.

Fig. 5.16 A cyclic voltammogram at silver working electrode for 1 wt.% $AlCl_3$ in the molten LiCl-NaCl mixture in the weight ratio of 40:50. T=700°C. Area: 0.097 cm^2. v=0.3 V/s.

Fig. 5.17 A plot of $\log[(i_p-i)/i]$ vs V on the cathodic wave for Al^{3+} at silver working electrode. $AlCl_3$ content: 1 wt.% in the molten LiCl-NaCl mixture in the weight ratio of 40:50. Area: 0.097 cm^2. T=700°C. v=0.3 V/s.

Fig. 5.18 A plot of the cathodic peak current vs (scan rate)$^{1/2}$ for the reduction of Al^{3+} at gold electrode. $AlCl_3$ content: 1.5 wt.% in the molten LiCl-NaCl melt in the weight ratio of 40:50.

T=700°C. Area: 0.173 cm^2.

Fig. 5.19 A plot of the cathodic peak current vs (scan rate)$^{1/2}$ for the reduction of Al^{3+} at silver electrode. $AlCl_3$ content: 1.5 wt.% in the molten LiCl-NaCl melt in the weight ratio of 40:50. T=700°C. Area: 0.18 cm^2.

ACKNOWLEDGEMENTS

I should like to thank my thesis advisor, Professor Donald R. Sadoway, for his excellent guidance and support throughout this work.

I thank my wife, Hyun Sook, for her constant patience and sacrifices she made during my doctoral studies. I owe special thanks to my daughter, Yo-Eun, and my parents for constant love and support.

I should like to express my appreciation to J.H. Flint, R.P. Singh, A. McLeod, J. Koziol, and other officemates for numerous helpful discussions and suggestions in relation to the experimental work.

I thank Prof. G.E. Wnek and Prof. R.E. Spjut for their helpful discussions and for serving on my thesis committee.

Finally, I should like to acknowledge the support of the U.S. Department of Energy, Office of Industrial Programs, through Grant No. DE-FG07-82CE40545.

1. INTRODUCTION

Molten salt electrolysis, a very energy-intensive process, is used in the extraction of light metals. Molten (or fused) salts are a class of liquids generally characterized by high ionic conductivities and melting points much higher than room temperature. The high electrical conductivity of molten salts is a major factor in making this class of liquids an attractive medium for electrowinning, particularly of those electropositive metals that cannot be deposited from aqueous solutions.

Aluminum production by the Hall process and magnesium production in the Dow and I.G. Farbenindustrie cells constitute the major commercial applications of metal electrowinning from molten-salt media at present. The production of primary aluminum and magnesium has been estimated to have consumed 2.8 percent of the total generated electric power in the United States during the year 1984.[1] It is somewhat ironic that the least dense structural metals, which can reduce energy consumption when used as materials of construction in transportation vehicles, are the most energy-intensive metals to produce. Therefore, efforts are being made in these extraction processes to decrease net energy utilization.

The electrolytic production of magnesium accounts for about 70% of the total magnesium production in Western World.[2] Magnesium production by the electrolytic processes requires 15 - 18 kWh per kilogram of Mg metal. The current efficiency of I.G. Farben anhydrous process is 80 - 90% and that of Dow partially hydrous process is

75 - 80%.[2] The only commercial way of extracting aluminum is the Hall-Heroult process. Aluminum production requires not less than 12 kWh/kg of Al metal in recent industries, with a current efficiency of exceeding 90%.[3,4]

The energy input into the electrolysis cell is in the form of direct current, and the energy efficiencies in the magnesium or aluminum processes are only in the 30 to 40% range. The energy efficiency is defined as

$$\text{Energy Efficiency} = \text{Voltage Efficiency} \times \text{Current Efficiency}$$

where

$$\text{Voltage Efficiency} = \frac{\text{Decomposition voltage}}{\text{Actual cell voltage}}$$

$$\text{Current Efficiency} = \frac{\text{Charge used in forming product}}{\text{Total charge delivered by power supply}}$$

Major energy reductions are achieved by reducing the cell voltage or by increasing the current efficiency. Many sources of current inefficiency in the molten salt processes have been reported.

As major sources of the current losses during electrolysis of molten salts, the following have been reported.[5-9]

1. The back-reaction between the deposited metal and the gas liberated at the anode.
2. Simultaneous discharge of other metal ions.
3. The reaction of the deposited metal with the impurities contained in the electrolyte or with the products of simultaneous electrochemical side-reaction.
4. Redox reaction due to the multiplicity of valence of the metal ion in the electrolyte melt.

It has also been reported that the current inefficiency may be associated with the occurrence of "metal fog" (or streamers) and coloration of the normally transparent electrolytes during electrolysis. During magnesium electrolysis, Komura et al.[10] observed that the degree of the dispersion of Mg into the melts was 18 times as much as the true solubility. A brown cloud was also observed[11,12] with the on-set of electrolysis of magnesium chloride containing melt, which disappeared after some time. It was assumed that this phenomenon was also due to the dispersed magnesium which are probably formed by electrolysis. Ishikawa[13] reported that, during electrolysis of $AlCl_3$ in equimolar mixture of NaCl-KCl, a yellow coloration was observed starting in the vicinity of the anode and spreading to the entire melt. The color was found to fade with discontinuation of electrolysis. These streamer formation and coloration phenomena might be indirectly linked to the current inefficiency, for example, through the recombination reaction.[14]

Even though much work has been done to increase current efficiency, the natures of the metal fog and the coloration of the electrolytes have not yet been identified. No work has been reported on the study of multivalent species occurring during magnesium or aluminum electrolysis in molten chloride baths.

It was the intention of this research to study these issues using a spectroelectrochemical technique which is the combination of spectroscopy and electrochemistry. In this technique, spectroscopy is used as a probe to observe the electrochemical phenomena which occur in the solution undergoing electrolysis, and therefore, spectral and electrochemical information can be obtained simultaneously. As spectroscopic method, Raman spectroscopy was applied in this research since it is acknowledged to be the most powerful means for the study of coordinated ionic species.[15,16] Raman spectroscopy involves only visible radiation, and has the potential to study a wide range of electrolyte systems over an extensive frequency range.

In the past, electrochemists have relied on the data derived from conventional measurement of current, potential, and charge to provide information about the structure of the electrode/electrolyte interphase, and on the mechanism and kinetics of electrode processes. Such information is necessarily indirect, and thus, spectroelectrochemical techniques have been increasingly applied in this area of investigation, because this combined technique can yield simultaneous spectral and electrochemical information which may help in identifying and obtaining kinetic reaction intermediates, and also deriving structural data.

The spectroelectrochemical technique has been applied to molten salt systems so recently that few data or experimental techniques are available. For a successful application, as many data and experimental techniques as possible have to be accumulated first. Therefore, the purpose of this spectroelectrochemical study was to establish the basis for future work on the fluoride-based systems, which are commercially important, but very difficult to handle. From a practical point of view, the study had to begin with the less corrosive systems that still have the occurrences causing the current inefficiency mentioned above. Thus, for the present study, the I.G. magnesium process and Alcoa smelting aluminum chloride process were selected.

The reasons for selecting the I.G. Farben magnesium process for this research were:(a) this system is easy to handle because the electrolyte for the magnesium electrolysis does not react with fused quartz container and is molten at a relatively low temperature (650°C); (b) the electrochemical reactions in this anhydrous magnesium chloride process are less complex than in the hydrous $MgCl_2$ process (Dow process); and (c) the formation of the metal fog at the cathode and coloration of the electrolyte during electrolysis have been reported, but not identified.[11,12]

The Alcoa Smelting Process (electrolysis of $AlCl_3$-NaCl-LiCl) was selected, because these chloride-based systems can be contained in a fused quartz cell and are molten at a relatively low temperatures, as in the case of the anhydrous magnesium process. More importantly, the

effect of multiple valency on the electrodeposition might be studied from this system, because it has been assumed that aluminum exists in the alkali chloride melts as both Al^{3+} and a subvalent form thought to be Al^{+}.[17-19]

The possibility of the formation of univalent aluminum ion follows from the structure of the valence electron shell of its atom, where $3s^2$ and $3p^1$ - electrons are found. In this case, the effect of the inert pair of s-electrons with antiparallel spins for elimination is manifested, in accord with which the first ionization potential proves substantially smaller than the second and third (574.4, 1799.9 and 2784.4 kJ/g-atom, respectively).[18] In chloride melts, Al^{3+} has been reported to coordinate with four chloride ions to form tetrachloro-aluminate complex $AlCl_4^-$, which can be readily identified in the vibrational spectrum of the melt.[20 25] Electrolysis of $AlCl_3$-bearing melts favors the formation of subvalent species,[26] whose coordination has not been cited in the literature. But its vibrational spectrum would be identifiably different from that of $AlCl_4^-$. Thus, by studying the $AlCl_3$ system, the researcher expected to obtain direct information on the nature of the chemical species present and on their interactions.

No Raman spectra have been reported for the magnesium or aluminum chloride systems undergoing electrolysis. For a successful spectro-electrochemical study, therefore, the research began with thorough investigation of the basic components of the electrolytes for aluminum and magnesium electrolysis. Raman spectra were measured and analyzed for each electrolyte component and their mixtures. Raman measurements

were conducted on the melts of industrial composition for aluminum and magnesium electrolysis. Raman spectra were measured in situ during electrolysis in attempts to identify the streamers, coloration of electrolyte, and any subvalent species. Cyclic voltammetry was conducted as an electroanalytical technique to obtain information about the generation of new subvalent species which were not detected by Raman measurement. These are thought to be kinetic entities present only during electrolysis.

2. LITERATURE

In spectroelectrochemical techniques, the combination of spectroscopy and electrochemistry, spectral measurements of the solution adjacent to the electrode are made simultaneously with electrochemical reaction. Here, spectroscopy is used as a probe to observe the electrochemical phenomena which occur in the solution undergoing electrolysis. This combined analytical technique has been developed recently,[27] and thus, most previous work has been conducted either spectroscopically or electrochemically. Raman spectroscopy has been widely applied to molten salt systems as a spectroscopic technique.[28]

Most work has been conducted to measure Raman spectra of molten $MgCl_2$ or $AlCl_3$ in alkali or alkaline earth metal chloride melts. However, the purpose was to determine the structure of molten salts and to understand the principles which explain the structure and behavior of molten salts, and thus, the spectra have been measured in the absence of an applied electric field.

Balasubrahmanyam[29] reported in 1966 Raman spectra of molten $MgCl_2$ at 730°C, a mixture of 50 mol.% $MgCl_2$ and KCl at 525°C and a mixture of 33 mol.%, $MgCl_2$ and KCl at 475°C. These spectra were measured with mercury arc radiation. Later, however, Raman spectra of molten $MgCl_2$ were obtained using laser radiation,[30,31] and refined Raman spectra were reported for magnesium chloride - alkali metal chloride systems at various compositions ($MgCl_2$ + nACl where n = 0 - 4,

and A = Cs, K, Na, Li).[32] It has been established that magnesium does not exist as a discrete cation in chloride melts, but in the form of tetrachloro complex, $MgCl_4^{2-}$.

Raman spectra for $AlCl_3$ system were measured also to determine the ionic structure, as in the case of $MgCl_2$. Since $AlCl_3$ sublimes without melting, Raman spectra of pure molten $AlCl_3$ cannot be measured under normal conditions. ($AlCl_3$ sublimes at a low temperature of 182°C.) Most of work has been done, therefore, with KCl or NaCl, but not with both, and usually higher $AlCl_3$ content than our concern.[20,33-36] As in the case of magnesium chloride systems, aluminum has been reported to exist in the form of chlorocomplexes, predominantly $AlCl_4^-$, in chloride melts.

The electrochemical reduction of Mg^{2+} from alkali chloride and/or alkaline earth chloride melts have been studied.[37-40] It has been established that the reduction process is diffusion controlled. During electrolysis, melt coloration and metal fogging have also been observed, without identification of their nature.[11-12] Subvalent forms of Al^+ and/or Al^{2+} have been suggested from the electrochemical study of $AlCl_3$ in the alkali chloride melts.[41-43] Metal fogging and coloration of the melt have also been observed during electrolysis of $AlCl_3$-containing melt.[13,26] However, the nature of metal fogging, coloration and the complexes of these lower oxidation states has by no means been confirmed.

It can be said that these spectroscopic and electrochemical studies presented an almost clear picture of the coordination behavior

of magnesium and aluminum in their chloride - alkali chloride melts. However, Raman spectra or electrochemical studies of $MgCl_2$ and $AlCl_3$ at their industrial composition have not been reported, nor have they not been combined with each other.

3. ELECTROLYSIS OF $MgCl_2$ AND $AlCl_3$ IN INDUSTRY

3.1 I.G. Farben Magnesium Chloride Process

Magnesium, the lightest structural metal, is produced mostly by the electrolysis of magnesium chloride dissolved in alkali and alkaline earth metal chlorides using technologies developed by I.G. Farbenindustrie and Dow Chemical Company. The starting material for electrolytic process is some form of an aqueous solution of magnesium chloride. Before electrolysis, this material is dehydrated and purified. Because of the high chemical affinity of water to magnesium chloride, however, the dehydration is not trivial. Most processes (e.g. I.G. Farben) use anhydrous magnesium chloride, while one process, Dow Chemical, uses the partially hydrated compound (15 - 20% water of crystallization).[44]

Magnesium is electrowon from a chloride electrolyte which is more dense than the magnesium metal itself. For this reason, in commercial magnesium chloride electrolysis cells, the cathodes are equipped with collection systems that trap the rising metal droplets. The basic cell design of the I.G. Farben process is shown in Fig. 3.1.[45] The cell reaction is

$$MgCl_2(liq) = Mg(liq) + Cl_2(gas).$$

At 700°C, ΔG° = 116.07 kcal/mol for this reaction and the standard reversible potential is -2.52 V. The practical decomposition voltage varies between 2.60 and 2.85 V, depending on the supporting electrolyte

and the operating temperature.[46] Graphite anodes are positioned between steel cathodes. Magnesium metal should wet the cathode and move upward along with the electrolyte by gas lift circulation. Cathode tops are designed to discharge the magnesium into the metal collection zone effectively. The anodic compartments are always completely sealed for efficient and economic recovery of chlorine. It is important to prevent escape of chlorine to the immediate work area and to the atmosphere.

Diaphragms constructed of refractory materials are immersed into the electrolyte between each anode and cathode to separate chlorine from the metal product to prevent the loss of magnesium by their recombination reaction. Since feed to the cell is anhydrous $MgCl_2$, concentrated chlorine is evolved at the anodes and can be recovered for chlorination of magnesium oxide ore. There is no external heating of the cells, which are insulated with refractory brick and contained in a steel tank.

The composition of the electrolyte is dictated primarily by the source of $MgCl_2$, e.g., sea water or brine, but a wide variation is possible as long as $MgCl_2$ is held above 10 wt.%. The operating temperature is 740°C. An anode - cathode spacing has to be large enough for chlorine recovery, which increases cell resistance and thus decreases current efficiency. Current density is 0.35 - 0.5 A/cm^2 and cell voltage is 5 - 7 V, with a current efficiency of 80 - 90%. Energy consumption is 15 - 18 kWh/kg of Mg metal.[5,47]

3.2 Alcoa Aluminum Chloride Process

Aluminum is extracted primarily by electrolysis of Al_2O_3 in Hall-Heroult cells. The source of Al_2O_3 is bauxite, which is treated by the Bayer process. The electrolyte is essentially a solution of aluminum oxide dissolved in molten cryolite, Na_3AlF_6. From the consumable carbon anode, such gaseous products as CO_2, CO, and fluorides are generated. In addition, particulates, halocarbons, and polynucleararomatics are produced, which may pose hazards to human health and the environment. Since the melting point of 10 wt.% Al_2O_3 in cryolite is about 960°C, the Hall cell must be operated about 300°C above the melting point of aluminum (660°C),[4] which may result in energy inefficiency.

In this regard, chloride metallurgy has been particularly attractive in electrowinning from molten salt supporting electrolytes. The Aluminum Company of America (Alcoa) developed a process for electrowinning aluminum primarily from a fused alkali chloride melt, with the following advantages over the Hall process: (1) The difficulty of continual adjustment of carbon anodes can be avoided by using non-consumable stationary electrodes. (2) The use of non-consumable anodes allows the employment of bipolar electrodes, which increases cell throughput. (3) The cell resistance in the chloride cell may be appreciably less than that in the Hall cell due to the smaller spacing between the anode and cathode. (4) No fluoride-bearing gases are produced at the anode, and the anodic product of fused-chloride electrolysis is usually gaseous chlorine, which can be recovered and recycled for direct chlorination.

The Alcoa process uses $AlCl_3$ prepared by chlorination of Al_2O_3 which is obtained by the Bayer process. The cell (Fig. 3.2) for electrolysis is constructed from a steel mantle lined with a thermally-insulating, non-conducting refractory material.[48,49] (The details of the process have not been disclosed.) The cell reaction is

$$AlCl_3(liq) = Al(liq) + 3/2Cl_2(gas).$$

At 700°C, ΔG° = 121.2 kcal/mol for this reaction, and the standard reversible potential is 1.75 V. The metal is collected in a graphite compartment at the bottom of the cell, and chlorine is collected for recycling. Inlets for electrolyte and outlets for products pass through the lid lined with a refractory material.

The electrodes which consist of a horizontal anode at the top, a horizontal cathode at the bottom, and bipolar electrodes in between, are stacked at a separation of less than 1.3 cm in the cell.[50] Electrons enter the lower graphite from the cathode bars, pass through the electrolyte to the next bipolar plate, and finally out the top anode bars. Aluminum chloride is decomposed to produce aluminum and chlorine in each compartment. The operating temperature is 700 ± 30°C. The typical cell composition is 5 wt.% $AlCl_3$, 53 wt.% NaCl, 42 wt.% LiCl. The pumping effect of the chlorine bubbles improves melt circulation and supplies new electrolyte to the inter-electrode gap.

Current density is 0.8 - 2.3 A/cm^2 and cell voltage is 2.7 V.

Energy consumption has been reported to be less than 9.5 kWh/kg of Al metal, which is lower than that of Hall cell process, about 12 kWh/kg of Al metal in the latter case.[3]

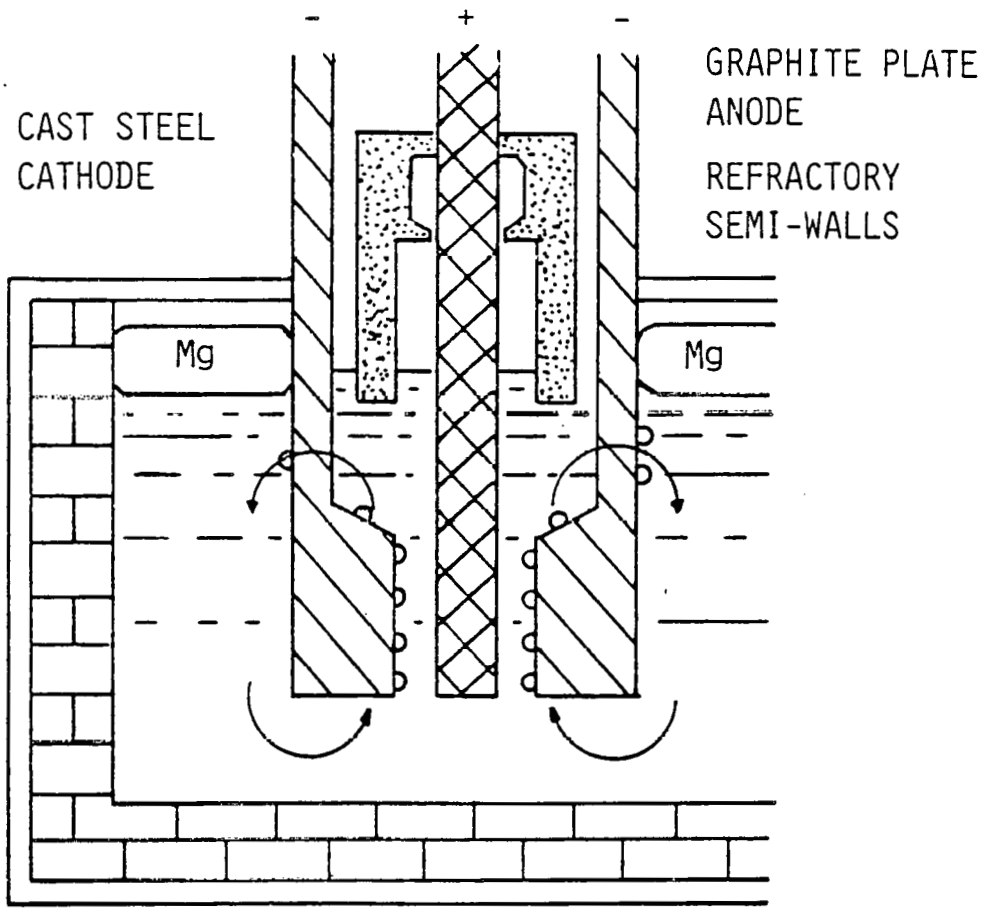

Fig. 3.1 Schematic of I.G. Farben magnesium electrolysis cell.[45]

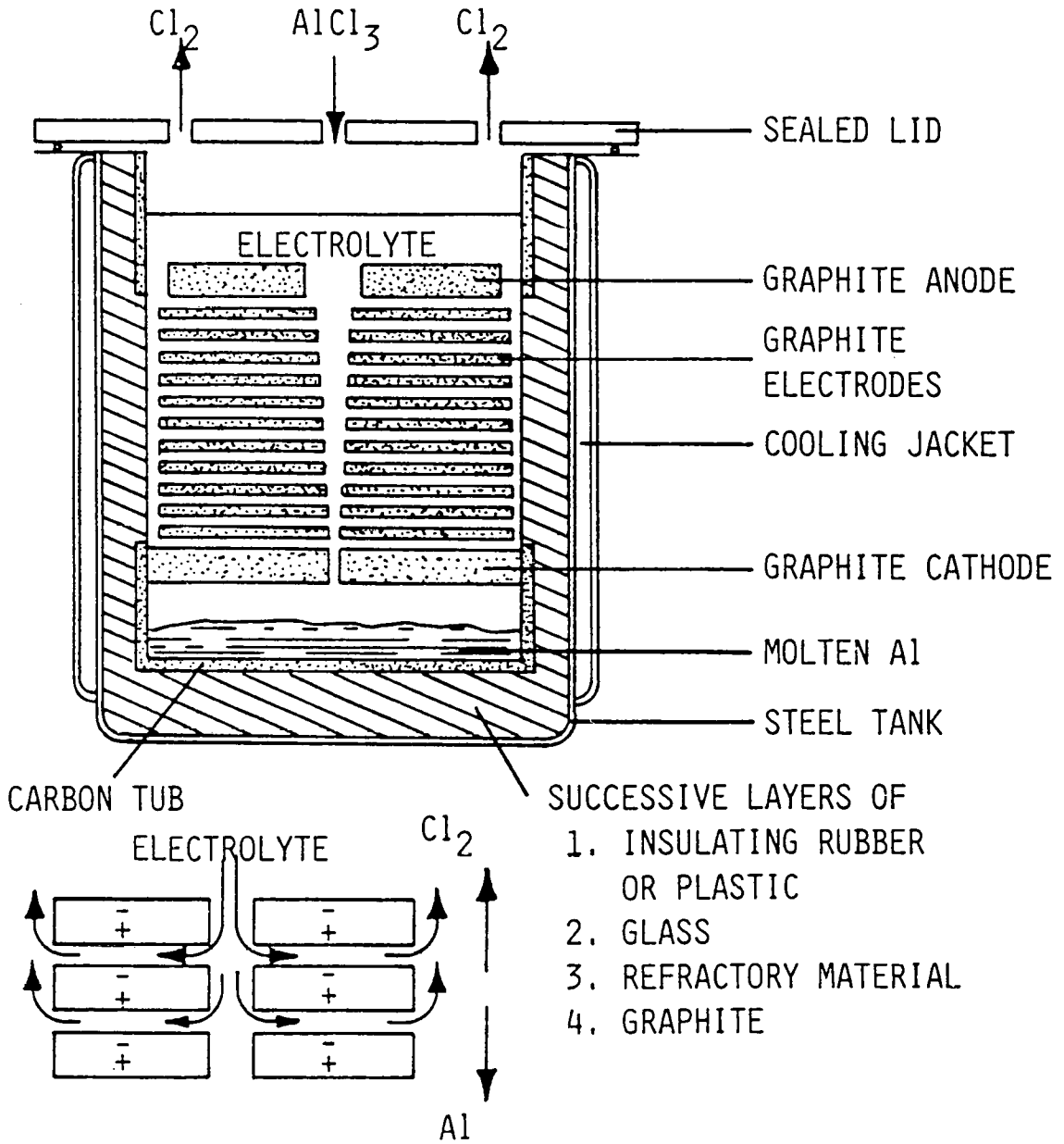

Fig. 3.2 Schematic of Alcoa aluminum chloride electrolysis cell.[49]

4. RAMAN SCATTERING STUDIES

Complex ion formation in molten salt solutions has been a general concept used to characterize and interpret spectroscopic, kinetic, and thermodynamic data of a class of strongly interacting mixtures of alkali halides with polyvalent metal halides.

Evidence for the tetrahedral complex, MX_4^{2-} anions from phase diagram calculations was first noted by Flood and Urnes[51] for the $MgCl_2$ - alkali metal chloride system. The relatively sharp Raman peaks for the $MgCl_2$.nACl melts[29-32,52-54] have suggested that these systems cannot be treated as simple ionic liquids, because the Raman intensity of a purely electrostatic interaction is 10^{-2} - 10^{-5} times that of covalently linked atoms.[55] There have been many reports on thermodynamic[56-60] and spectroscopic[20,29,52,53] evidences of the presence of complex entities in molten salt mixtures of the type $AX-MX_2$ or $AX-MX_3$, where A is an alkali metal cation, X a halide ion, and M is metal cation.

During the last two decades, Raman spectroscopy has become a standard method for structural investigations of molten salts, particularly for identifying complex ions and other structural entities. From a Raman study on $MgCl_2$ and the $MgCl_2$-KCl system, Balasubrahmanyam concluded[29] that the layered structure of solid $MgCl_2$ was partly broken up to form $MgCl_6^{4-}$ units in $MgCl_2$, but the addition of KCl to the

$MgCl_2$ melt led to formation of $MgCl_3^-$ and possibly $MgCl_4^{2-}$. However, later Raman works[52,53,55] proposed that $MgCl_6^{4-}$ does not exist in molten $MgCl_2$, and interpreted the spectra in terms of a residual ionic lattice, i.e., a polynuclear complex $(MgCl_2)n$. For the $MgX_2.2KX$ systems (X = Cl, Br, I), Maroni[53] observed Raman spectra that were in excellent agreement with the tetrahedral complex $MgCl_4^{2-}$. No evidence for the $MgCl_3^-$ species was detected.

The Raman study by Brooker[54] of K_2MgCl_4 and Cs_2MgCl_4 in the molten state was strongly in favor of the tetrahedral $MgCl_4^{2-}$ ion proposed by Maroni et al.[29,52] Additional studies[31] on molten $MgCl_2$ suggested the presence of discrete polyatomic species, including $MgCl_4^{2-}$, and did not favor the residual ionic lattice model proposed by Capwell.[30] Later, Brooker et al.[32] concluded that the structure of the species present in the melts was not related to the structure present in the solid. It was also found that the network lattice structures with distorted octahedral coordination of magnesium gave way to the smaller tetrahedral coordination on fusion. It is generally accepted that $MgCl_4^{2-}$ is the predominant complex ion in the melts of $MgCl_2$ - ACl.

Even though the Al-X bond is largely ionic, aluminum halides do not melt to form ionized liquid in pure state.[61,62] However, with other halogen compound, aluminum halides behave as strong Lewis acids as demonstrated by the formation of the anion, AlX_4^-,[61] which makes the mixture melt highly ionic.

Chloroaluminate melts may be defined as mixtures of aluminum chloride and other metal chloride(s). The most investigated chloroaluminates are the aluminum chloride - alkali chloride mixtures. The existence of complex ions in these melts has been reported using an analysis of thermodynamic properties,[63-65] via X-ray diffraction method,[66] by neutron scattering,[67] and by IR[16,68,69] and Raman spectroscopy.[21-23,34,56]

All the previous Raman works have concentrated on the structural aspects of solutions of alkali chlorides containing aluminum chloride in excess of the equimolar compositions. These systems have been used as molten salt solvents, due to the low melting points, a wide range of acidities, and high decomposition potentials. There appears to be little disagreement between the earlier and the more recent studies in the literature as to the structure of the complexes present in the melt. The $AlCl_4^-$ tetrahedron has been confirmed as a fundamental structural unit. Higher complexes, $Al_2Cl_7^-$ and $Al_3Cl_{10}^-$, have also been identified in melts with mole fraction of $AlCl_3$ larger than 0.5, but they are not believed to be of importance in the composition range studied in this research.

There have been no reports on Raman spectrum of a melt of composition resembling that of the industrial electrolyte. No Raman spectra have been measured during electrolysis of the systems mentioned above, either. Each component or their mixtures of the $MgCl_2$ or $AlCl_3$ electrolyte were investigated in detail by Raman measurement. Raman spectra were also measured in the systems of $MgCl_2$ and $AlCl_3$ in their

supporting electrolytes, primarily during electrolysis.

4.1 Fundamentals of Raman Spectroscopy

When monochromatic radiation of certain frequency is incident on systems like dust-free transparent gases and liquids, or optically transparent solids, most of beam is transmitted unchanged in its frequency even with some scattering.(Fig. 4.1) However, the analysis of the scattered beam shows a difference in its frequency content: in addition to the original frequency, several pairs of new frequencies of the type, $\nu' = \nu_0 \pm \nu$. The frequency, ν, and the wavenumber, $\tilde{\nu}$, are related to each other by the equation, $\tilde{\nu} = \nu/c$, so they can be used alternatively. (c = speed of light.)

The theory of Raman spectroscopy may be explained by quantum or classical physics, but the scattering process may also be given a simple graphical representation of the collision between the incident radiation and the molecular species, as in Fig. 4.2.[70] By the collision with the incident radiation, the vibrational energy state of the molecule is raised to a certain high energy level. Most of it returns to the original energy state due to the elastic collision (Rayleigh scattering). However, by inelastic collision between the molecule and the radiation, the molecular energy does not return to its original energy state. Instead, the final energy level is higher or lower than the original state. This inelastic scattering process is called Raman scattering, and it is shown by peaks in the spectra. These peaks are

called Raman peaks.

In the spectra, the Raman peaks are identified by their wavenumber shift from the incident value. This wavenumber shift is closely associated with vibration frequency of in the molecular structure. Even though one molecular structure may have several modes of vibration, all the vibrations are not active in Raman scattering.

The number of Raman-active vibrational modes depends on the molecular structure. For example, diatomic or linear triatomic molecules have only one, and non-linear triatomic molecules may have three Raman peaks.

The intensity of Raman peak is given as follows;[71]

$$I = \frac{K\, I_o\, N\, (\nu_o - \nu_\kappa)^4\, [\, 45\, \alpha^2 + 7\, \gamma^2]}{\nu_\kappa\, [1 - \exp(-hc\nu_\kappa/kT)]}$$

where

K = constant,

I_o = intensity of the incident radiation,

N = number of molecules,

ν_o = incident wavenumber,

ν_κ = wavenumber shift due to the molecular vibration,

α = mean value of polarizability change during the vibration,

γ = anisotropy of polarizability change during the vibration,

and others have their usual meanings. According to this equation, the intensity is proportional to the concentration. This equation also shows that the relative intensity ratio is governed by the term, $45\alpha^2 + 7\gamma^2$, indicating that the shape of the Raman spectrum of a certain molecular species would be the same in any case.

Fig. 4.3 shows the Raman spectra measured in the molten mixture of 25 mol.% $AlCl_3$ - 75 mol.% CsCl. In the figure, the spectrum on the ${}^{\perp}I_{\perp}$ curve and that on the ${}^{\parallel}I_{\perp}$ curve were obtained at two different polarization states. Here, ${}^{\perp}I_{\perp}$ means that polarization state of the incident beam (${}^{\perp}I$) is parallel to the state of the scattered beam at the entrance slit of the spectrometer ($I_{\perp}$), while ${}^{\parallel}I_{\perp}$ stands for the perpendicular states of the two beams. This measurement allows the determination of the depolarization ratio. The depolarization ratio is given as follows;[71]

$$\rho = \frac{3\gamma^2}{45\alpha^2 + 7\gamma^2}$$

As we can see, if $\rho = 0$ (i.e., $\gamma = 0$), the vibration is totally symmetrical, and if $\rho \neq 0$, the vibration is asymmetric. The depolarization ratio may be helpful in identifying species since it can give information about which peaks are due to symmetric vibration and which ones are due to asymmetric vibration in the molecular structure.

Consequently, with the wavenumber shift, the number of Raman

peaks, shape of the peaks, and polarization, Raman spectra may be considered as a fingerprint of some molecular species, and might be used for detecting the presence of unknown substances.

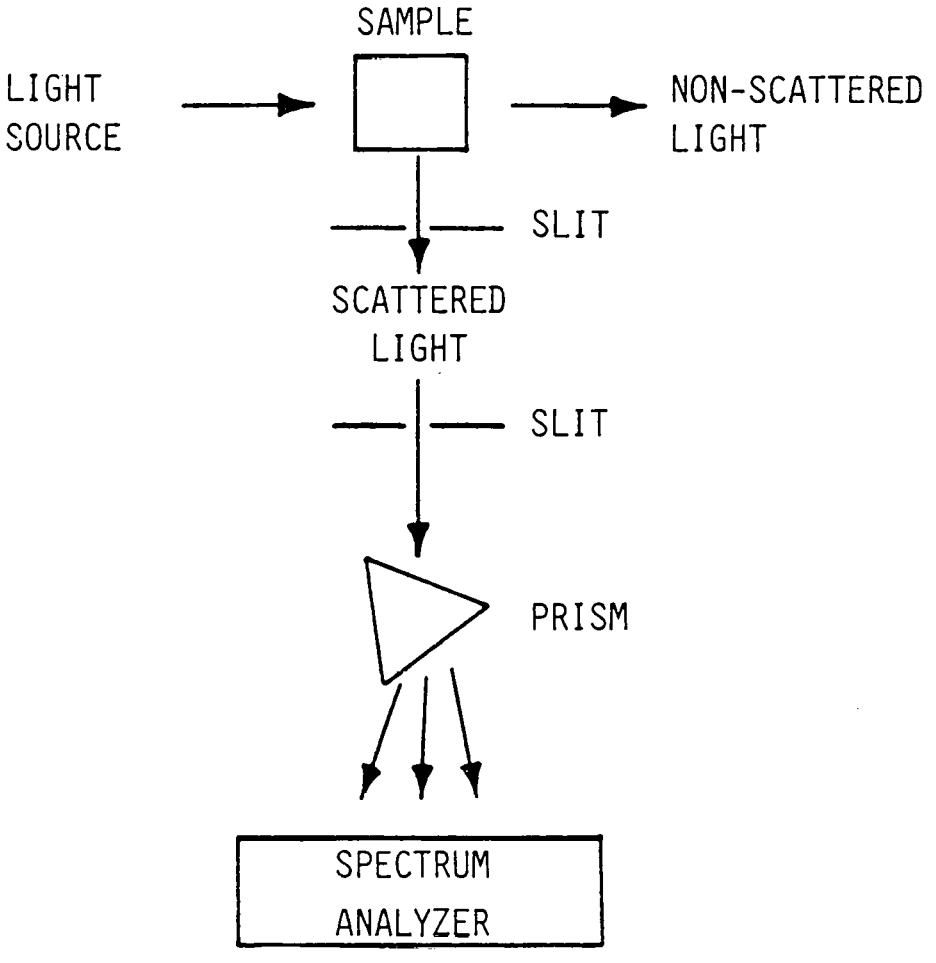

Fig. 4.1 Schematic of Raman spectroscopy

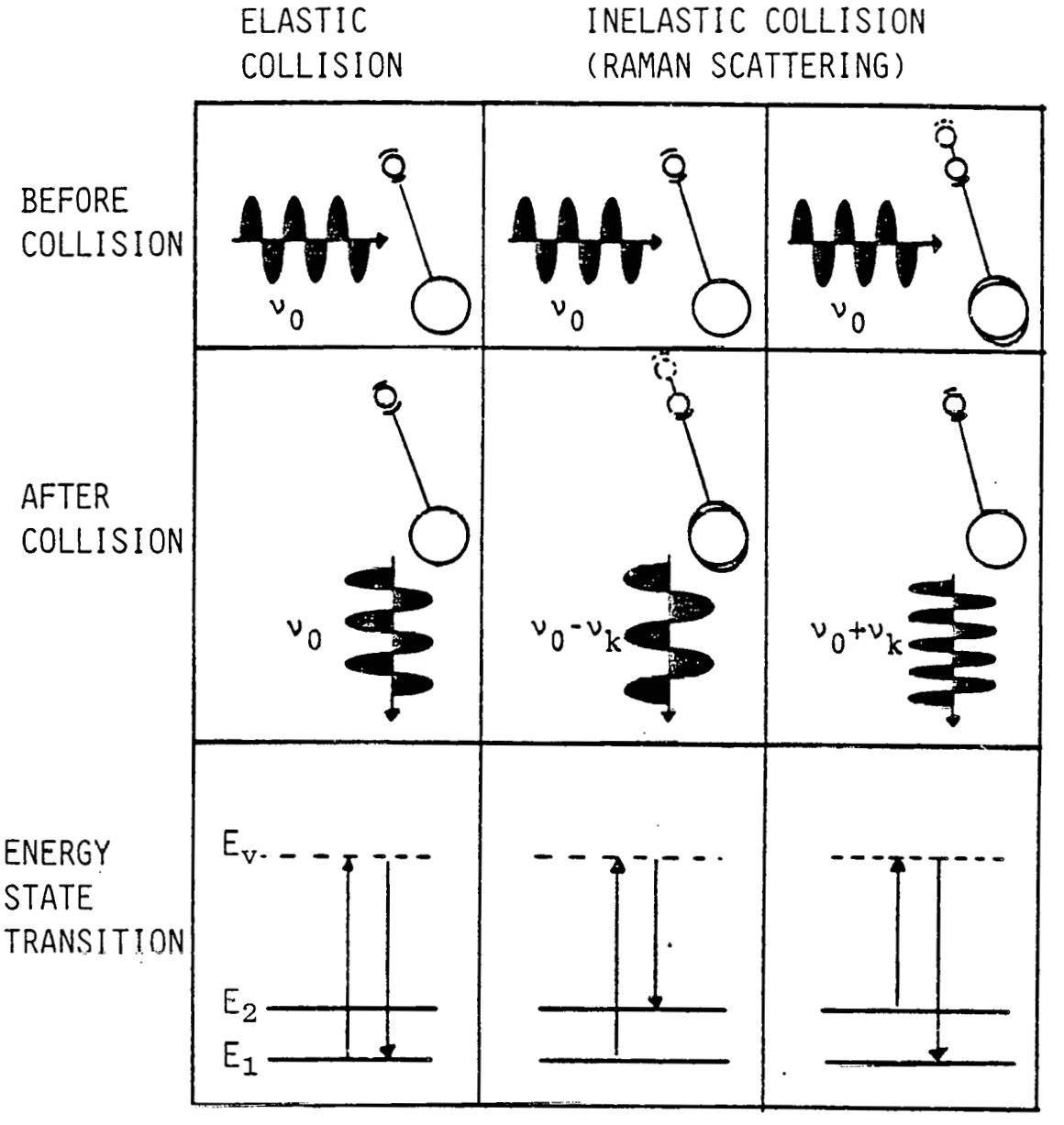

Fig. 4.2 Schematic illustration of elastic and inelastic collisions between the incident radiation and the chemical species. ($E_v > E_2 > E_1$, E_v: virtual energy state)[70]

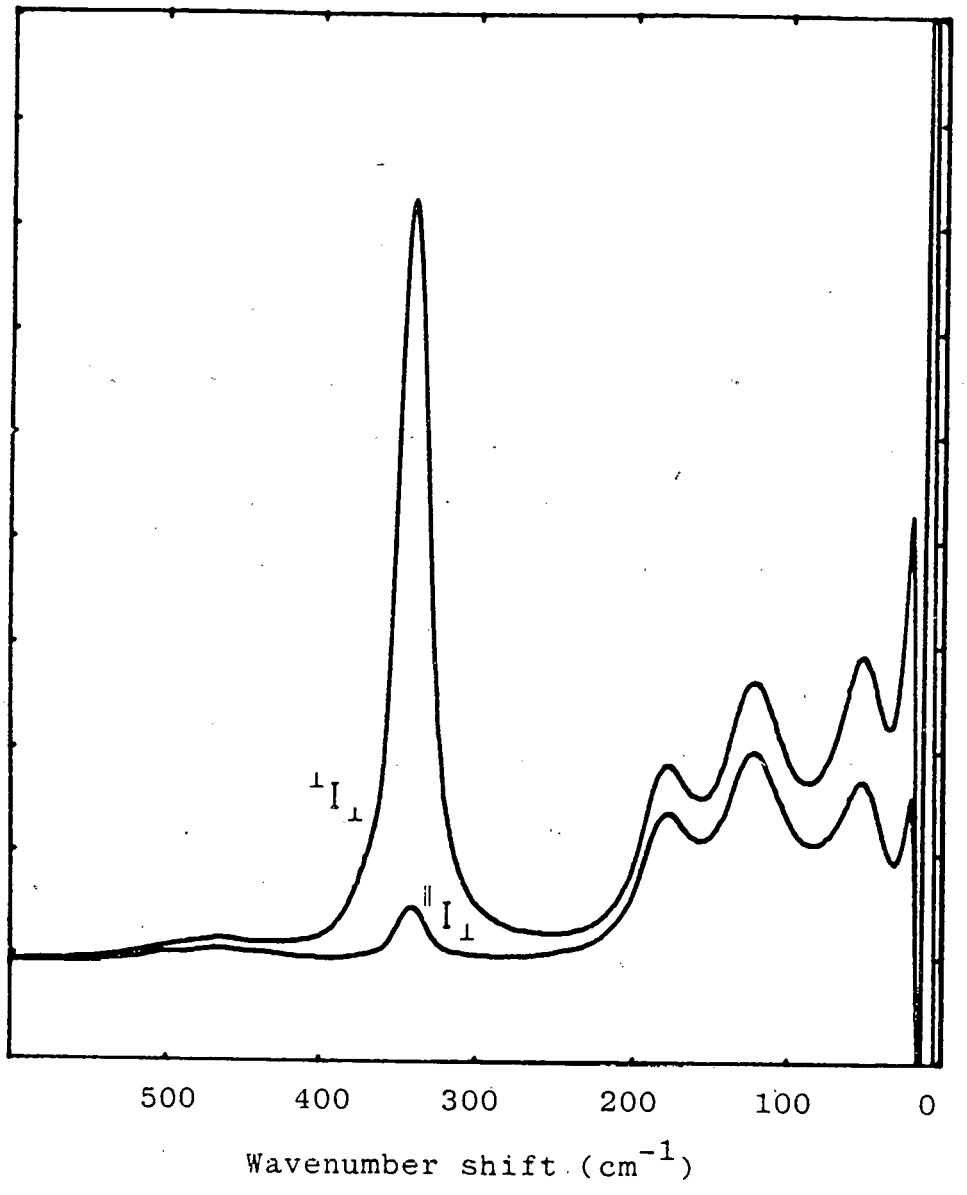

Fig. 4.3 Raman spectra of 25 mol.% $AlCl_3$ + 75 mol.% CsCl. T=700°C. λ=514.5 nm

4.2 Experimental

4.2.1 Instrumentation

The schematic diagram of the instrumentation for Raman study is given in Fig. 4.4. Linearly polarized monochromatic laser beam from either an Ar^+ laser (Coherent Innova 90-4) or a Kr^+ laser (Coherent Innova 90-K), passes the optical instruments, mirrors to change beam direction and a focusing lens. The orientation of the incident laser electric vector is varied using a polarization rotator. Plasma lines from the laser are removed with narrow bandpass interference filters. The focused beam irradiates the sample in the cell which is held inside a furnace. (The cell and furnace are described later in detail.) Electrolysis is conducted galvanostatically or potentiostatically with a Galvanostat/Potentiostat (EG&G PARC, Model 173). The charge passed during electrolysis is measured by a coulometer (EG&G PARC, Model 179).

Most of the incident beam is transmitted unchanged in its wave-number and strikes a power meter (Newport Research, Model 185) which measures the transmitted laser power. This measurement is used as a reference for the transparency or clarity of the melt. The scattered beam is focused through a polarization analyzer onto the entrance slit of the spectrometer by a lens at 90° from the beam propagation direction, which allows the conventional right-angle scattering geometry.

The spectrometer is a triple monochromator (Spex Industries, Triplemate 1403). In the spectrometer, the beam is collimated and dispersed several times and finally focused onto an exit slit of the spectrometer. At this stage, most of the stray light is eliminated. The refocused light is again collimated and dispersed on the grating which can be varied for a different resolution. The final mirror of the spectrometer projects a flat image onto the focal plane on the detector, an intensified silicon photodiode array (EG&G PARC, Model 1420-3).

When photons from the spectrometer strike the detector, electrons are emitted and multiplied. By this process, the light signal is converted to the electrical signal. This electrical signal is amplified, digitized by the detector controller (EG&G PARC, Model 1218), and finally transmitted as data to optical multichannel analyzer (EG&G PARC, OMA, Model 1215) where the data may be manipulated or stored.

The plane of polarization of the exciting radiation is set by a polarization rotator ($^{\parallel}I$ or $^{\perp}I$). The beam then passes horizontally through the molten sample. The scattered radiation is collected at 90° and is imaged onto the vertical entrance slit of the spectrometer while passing through a vertical polarization analyzer ($I_{\perp}$ always). The spectrometer slit width is 100 μm, equivalent to ~6 cm^{-1}. Typically, the spectra were recorded for approximately 1 minute, corresponding to 200 scans on the OMA, which was calibrated using the emission lines of neon lamp in the green. All spectra were measured using the 514.5 nm line of argon as exciting radiation, if not specified.

The scattering geometry was such that a horizontal laser excitation streak was imaged onto the vertical entrance slit of the spectrometer. In this configuration, only Raman-scattered radiation can enter the monochromator.[72] This is particularly important because it is obviously undesirable to simultaneously collect any contribution to the measured spectra associated with the continuum Raman scattering from the quartz-cell walls. The blackbody radiation from the melt, which can obscure the low-intensity high-frequency region of the spectra, was measured at the end of each experimental scan and subsequently subtracted from the raw data.

To reduce the noise which is inherent in all spectroscopic measurements, Raman spectrum is obtained with many scans (up to 400), because the signal-to-noise ratio varies as the square root of the number of measurements. Signal-to-noise ratio is further enhanced by the Savitzky-Golay technique[73,74]: a polynomial approximates local regions of raw data; then, weighting coefficients are convoluted with raw data to yield smoothed values. This technique reduces noise (high frequency fluctuations) by acting as a mathematical low pass filter. The Optical Multichannel Analyzer (OMA) employed in this research also has the differentiating function which can aid in pinpointing an observed peak.[75]

4.2.1.1 Furnace

Specimens are heated by a method somewhat different from those previously employed in spectroscopic studies.[76] This is due to the need to accommodate the laboratory-scale electrolysis cells, which are quite large compared to spectrocells commonly employed in such works. Specifically, an electrical resistance tube furnace was designed and built (Fig. 4.5), which consists of nichrome wire wrapped around a vertical fused quartz tube, 5.1 cm in diameter - 30 cm long, contained in a can packed with aluminosilicate insulating fiber. To permit irradiation and observation of the sample in the furnace, three sidearm tubes were connected to the vertical tube to serve as windows. Located in the same horizontal plane and in a tee configuration, the sidearms are heated by independently-controlled nichrome windings to maintain a constant temperature in the sample. This configuration eliminates the cold-spot on the sample without using shields for the side holes. The furnace could be used up to 1373 K.

The furnace was calibrated for various temperatures with solid iron oxide powder before use. The temperature of the level up to 6 cm from the bottom of the cell did not have any gradient. In the real experiment, the melt did not show any convection due to the thermal gradient.

4.2.1.2 Melt container

For the measurement of Raman spectra without electrolysis, the container was made by joining a 12 mm square fused quartz tubing to 20 mm dia. round tubing (Fig. 4.6 (a)). This fused quartz cell was sealed by a 304 stainless steel cap, which had a hole on top for temperature measurement and two ports for gas circulation.

The electrolysis cell was made of optical grade square fused quartz tubing, 25 mm on edge, joined to a commercial-grade round tubing 41 mm O.D. (Fig. 4.6 (b)). A compression fitting made of 304 stainless steel served as cell cap. It had 4 fittings on the top for cathode, anode, inert gas inlet, and thermocouple, and a port on the side for gas outlet.

4.2.2 Salt preparation

Purification of the melt is extremely important. Impurities can participate in side reactions which are not representative of electrolysis but which may produce species that may affect the Raman spectroscopy or voltammetric studies. The most deleterious substances are insoluble particulates which scatter the incident laser light and make spectroscopy difficult, and water, which can react to form a variety of hydrolysis products. Various procedures have been developed and adopted to remove these hydrolysis products employing anhydrous hydrogen chloride or chlorine, vacuum pre-electrolysis, or a combination of these

techniques, as suggested in the literature. However, the melts of the salts prepared by these methods were not satisfactory for this spectro-electrochemistry work.

This research has developed a different purification procedure using **thionyl chloride** ($SOCl_2$). The possible reactions of thionyl chloride with oxides can be thought as follows;

$$MgO(s) + SOCl_2(g) \rightarrow MgCl_2(l) + SO_2(g)$$

$$\Delta G^\circ_{973\ K} = -31\ kcal\ mol^{-1}$$

$$Al_2O_3(s) + 3SOCl_2(g) \rightarrow 2AlCl_3(l) + 3SO_2(g)$$

$$\Delta G^\circ_{973\ K} = -18\ kcal\ mol^{-1}$$

These thermodynamic data are not complete; however, the marginally negative ΔG°'s were calculated from information in Barin, Knacke, and Kubaschewski.[77,78]

Anhydrous magnesium chloride was prepared in principle by the method of Behl and Gaur.[79] The preparation involves the dehydration and decomposition of a double salt, ammonium carnallite ($MgCl_2.NH_4Cl.6H_2O$), followed by chlorination of $MgCl_2$ with $SOCl_2$.

The double salt is heated and evacuated in a cylindrical fused quartz vessel at a temperature of 175°C until dehydration is complete

(about 8 hours). The resulting anhydrous magnesium ammonium chloride is heated slowly to 340°C (30°C every two hours) to decompose the double salt and to separate the NH_4Cl. This treatment is conducted in a long fused quartz tube (Fig. 4.7). Ammonium chloride vaporizes to deposit on the cooler upper part of the tube, and magnesium chloride remains in the bottom of the tube.

After ammonium chloride is removed in the glove box, the remaining magnesium chloride is heated to 550°C. At this temperature, higher than that at which all possible water can be removed,[80] argon gas bubbled through $SOCl_2$ is passed over the salt to remove any remaining oxide, oxychloride, or moisture for 1 - 2 days. After chlorination, the magnesium chloride is evacuated at 800°C, just above the melting point. The distilled $MgCl_2$ is taken out and stored in the glove box for future use.

$AlCl_3$ is highly hygroscopic and sublimes at a very low temperature, 182°C, at normal pressure. Analytical grade $AlCl_3$ is used for the starting material. Before the thionyl chloride treatment, this salt is pre-purified several times by subliming under vacuum at 170°C. Over this pre-purified salt, the Ar gas bubbled through $SOCl_2$ is passed at 100°C for a day, and then it is sublimed under $SOCl_2$ atmosphere at 150°C. The purpose of $SOCl_2$ treatment is the same as in the case of $MgCl_2$ purification. This salt is finally sublimed under vacuum at 180°C.

The procedure for the preparation of other salts such as NaCl,

KCl, LiCl, and CsCl is simpler than that for $MgCl_2$ or $AlCl_3$ and consists of following steps: The salt is dried under vacuum at 150°C, 300°C, and 500°C for 5 hours at each temperature. The Ar gas saturated with $SOCl_2$ is passed over the salt for a long period (1 day) at 550°C. Finally, they are distilled by subliming at their melting temperature.

Since $CaCl_2$ has a low vapor pressure even at its melting point, it cannot be sublimed as easily as $MgCl_2$ or the other salts. $CaCl_2$ packed under argon served as starting material. After drying the material under vacuum at various temperatures (150°C, 300°C, and 500°C for 5 hours at each temperature), the Ar gas bubbled through $SOCl_2$ is passed over the $CaCl_2$ for a longer period (3 days). Without distillation, it is removed and stored in the glove box.

4.2.3 Typical Experiment

The electrolytic cell for experiments is prepared in the following manner. The fused quartz cell is cleaned with HF and rinsed with distilled water. After drying in air, the cell is flame-polished to restore the optical quality of the square part of the cell. In the glove box, salts are charged into the cell and the electrodes and the cap are installed. The assembled cell is placed in the furnace where the salts are melted under high purity argon (below 5 ppm of oxygen).

For $MgCl_2$ experiments, the usual melt composition is 11% $MgCl_2$,

6% $CaCl_2$, 65% NaCl, and 18% KCl by weight percent. (This composition is currently employed in industry.) The melt is almost 3 cm deep. The temperature is usually maintained at 750°C. The composition for $AlCl_3$ experiments is usually 5 wt.% $AlCl_3$, 53 wt.% NaCl, and 42 wt.% LiCl, but sometimes 10 wt.% $AlCl_3$, 50 wt.% NaCl and 40 wt.% LiCl. The temperature is measured with a chromel-alumel thermocouple in the melt, and maintained at 700°C.

The spectra are measured in the bulk and on the cathode surface before and during electrolysis using 514.5 nm argon laser radiation. Typical laser power was in the range of 0.7 - 1.5 W.

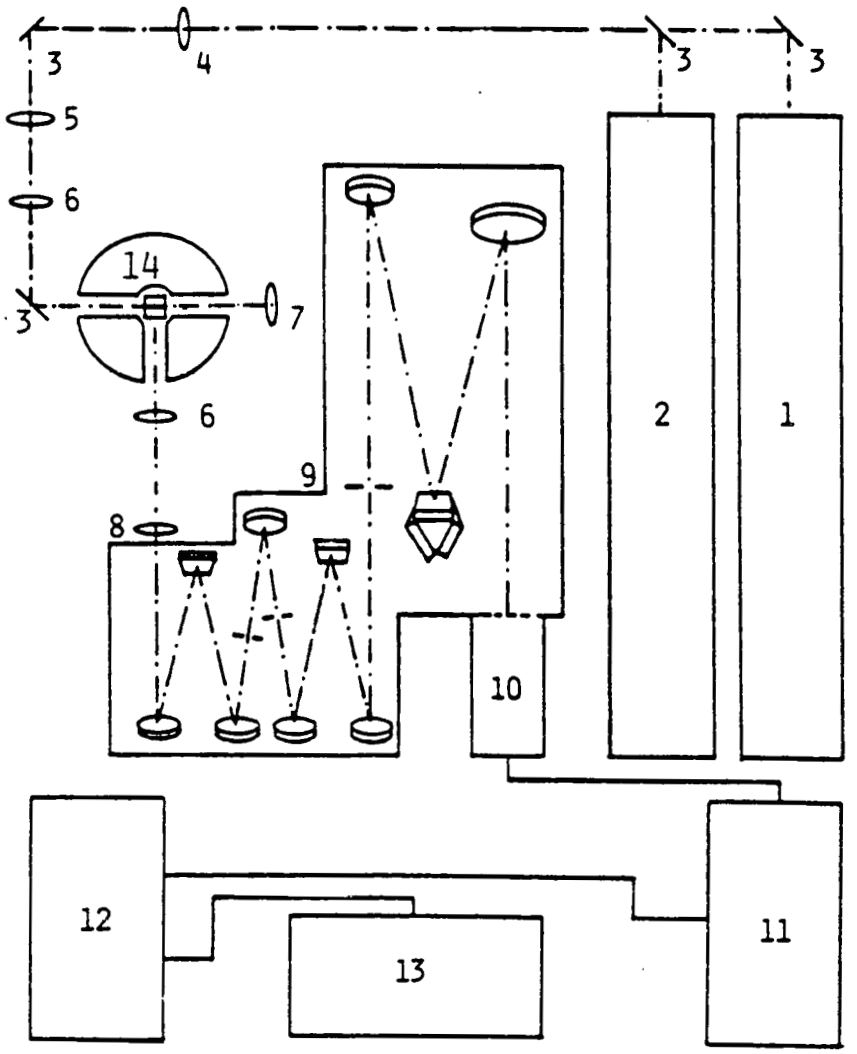

Fig. 4.4 Schematic diagram of Raman instrumentation.

(1) Ar laser; (2) Kr laser; (3) Mirrors;

(4) Polarization rotator; (5) Bandpass filter;

(6) Focusing lenses; (7) Power meter;

(8) Polarization analyzer; (9) Spectrometer;

(10) Detector; (11) Detector controller;

(12) Optical multichannel analyzer; (13) Plotter;

(14) Furnace and melt container

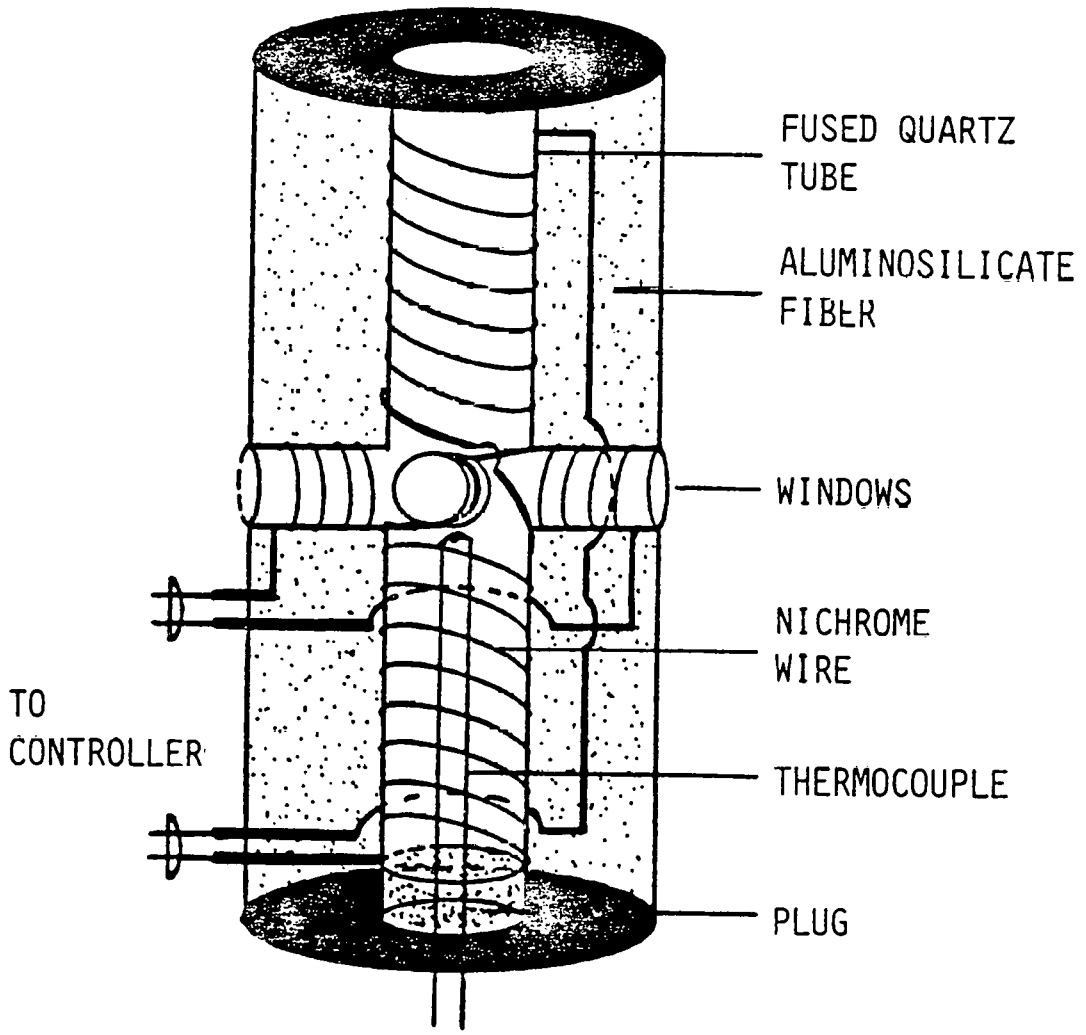

Fig. 1.5 Schematic of the furnace for Raman measurement.

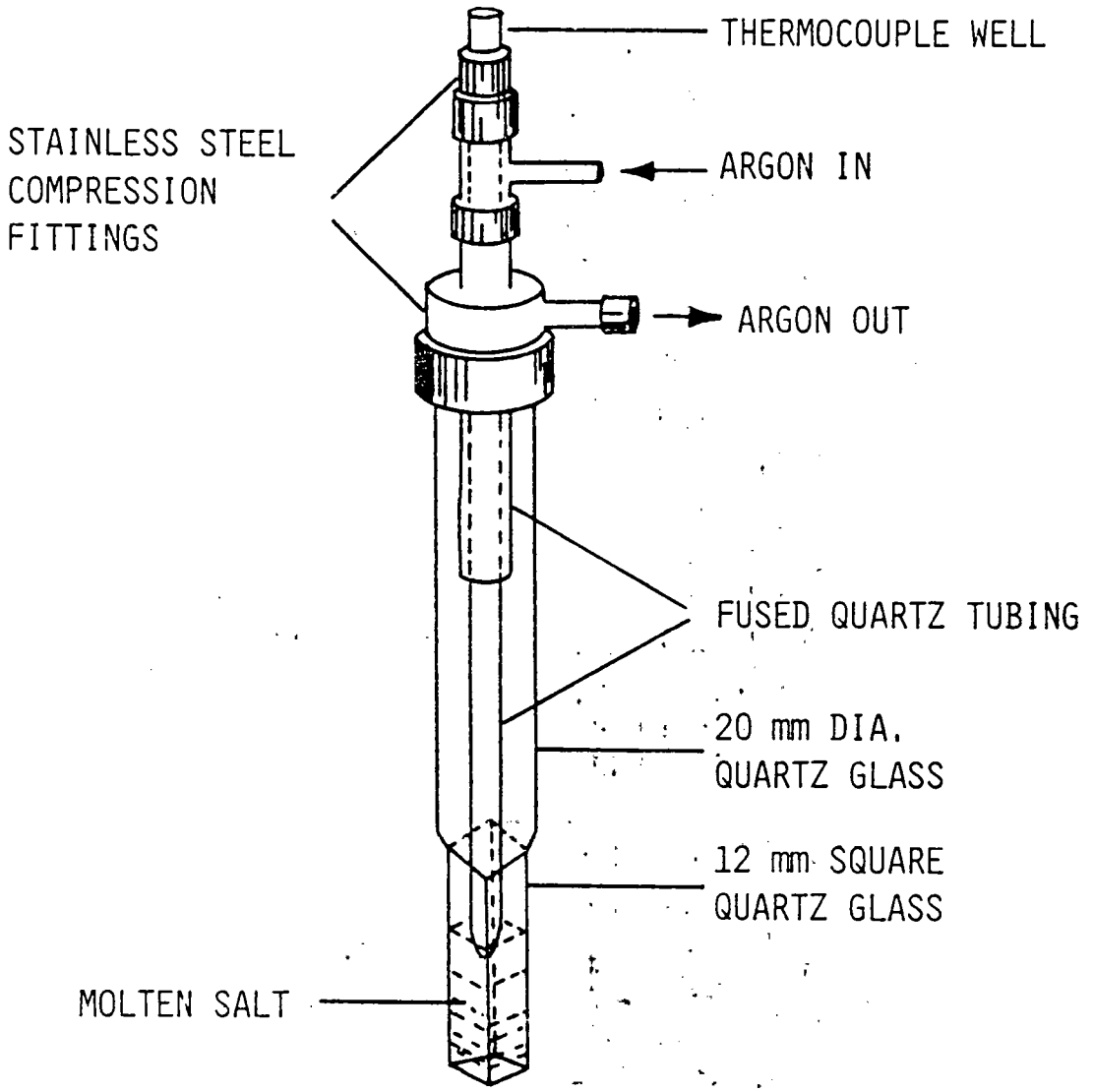

Fig. 4.6 Schematic of molten salt container.

(a) For Raman measurement without electrolysis.

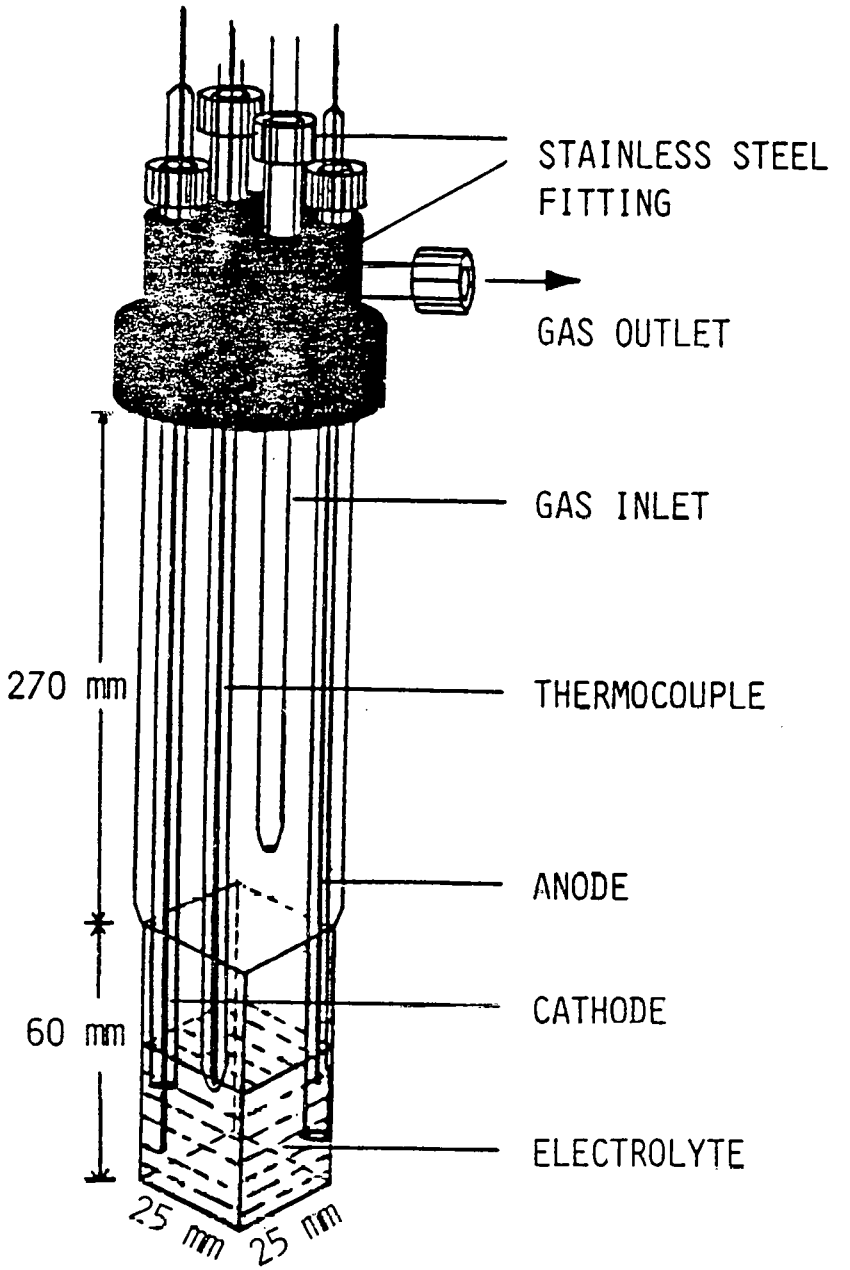

Fig. 4.6 (b) For Raman measurement during electrolysis

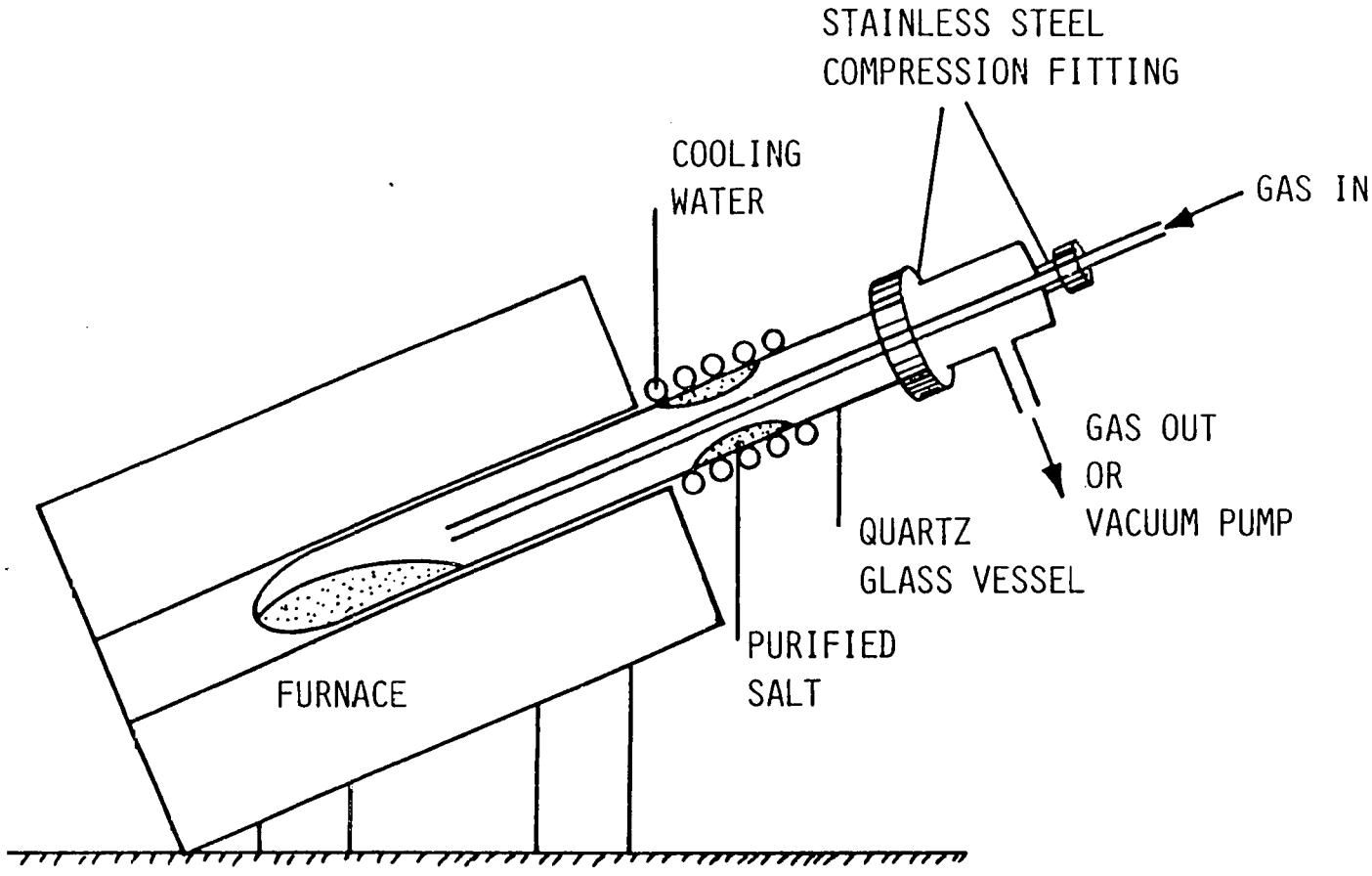

Fig. 4.7 Schematic of the apparatus for salt purification

4.3 Results and Discussion

4.3.1 Raman spectra of melts without electrolysis

4.3.1.1 Melts of $MgCl_2$ and additives

Raman spectra measured for pure molten $MgCl_2$ at 740°C show a completely polarized peak at 205 cm^{-1} and a broad depolarized band at about 385 cm^{-1} (Fig. 4.8). Raman spectra are usually plotted intensity vs wavenumber shift from the value of the incident radiation. The intensity is scaled arbitrarily, and thus, the relative peak intensity is important in the Raman spectra. Wavenumber is used in the spectroscopy more often than wavelength or frequency, and in Raman spectra, wavenumber shift is more important than the absolute value, as described in earlier sections.

Most spectra were measured at two different polarization states by rotating the polarization of the incident laser beam, one at the parallel polarization state of the laser beam to the state of the scattered beam at the vertical entrance slit on the spectrometer ($I_{\parallel}$), and the other at the perpendicular state ($I_{\perp}$). For the upper curve in Fig. 4.8, the polarization state through the polarization analyzer was parallel to that of the incident radiation, and for the lower one, it was perpendicular to that of the incident beam. Peaks at about 90 cm^{-1} are not true Raman peaks, but rather artifacts of the filter cut-off which is employed to protect the photodetector from the high intensity

radiation at the incident frequency. A filter cut-off peak is always found in the measured Raman spectra unless otherwise specified. The Raman spectra in this figure have been scaled for comparison and found to be identical to those of Brooker and Huang.[31,81]

Alkali chlorides were investigated in detail because they are basic components of the supporting electrolytes for magnesium and aluminum chlorides electrolysis. Fig. 4.9 - Fig. 4.12 show Raman spectra of molten LiCl, NaCl, KCl, and CsCl, respectively, measured at the temperatures specified in each figure. The Raman spectra of the molten equimolar mixtures of NaCl-KCl and LiCl-NaCl are shown in the Fig. 4.13 and Fig. 4.14. In the Raman spectra of these alkali chlorides or their mixtures, there are no peaks like those seen in Fig. 4.8. However, Rayleigh shoulders due to the elastic collision between the radiation and the species are clearly found in the spectra, and thus, the featureless traces in these figures for the alkali chlorides are proper Raman spectra.[72,82]

Even though the alkali chlorides do not have any appreciable Raman peak, the addition of the alkali chloride to $MgCl_2$ changes the spectra. Fig. 4.15 shows the Raman spectra of molten mixtures of $nMgCl_2$ + (1-n)CsCl at 800°C (n = mole fraction), which show that the maximum peak seen in the spectra of molten $MgCl_2$ shifts from 205 cm^{-1} to 245 cm^{-1} with the increase of CsCl content in the melt. The peak movement may be explained by considering the difference in the charge densities (z/r^2) of magnesium and alkali metal ions. Because of the high charge density, magnesium ion draws chlorine ion from the alkali chloride to form a more

stable complex ion than that in the pure $MgCl_2$ melt. The stronger Mg-Cl bond in the complex ion makes the frequency higher, which causes the peak to shift to higher value in the spectra. Table 1 shows the ion radii of several elements which are important in this research. The values in the table are actually ionic crystal radii,[83] and they may be different in liquid state. However, the trend is thought to be correct.

It has been reported that alkali chloride act as a donor of chlorine ion to magnesium chloride to form tetrahedral complex ion, $MgCl_4^{2-}$, by the following reaction.[31,32]

$$2ACl + MgCl_2 = 2A^+ + MgCl_4^{2-}$$

In Fig. 4.16 and 4.17, one may observe that the maximum peak does not shift any more when CsCl content exceeds 67 mol.%. The reason is thought to be that, above this level, the CsCl content is more than enough for all $MgCl_2$ to form the complex ions under the above reaction. This observation strongly supports the tetrahedral complex ion theory. The tetrahedral complex ion formation is further supported by the fact that Raman spectra of molten $MgCl_2$ - 2CsCl mixture have four peaks at 106, 143, 247, and 350 cm^{-1}, and the peak at 247 cm^{-1} is completely polarized (Fig. 4.18), because these spectra look like those of CCl_4, a typical tetrahedral-structure molecule,[84] in that there are four Raman peaks, one of them polarized. Although all the peaks in Fig. 4.18 are not distinct, it is possible to locate the peaks with techniques of fitting and differentiating the curves, which are internal functions of

the microprocessor employed in this research.

Table 4.1 Ionic Radii of Elements (in Å)[83]

Ion	Ionic Radius	Ion	Ionic Radius
Al^{3+}	0.50	K^{+}	1.33
Li^{+}	0.60	F^{-}	1.36
Mg^{2+}	0.65	Cs^{+}	1.69
Na^{+}	0.95	Cl^{-}	1.81
Ca^{2+}	0.99		

With the addition of lighter alkali chlorides to $MgCl_2$, it was observed that the maximum peak moves to a slightly lower frequencies, while the halfwidth of the peak increases considerably over the cation series Cs^{+} to Li^{+} (Fig. 4.19). This may be again explained by the charge densities of alkali cations (Fig. 4.20); the small Li^{+} ion can compete quite favorably, due to the high charge density, for the chloride ion, which will weaken the Mg-Cl bond. This is reflected by the lower frequency in the Raman spectra. In Fig. 4.20, it may be observed that the wavenumber shift has an almost linear relationship with the charge density. The symmetric vibration mode of $MgCl_4^{2-}$ will occur in a greater range of environmental conditions in the neighborhood of the smaller Li^{+} than for the larger Cs^{+} ions, which could explain the larger halfwidth for the lithium melt.

From the above observations, it can be concluded that magnesium forms stronger complex ion when magnesium chloride is mixed with the heavier alkali metal chloride. The reason is thought to be that magnesium ion can easily draw chlorine ion from the lower charge density ion. The stronger complex ion formation is reflected by the sharper peaks and higher wavenumber shift in the Raman spectra. Temperature effect on Raman spectra could not be detected over the range experiments conducted.

The typical industrial composition of the electrolyte for magnesium electrolysis is 11 wt.% $MgCl_2$ - 65 wt.% NaCl - 18 wt.% KCl - 6 wt.% $CaCl_2$, and Fig. 21 and 22 show the Raman spectra of the supporting solvent melt only, and the electrolyte at the industrial composition, respectively. The peaks are not distinct in these spectra. However, since it is known where to look for the peaks from the above information, it was possible to locate the peaks with aid of the internal functions of the microprocessor (OMA) employed in this research. The peaks are at about 107, 142, 249, and 351 cm^{-1}. The peak at 249 cm^{-1} is completely polarized. All these information suggests that magnesium exists as a tetrahedrally coordinated complex, $MgCl_4^{2-}$, in the electrolyte of industrial composition.

4.3.1.2 Melts of $CaCl_2$ and with other additives

$CaCl_2$ is one of the major components of the supporting electrolyte for magnesium electrolysis. Since this Raman active chloride is not electroreduced during electrolysis, it was felt that it could serve as an internal standard for Raman measurement of $MgCl_2$ concentration in the cell-bath on-line in real time. The molten $CaCl_2$ and with other additives were investigated for possible use in this regard.

Fig. 4.23 shows the Raman spectra of pure molten $CaCl_2$ at 800°C. One sees a broad polarized band between 150 and 200 cm^{-1} which demonstrates that, just as $MgCl_2$, $CaCl_2$ has some tendency to form structural entities in the pure molten state. The broader band than that of $MgCl_2$ confirms the charge density effect on the spectra because the charge density (z/r^2) of Ca^{2+} is 0.43 times that of Mg^{2+} so that the possibility will be reduced for the formation of strong complex species. These results agree with the earlier measurements.[28,85]

Fig. 4.24 shows the Raman spectra of 33 mol.% $CaCl_2$ - 67 mol.% CsCl at 840°C. CsCl is a good ligand donor and as such would strongly promote complex formation, as described earlier. A polarized peak at 190 cm^{-1} is clearly evident, and other 3 depolarized peaks may also be found at about 113, 147, and 347 cm^{-1}. Here, the spectra have been smoothed by means of the Savitzky-Golay technique, which also helps in identifying peak positions by differentiation of the functional representation of the raw data. This result shows far better signal to noise ratio than that of Sakai et al.[86]

The strong polarized peak of what is believed to be the $CaCl_4^{2-}$ complex having been identified, the study turned to solutions of $CaCl_2$ in lighter alkali chlorides and finally in the supporting electrolyte for magnesium electrolysis. Fig. 4.25 shows the spectrum of 33 mol.% $CaCl_2$ in KCl. The Raman peak at 190 cm^{-1} is as evident as in the CsCl solvent melt. In Fig. 4.26, Raman spectra of 33 mol.% $CaCl_2$ in NaCl melt show a very weak band. Without the knowledge from the previous solvent melts, one would be tempted to conclude that $CaCl_2$ does not coordinate in NaCl solvent melt to form Raman active species. These results clearly show the fact that the stronger complex ion can be formed with the heavier alkali cation chlorides.

It is instructive to see the effects of the mixed $MgCl_2$ - $CaCl_2$ system. The spectrum of pure molten $MgCl_2$ has the predominant sharp peak at 205 cm^{-1} (Fig. 4.8). Fig. 4.27 shows the Raman spectrum of the equimolar solution of $MgCl_2$ - $CaCl_2$. Although it was difficult to prove quantitatively, this was thought to represent essentially the superposition of Fig. 4.8 and Fig. 4.28, both in a physical sense and from the standpoint of data analysis. Here, one can clearly see the additivity property of Raman spectroscopy. The peaks of pure $MgCl_2$ and $CaCl_2$ at 205 cm^{-1} and 180 cm^{-1} must be deconvoluted and the broad anomalous Rayleigh shoulder may have to be suppressed in order to derive quantitative information from these data.

4.3.1.3 Melts of $AlCl_3$ with additives

Raman spectra of pure molten $AlCl_3$ cannot be measured under normal conditions, because $AlCl_3$ sublimes without melting at 182°C. In this investigation, therefore, Raman spectra were measured for the molten mixtures of $AlCl_3$ with alkali chlorides.

The Raman spectra of the melt of 25 mol.% $AlCl_3$ - 75 mol%. KCl at 800°C showed similarity to those of CCl_4 in that four distinct peaks were observed (at 125, 183, 346, and 483 cm^{-1}) one of which is completely polarized (at 346 cm^{-1}), but others are not.(Fig. 4.28) As in the case of $MgCl_2$ experiments, most spectra were measured at two different polarization states. The filter cut-off peaks at about 70 cm^{-1} are not true Raman peaks. Filter cut-off was conducted for the protection of spectrometer from strong laser beam, and thus, these peaks are always observed at this location unless specified otherwise.

Fig. 4.29 shows the Raman spectra of $AlCl_3$ in KCl melt at several different compositions. The temperature was maintained at 800°C. KCl was chosen because it proved a strong chlorine ion donor during the study of $MgCl_2$ melt. One may see that the maximum peak becomes stronger with $AlCl_3$ content. No change was observed in the peak location within the composition range concerned. The same phenomenon was observed during $MgCl_2$ experiments, where the maximum peak did not shift any more when the alkali chloride content exceeds 67 mol.%, confirming the proposed tetrahedral complex ion formation by the reaction of

$$2ACl + MgCl_2 = 2A^+ + MgCl_4^{2-}.$$

Here, with the observation of four peaks one of which is polarized, the peaks' non-shift may again be in conformity with the reported tetrahedral complex ion formation reaction,[20,21]

$$ACl + AlCl_3 = A^+ + AlCl_4^-,$$

because, in the composition range concerned, the content of alkali chloride in the melt has already exceeded the value for all the aluminum ions to form complex ions under the assumption of the above reaction equation.

It was felt that the peak height measurement may be used as a reference for the determination of the concentration of $AlCl_3$ because the maximum peak at 346 cm^{-1} changes its height with the concentration without change in the location. Even though the peak intensity is proportional to the concentration only under the identical measuring conditions, the peak height measurement from the base line of the spectra was enough to obtain a quick information on the concentration. A plot of peak intensity vs mole fraction of $AlCl_3$ in KCl was drawn from Fig. 4.29 by normalizing the spectra (reference was the intensities at 65 cm^{-1} where no Raman peak was observed for this system), and it is shown in Fig. 4.30. The peak intensity measured from base line was drawn in arbitrary scale. In Fig. 4.30, one may see that the peak height is fairly proportional to the concentration of $AlCl_3$ in the melt.

It might be concluded here that Raman spectroscopy can be used as reference for measurement of the concentration in the systems like $AlCl_3$ electrolyte.

In the Raman spectra of Fig. 4.31, it can be observed that the maximum peak is the sharper for the melt with KCl than with NaCl or LiCl. This observation may again be explained by the lowest charge density of the K^+ ion of the three alkali metal ions, but the difference in the sharpness or peak location is not as great as observed in the $MgCl_2$ melts. This phenomenon is again explained by the high charge density of Al ion. (2.54 times that of Mg^{2+}.) It is also explained qualitatively by the greater tendency of Al to form covalent bond than Mg. It is well known that aluminum chloride does not form ionic melt when it is molten, and thus, it sublimes under normal condition. Because of this property, the strong Raman peaks can be observed and the small difference in the charge densities of the alkali metal cations may not be enough to cause an appreciable difference in the spectra. These observations are contrary to the Raman measurements by Rytter et al.[22], but agree well with the thermodynamic data.[87,88]

The composition of the supporting electrolyte in the Alcoa Smelting Process is 45 wt.% LiCl - 55 wt.% NaCl, and Fig. 4.32 shows Raman spectra of that melt measured at 700°C. There are no appreciable peaks, as expected. In the Fig. 4.33, Raman spectra are shown for the melt resembling an industrial composition (10% $AlCl_3$ - 40% LiCl - 50% NaCl by weight) at a temperature of 610°C. These spectra show four distinct peaks, at 125, 183, 349, and 483 cm^{-1}. The peak at 349 cm^{-1} is

polarized. The observation of four peaks, the relative intensities of the peaks, and the polarization of the strongest peak are characteristic of the tetrahedral structure which can be found in the Raman spectra of CCl_4.

All the observations are in strong conformity with the assumption that, in the electrolyte of industrial composition, aluminum coordinates with four chlorine ions to form a tetrahedrally coordinated tetrachloroaluminate ion, $AlCl_4^-$, by the following reaction.

$$ACl + AlCl_3 = A^+ + AlCl_4^-$$

4.3.1.4 Melts of $AlCl_3$ - CsCl

During the Raman study of $AlCl_3$ in CsCl melt, a new Raman peak was observed at 247 cm^{-1} for the melt of 10 mol.% $AlCl_3$ - 90 mol.% CsCl. (Fig. 4.34) This polarization-sensitive peak had not been expected for this melt because other alkali chloride melts did not show it, or phase diagram of $AlCl_3$ - CsCl system does not contain any compound or anomalous features in the composition range concerned. No literature on this phenomenon could be found. Therefore, Raman measurements were conducted carefully on this system.

In Fig. 4.35, one can see the peak at 247 cm^{-1} becomes as strong as that at 345 cm^{-1} as $AlCl_3$ content decreases in the CsCl melt. At a

low concentration of 0.5 mol.% $AlCl_3$ (Fig. 4.35 (c)), this peak is even stronger than that at 345 cm^{-1}. However, the Raman spectra of 5 mol.% or less of $AlCl_3$ in KCl, NaCl, or in LiCl did not show this peak (Fig. 4.36). As $AlCl_3$ content increases in the melt, the intensity of the peak at 247 cm^{-1} becomes weaker. This peak could not be found at the composition of higher than 25 mol.% $AlCl_3$. (Fig. 4.37)

Although other analysis techniques may be required to identify the species for that peak, a rough explanation can be given by comparing with another system. It has been reported that AlF_4^- is equilibrium with AlF_6^{3-} in cryolite melt.[89,90] By the same token, an equilibrium reaction can be imagined between the tetrahedral $AlCl_4^-$ and the octahedral $AlCl_6^{3-}$ complexes. This explanation is supported by the following observations: 1. For octahedral complex ion to be formed, chlorine ion has to be more easily obtained from the source than for tetrahedral complex formation. Here, Cs^+ ion has the lowest charge density of the alkali chlorides so that higher chlorine complex can be formed in this melt. As well, the presence of the large Cs^+ cations tend to open up the liquid structure to allow 6 Cl^- anions to associate with a single Al^{3+} cation. That is thought to be the reason why the peak at 247 cm^{-1} could not be observed for the mixtures of other lighter alkali chlorides. 2. As the concentration of CsCl increases in the mixture melt, the new peak intensity becomes great and at a very high concentration it is greater than that at 345 cm^{-1}.(Fig. 4.35) As Al^{3+} ions become less and Cl^- ions become more, Al^{3+} ions are surrounded by more chlorine ions, and thus, Al^{3+} ions have the higher chance of forming higher chlorine complex ion like $AlCl_6^{3-}$. That may explain why

the peak at 247 cm^{-1} becomes as strong as the peak at 345 cm^{-1} as $AlCl_3$ concentration decreases.

If one assumes that the octahedral complex forms only at high dilution in these Cs-rich chloroaluminate melts, then its formation can lead to loss of power efficiency. The electrodeposition of aluminum from an octahedral complex requires an additional step to that from a tetrahedral complex since the octahedral complex has to be decomposed to the tetrahedral complex first. This additional mechanistic step for Al reduction increases the overpotential through activation. Furthermore, the bigger octahedral complex is less mobile than the smaller tetrahedral complex, resulting in reduced diffusivity. This leads to an increase in concentration overpotential.

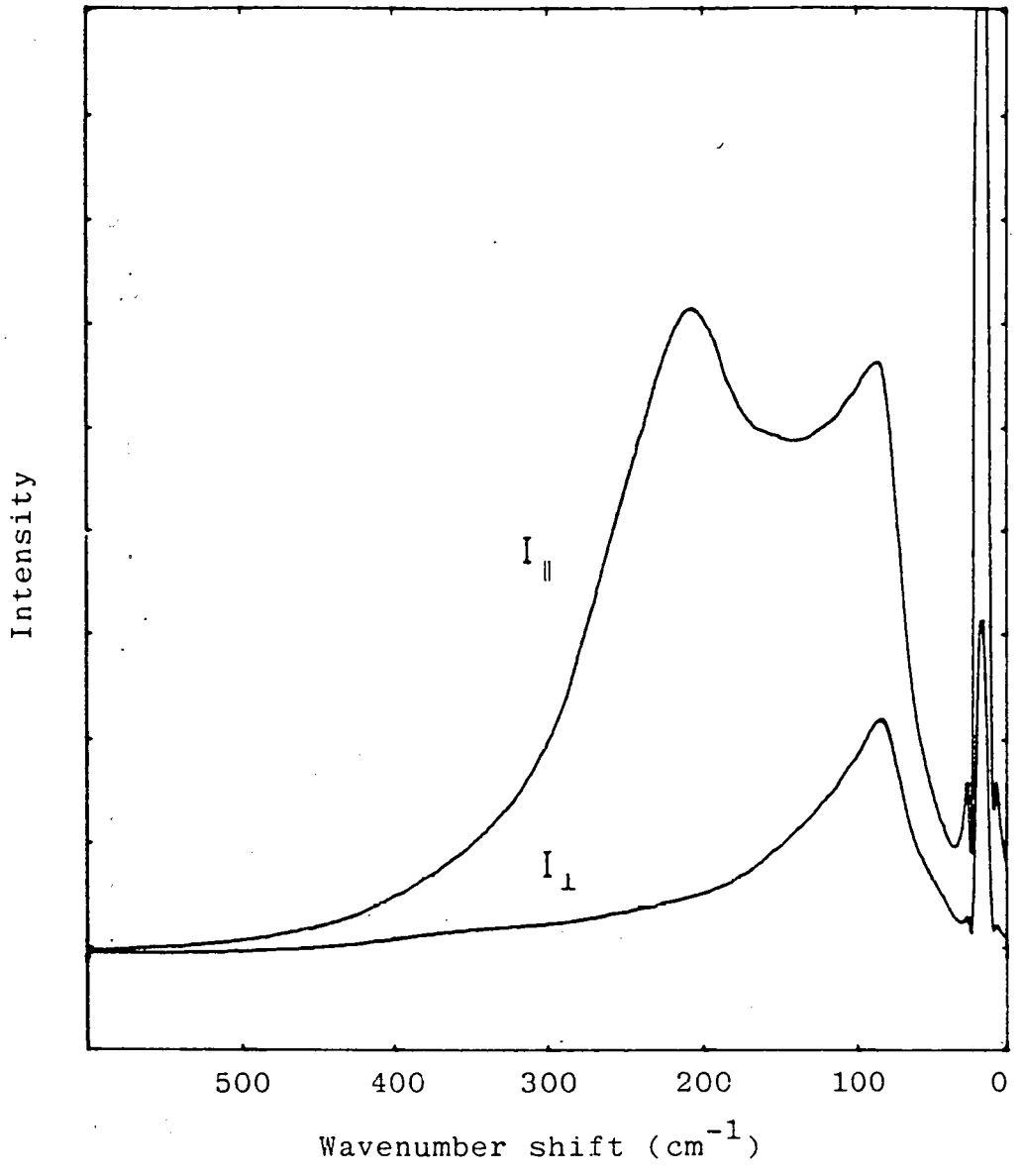

Fig. 4.8 Raman spectra of molten $MgCl_2$. T=740°C.

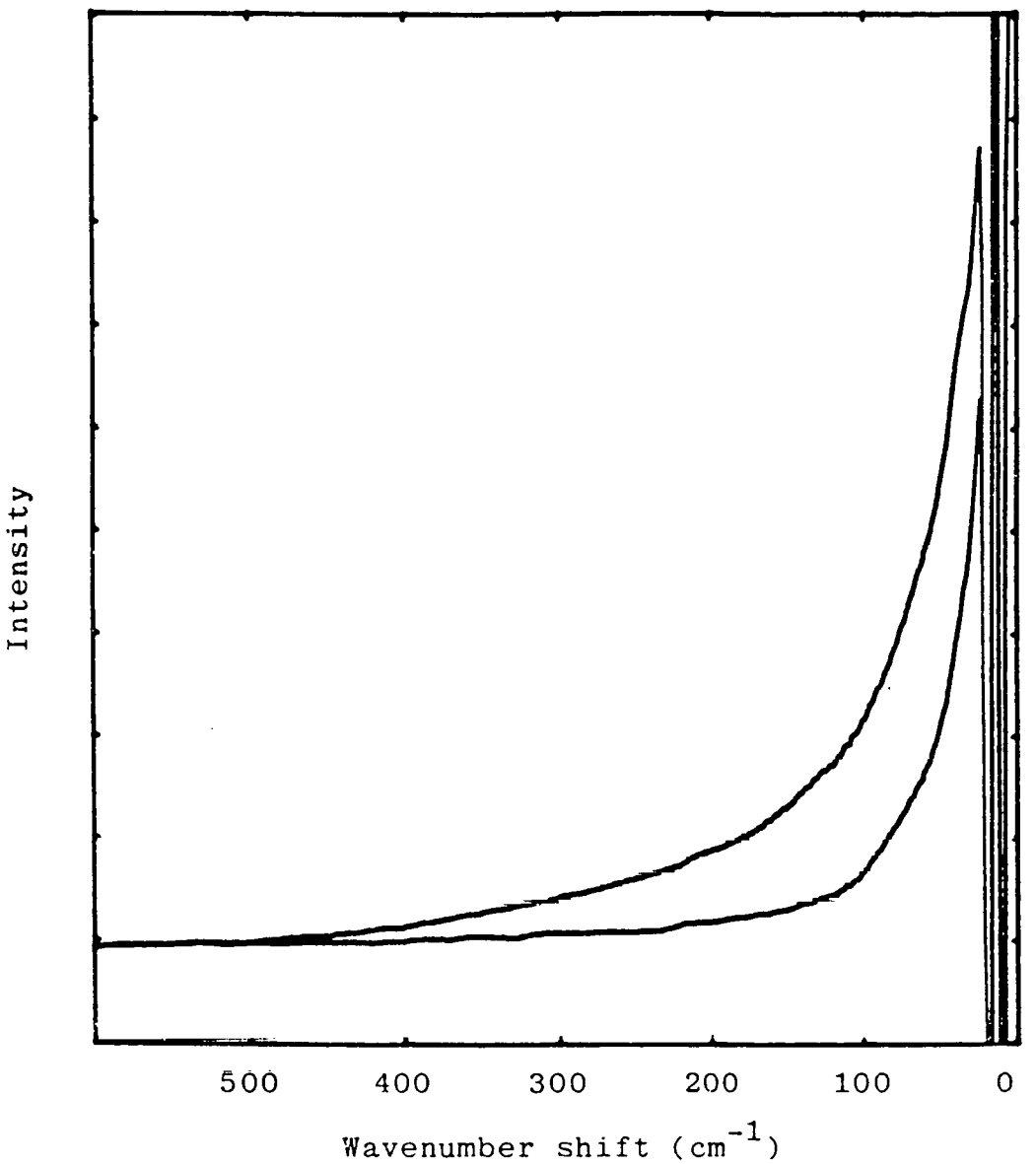

Fig. 4.9 Raman spectra of molten LiCl. T-800°C

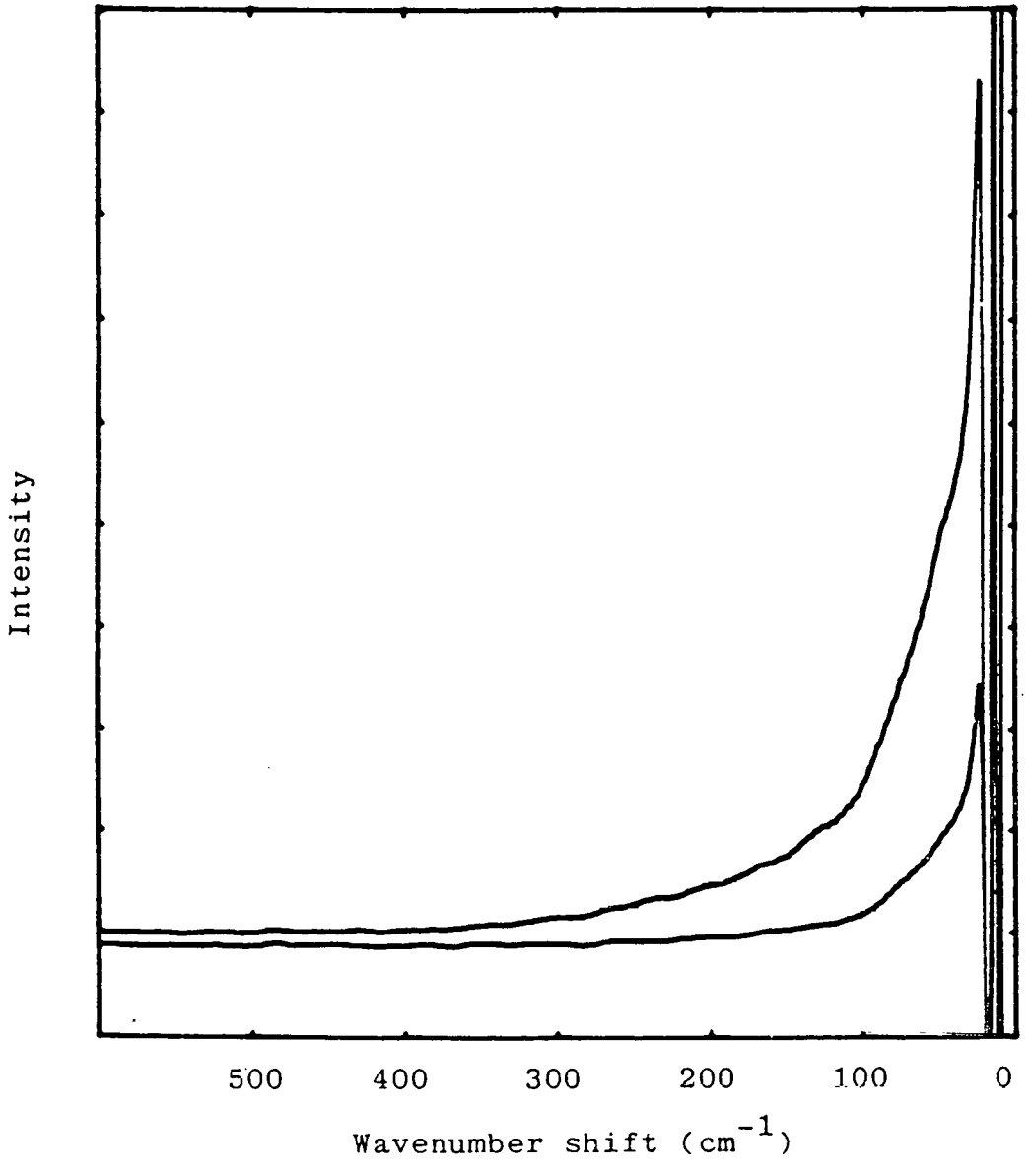

Fig. 4.10 Raman spectra of molten NaCl. T=830°C.

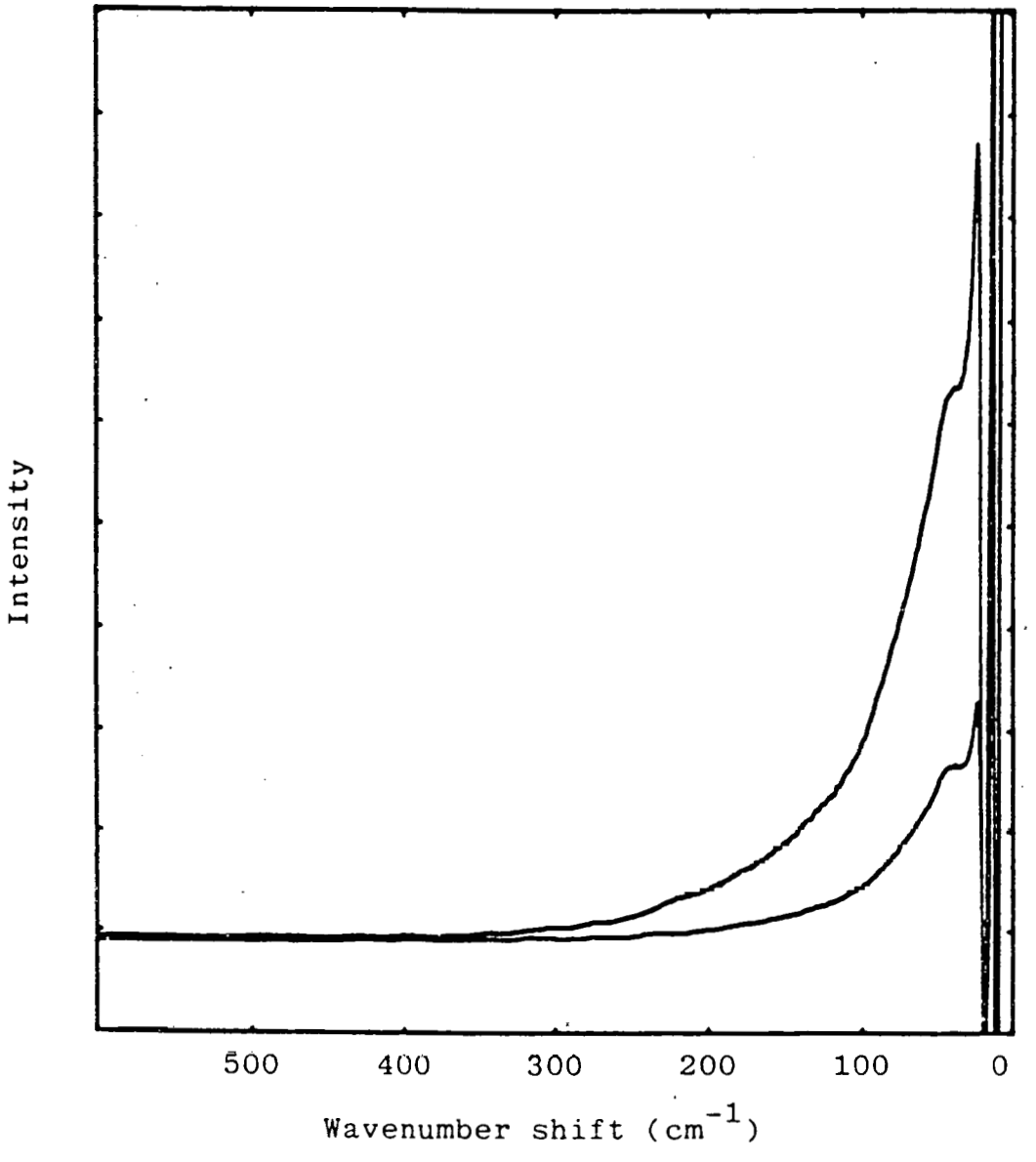

Fig. 4.11 Raman spectra of molten KCl. T=830°C.

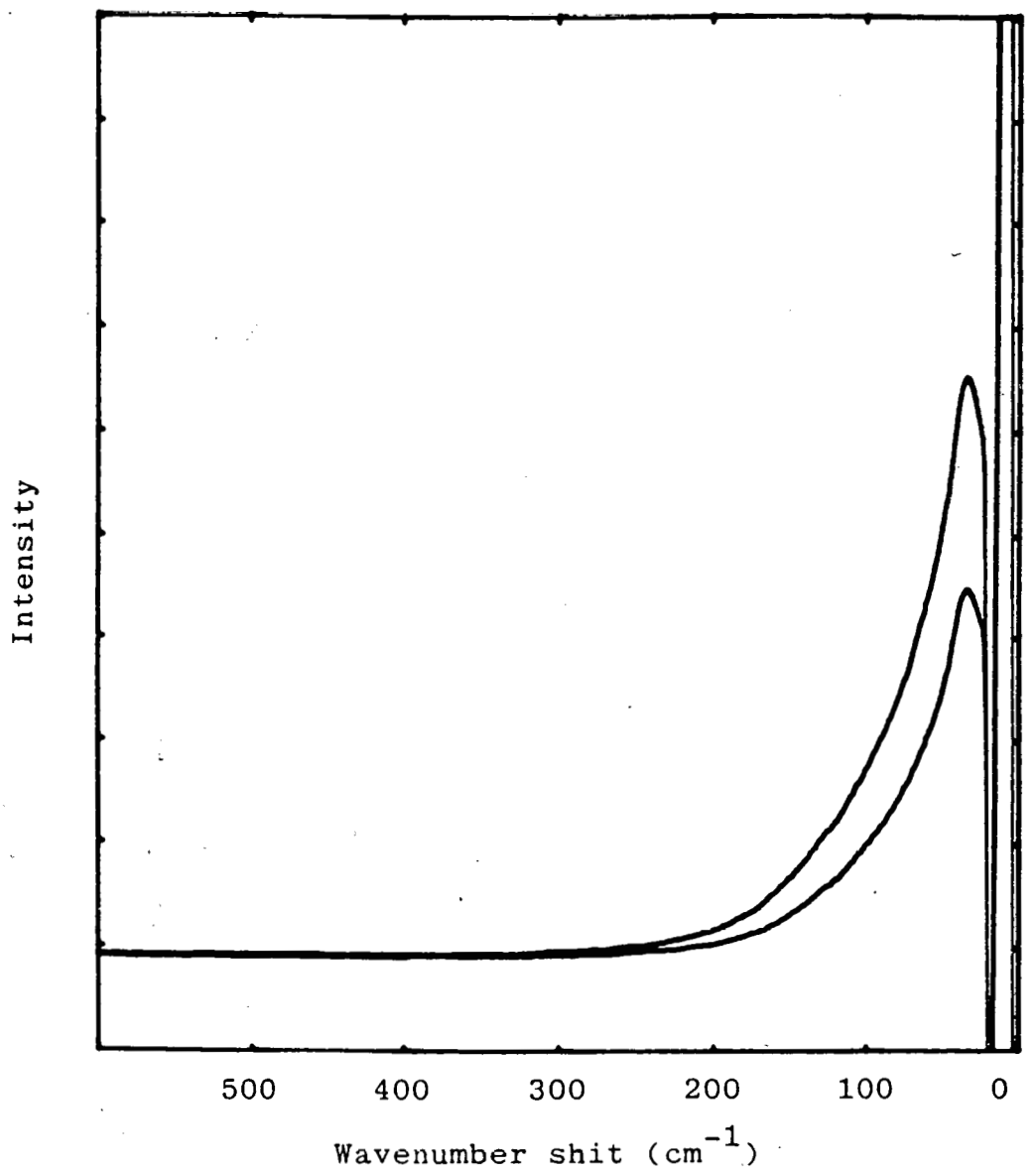

Fig. 4.12 Raman spectra of molten CsCl. T=750°C.

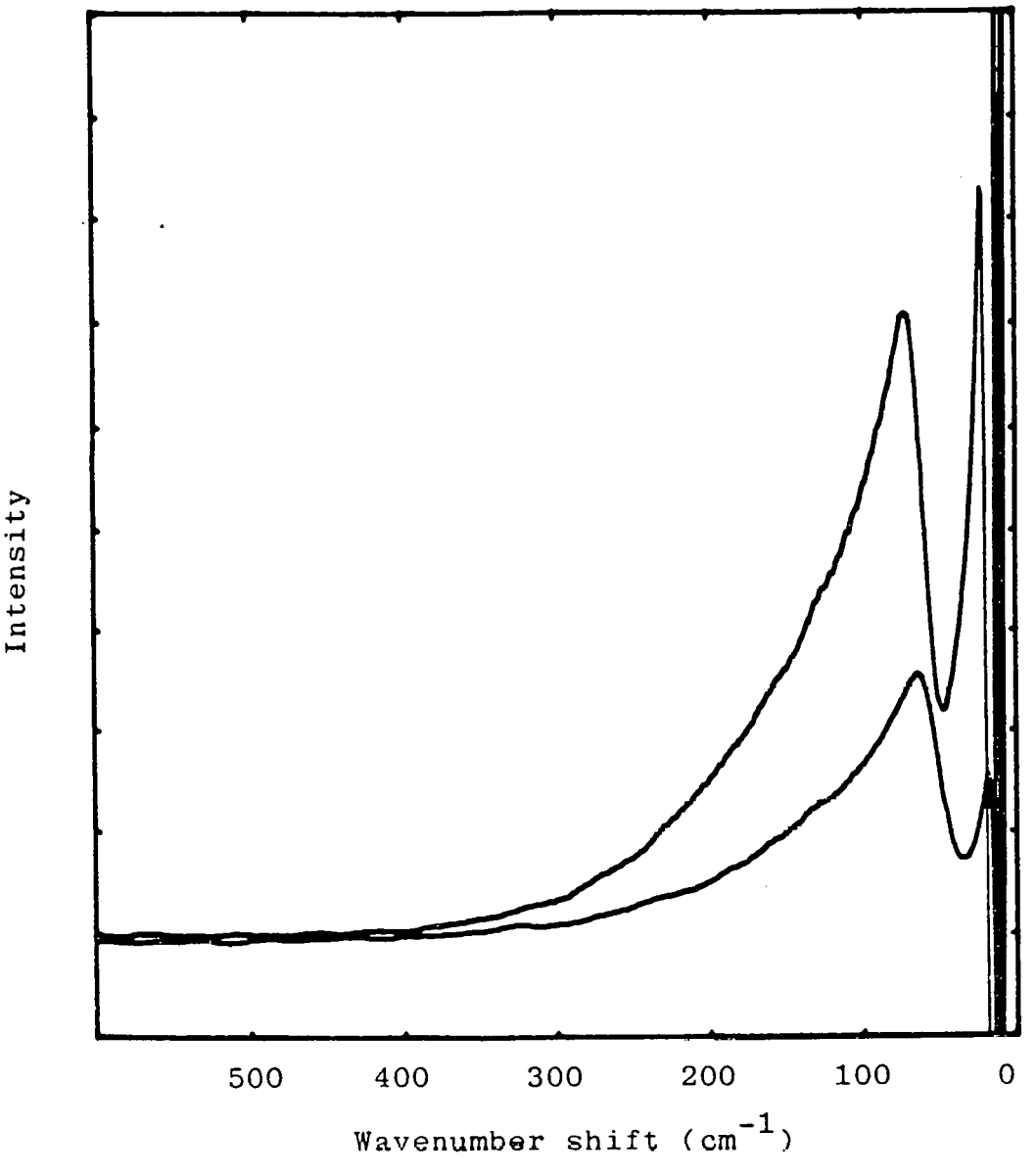

Fig. 4.13 Raman spectra of molten equimolar mixture of NaCl and KCl. T=750°C.

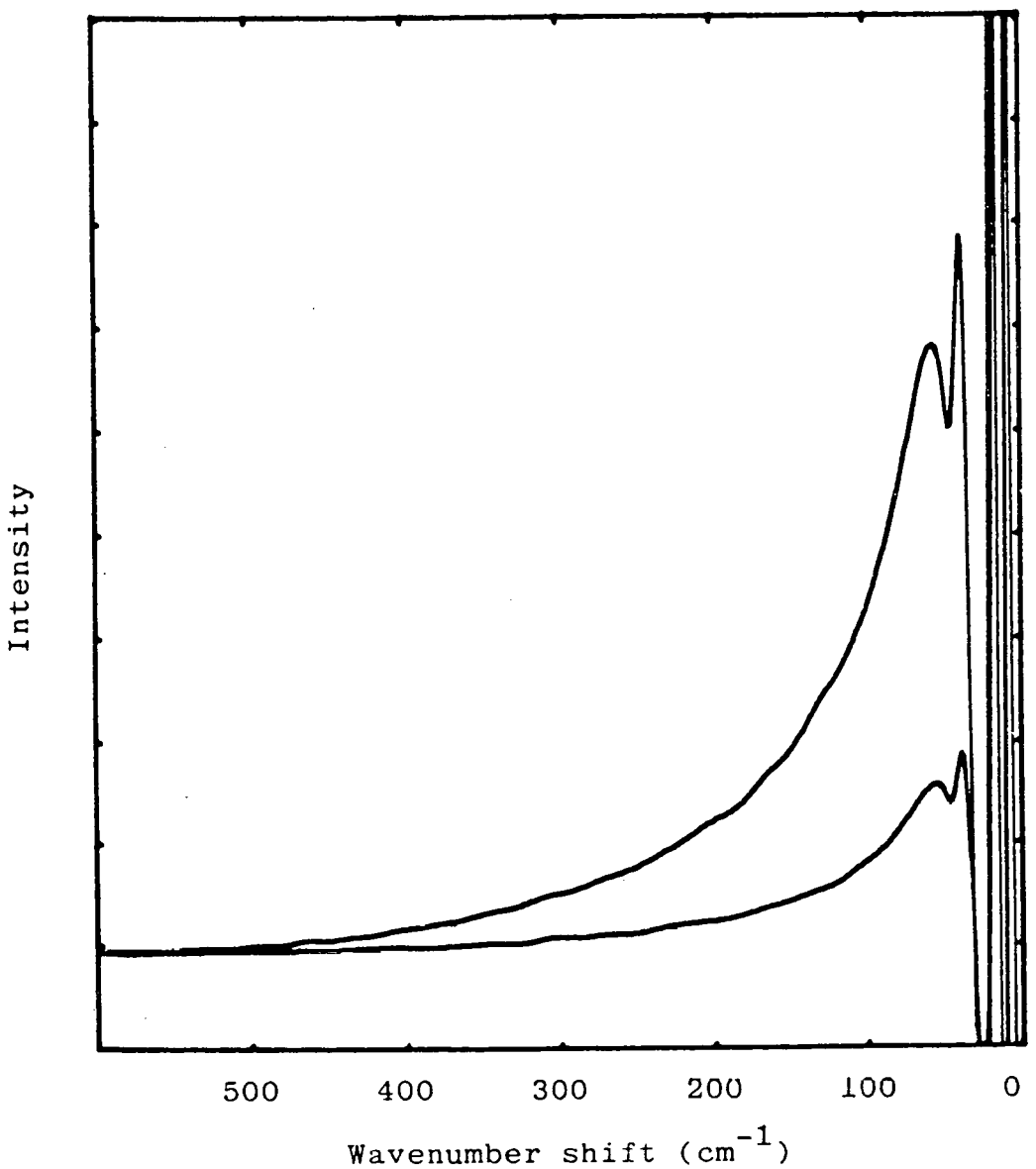

Fig. 4.14 Raman spectra of molten equimolar mixture of LiCl and NaCl. T=750°C.

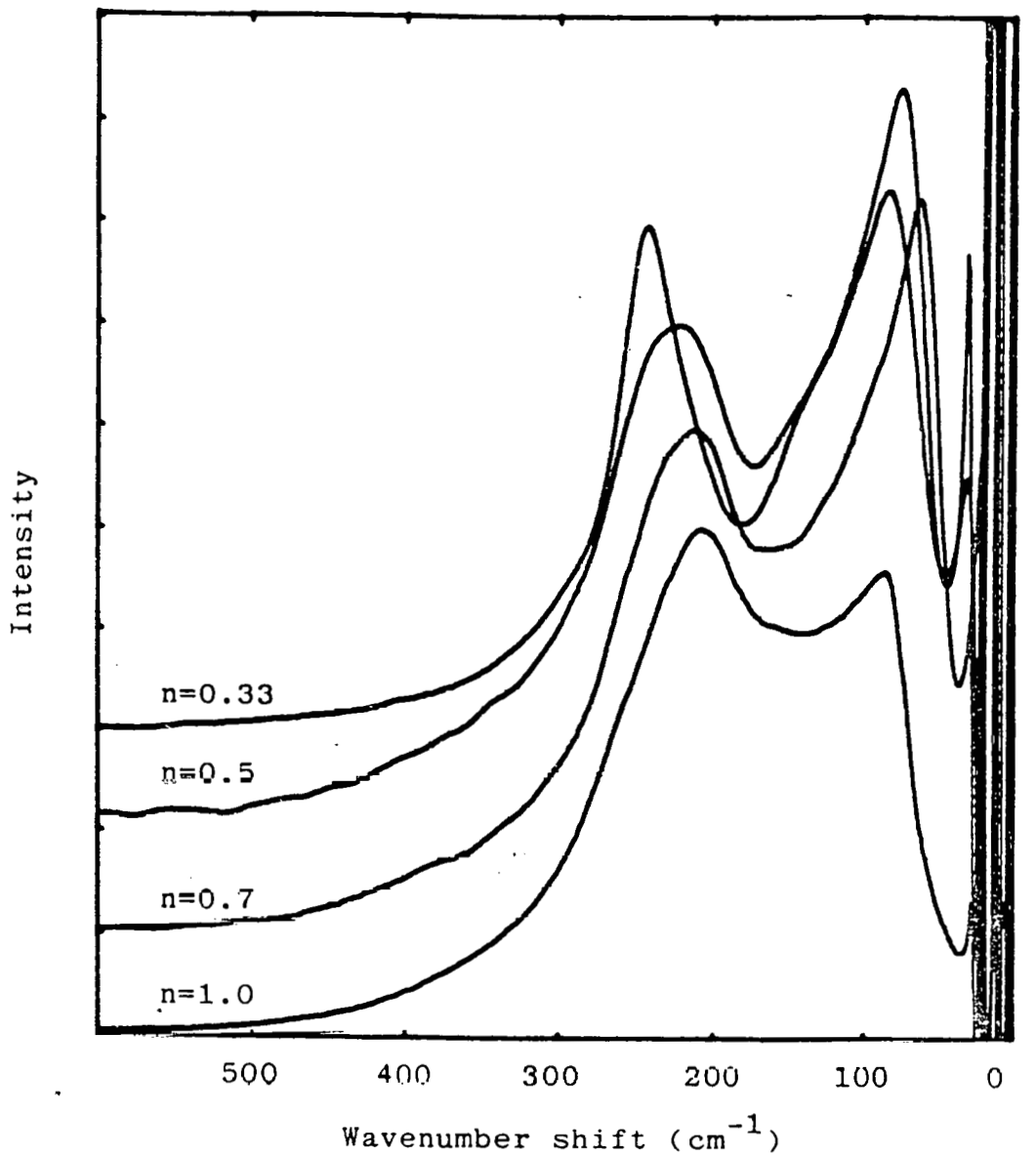

Fig. 4.15 Raman spectra of molten mixture of $nMgCl_2$ + (1-n)CsCl. n= mole fraction of $MgCl_2$. T=800°C.

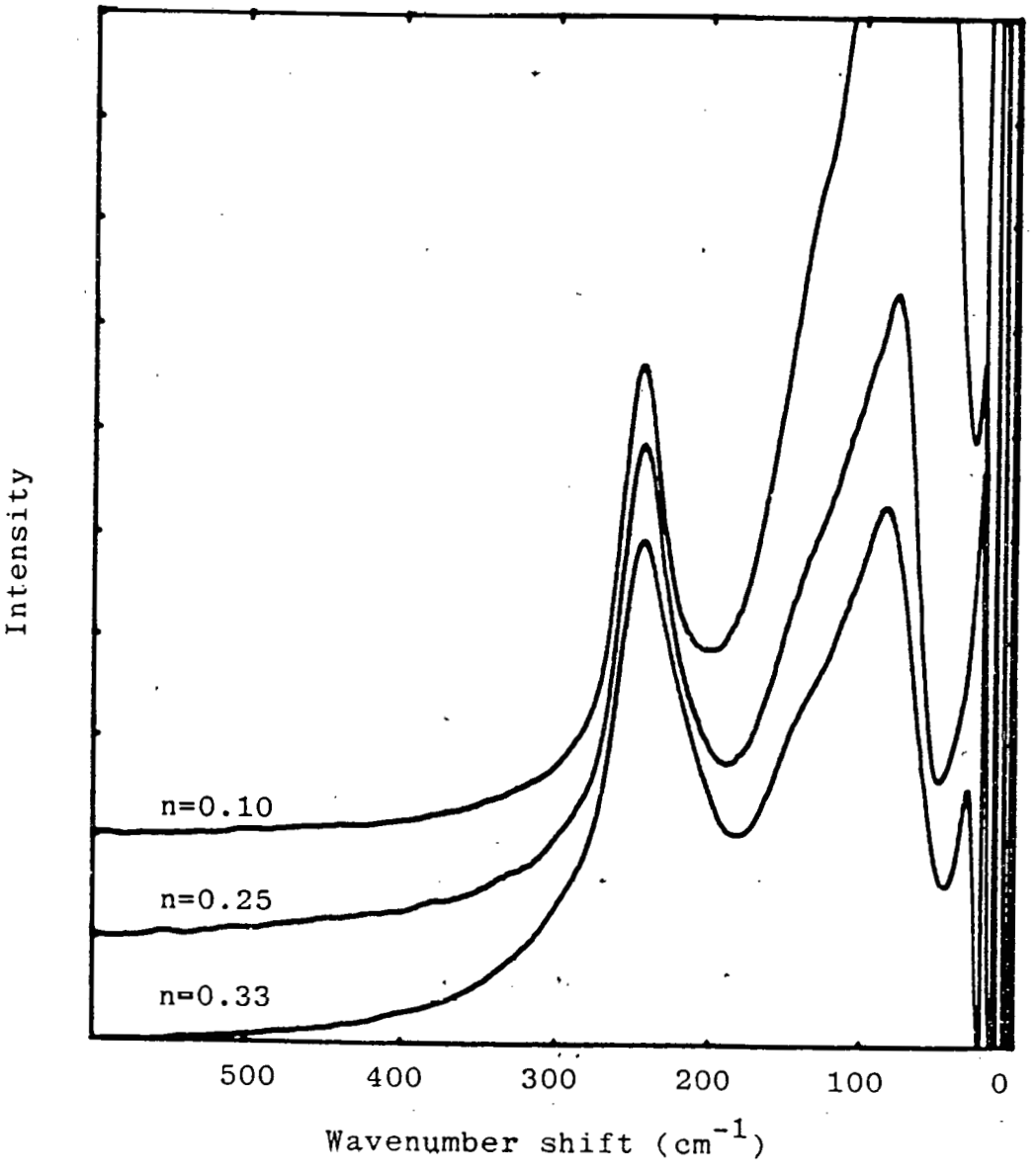

Fig. 4.16 Raman spectra of molten mixtures of $nMgCl_2$ + (1-n)CsCl. n= mole fraction of $MgCl_2$, <0.33. T=800°C.

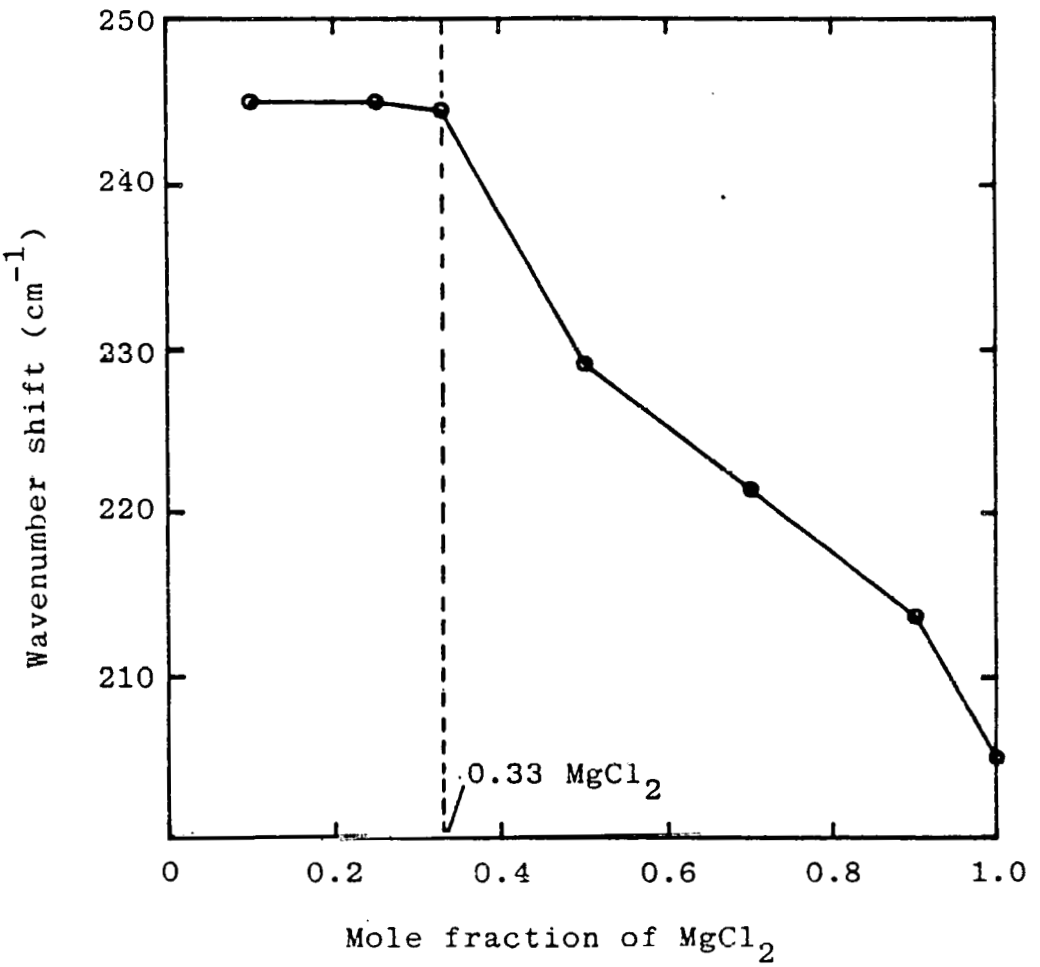

Fig. 4.17 Effect of CsCl concentration on Raman shift in the melt of $MgCl_2$ - CsCl. T=800°C.

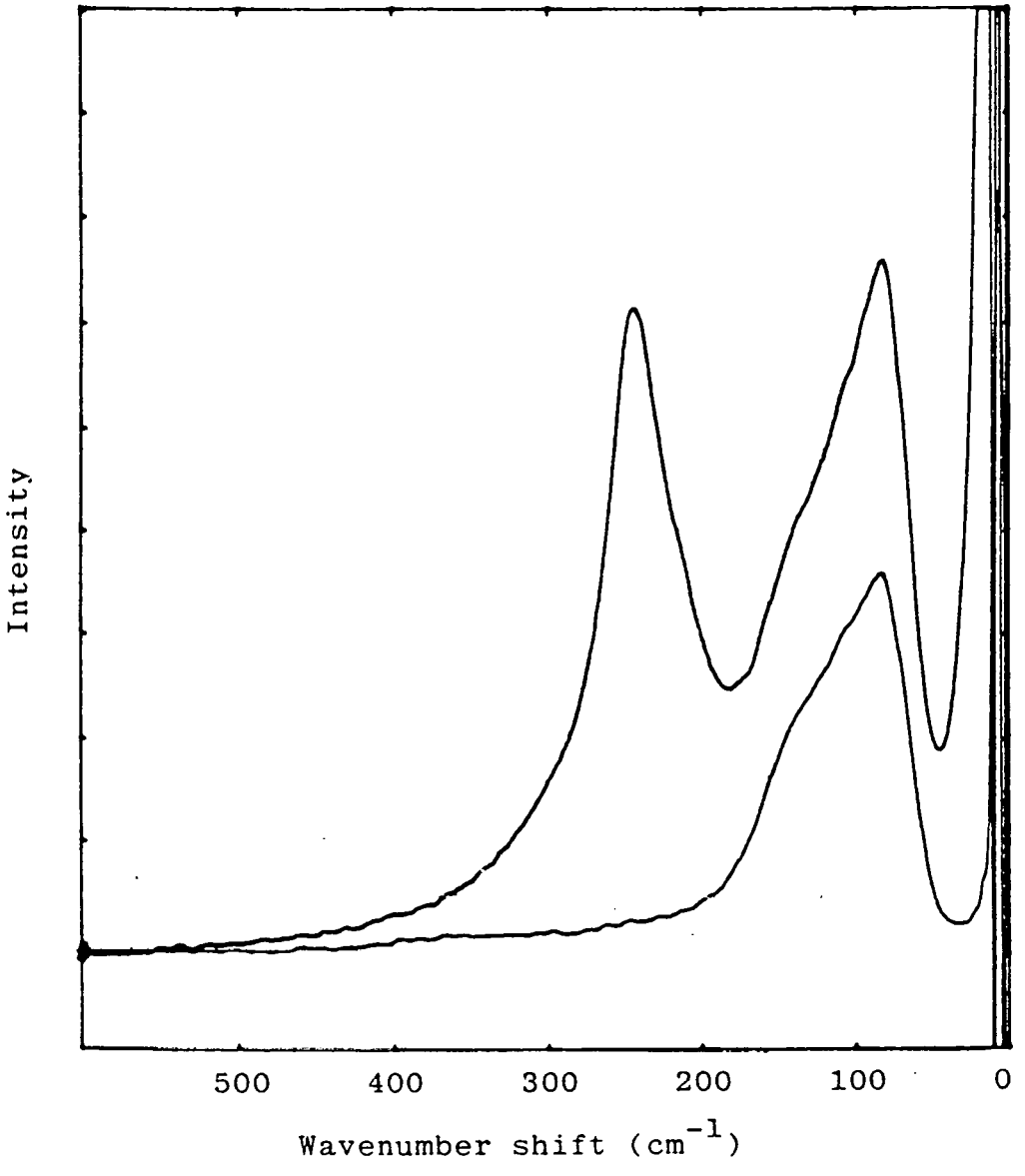

Fig. 4.18 Raman spectra of 33 mol.% $MgCl_2$ + 67 mol.% CsCl. T=750°C

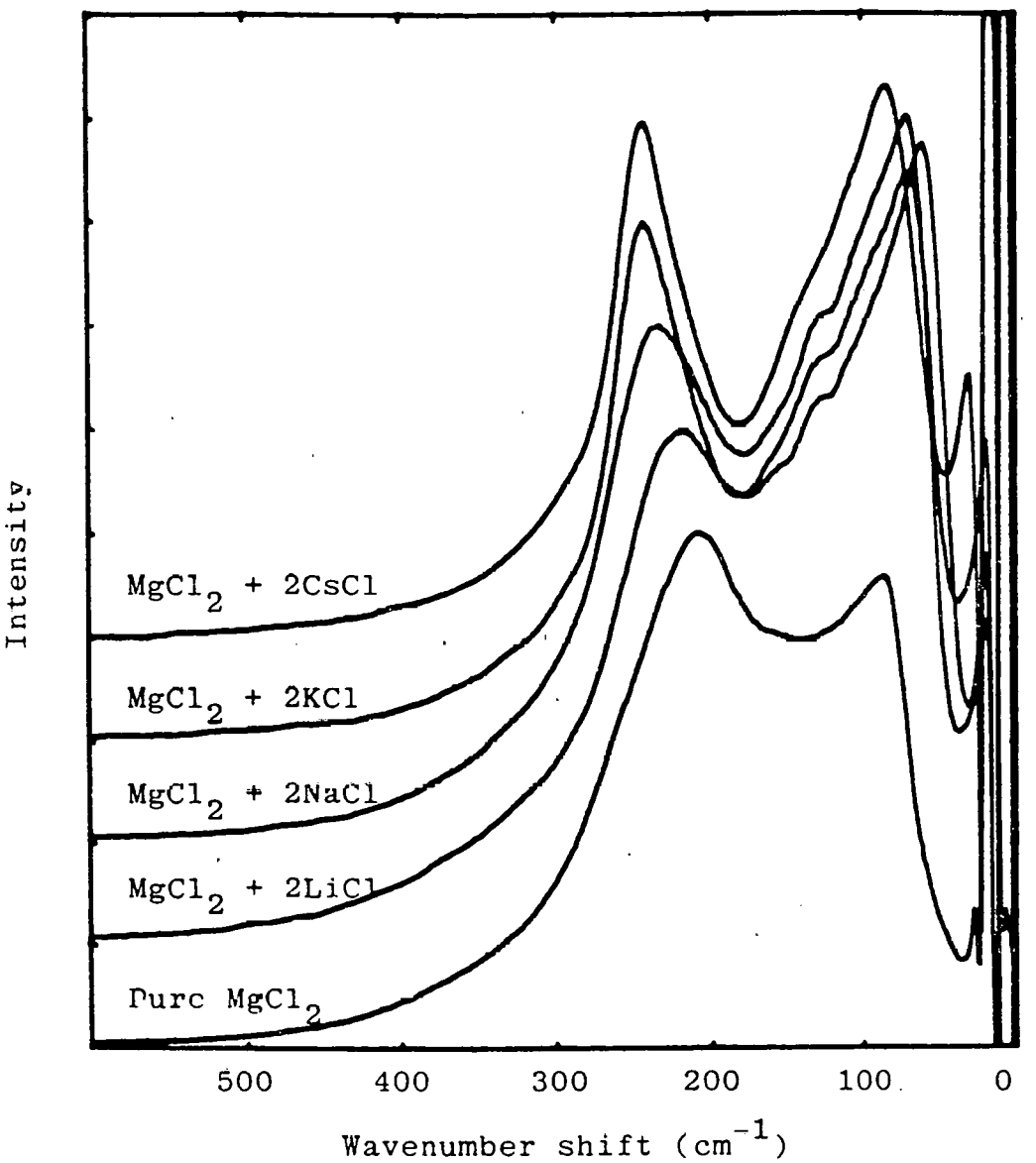

Fig. 4.19 Raman spectra of molten mixtures of $MgCl_2$ + 2ACl. T=750°C. (A= Cs, K, Na, Li)

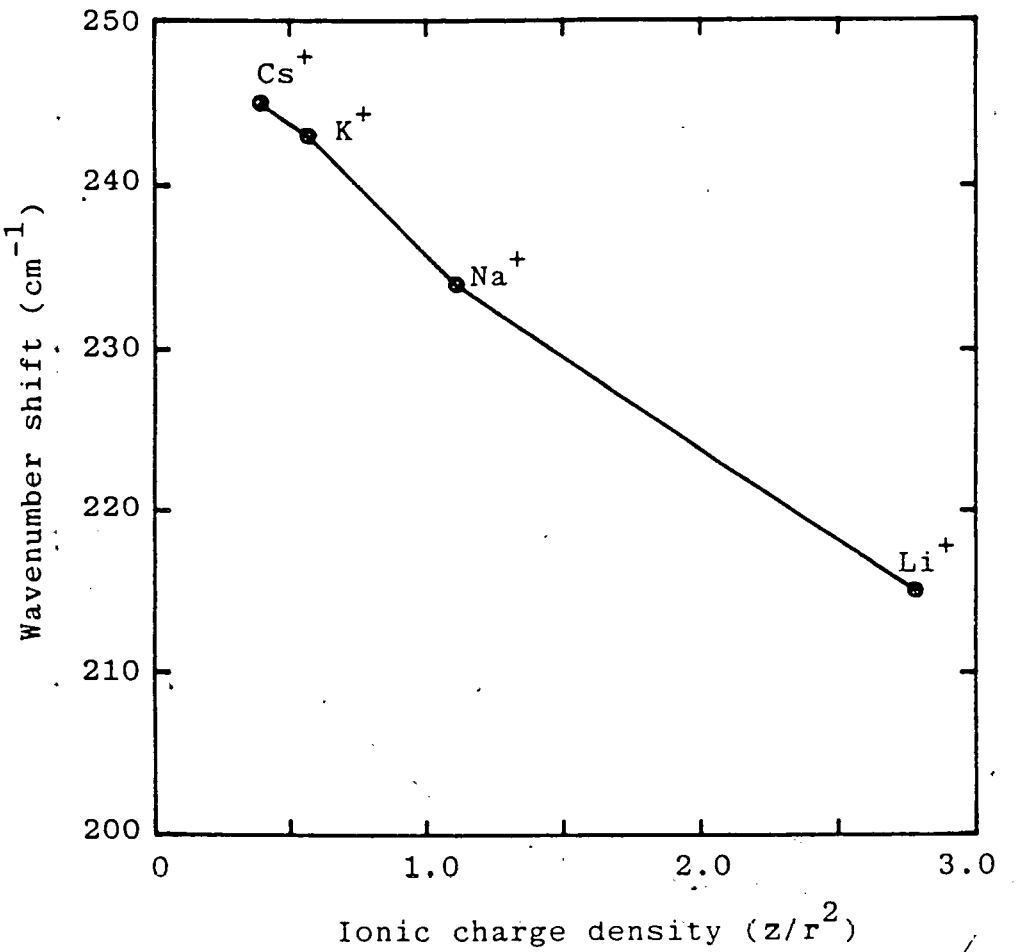

Fig.4.20 Effect of ionic charge density of alkali cation on Raman shift in the molten mixtures of $MgCl_2$ + 2ACl. T=750°C.

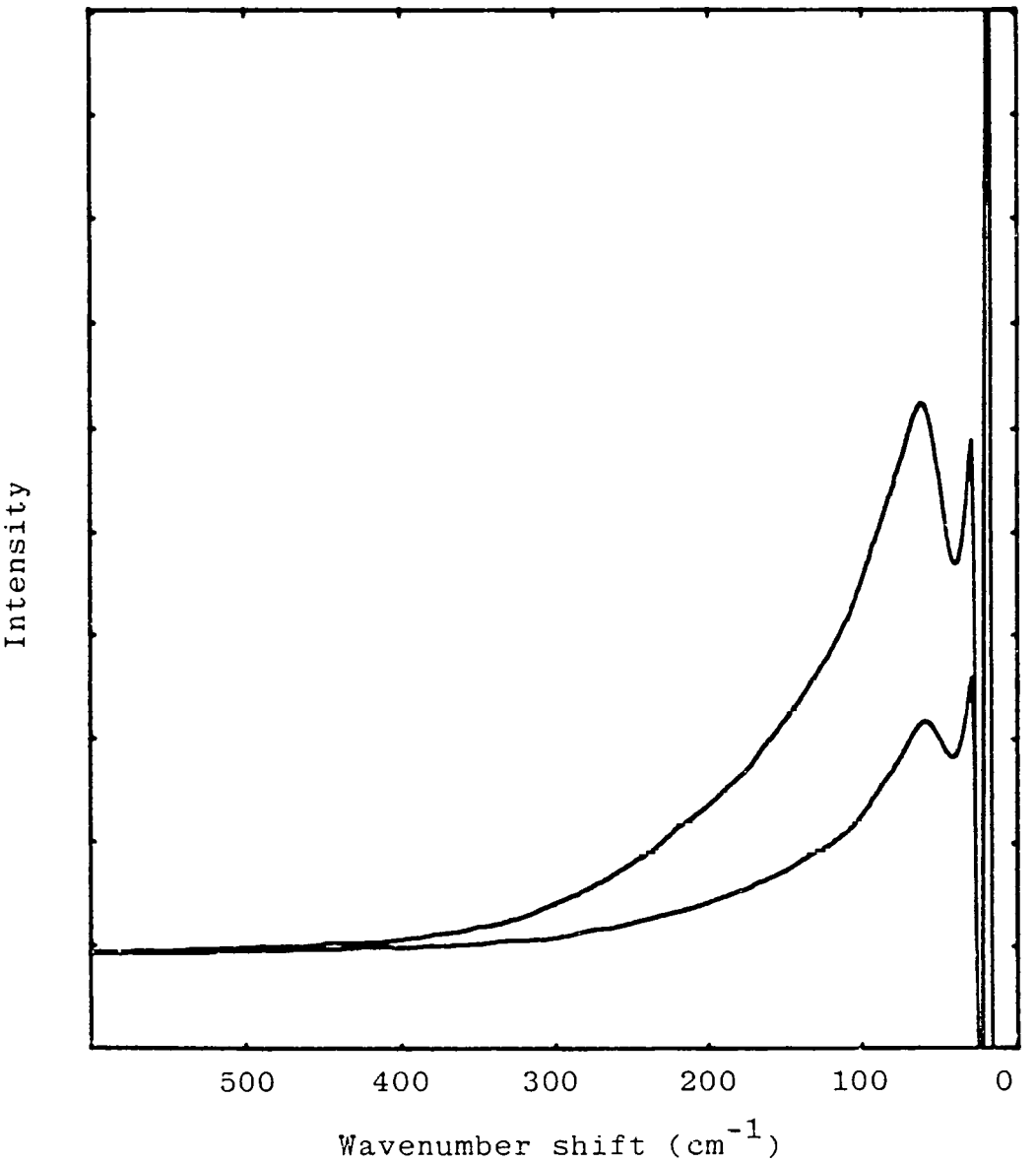

Fig. 4.21 Raman spectra of the supporting solvent melt for magnesium electrolysis. The weight ratio of $CaCl_2$, KCl, and NaCl is 6:18:65. T=770°C.

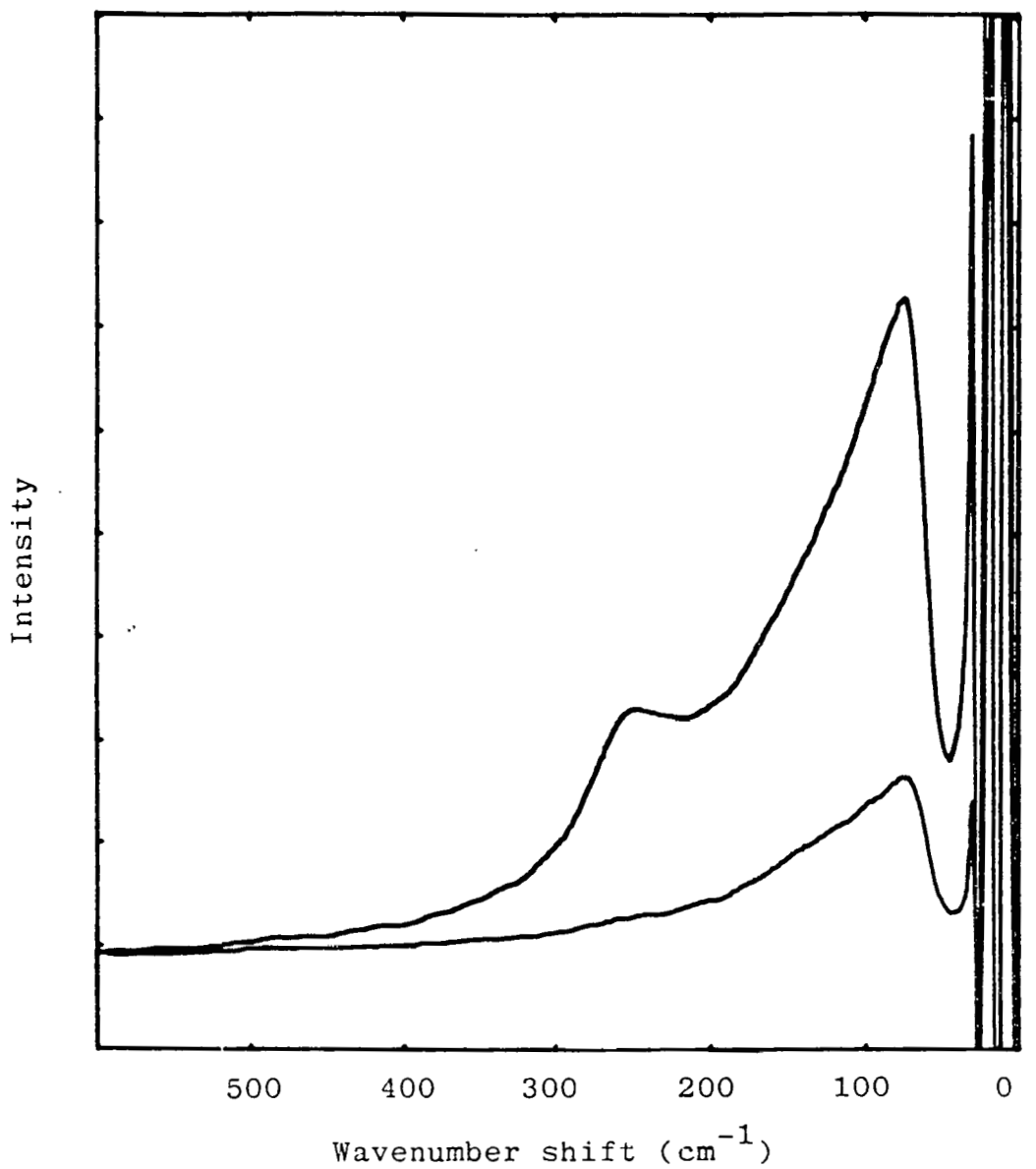

Fig. 4.22 Raman spectra of 11 wt.% $MgCl_2$ - 6 wt.% $CaCl_2$ - 18 wt.% KCl - 65 wt.% NaCl. T=760°C.

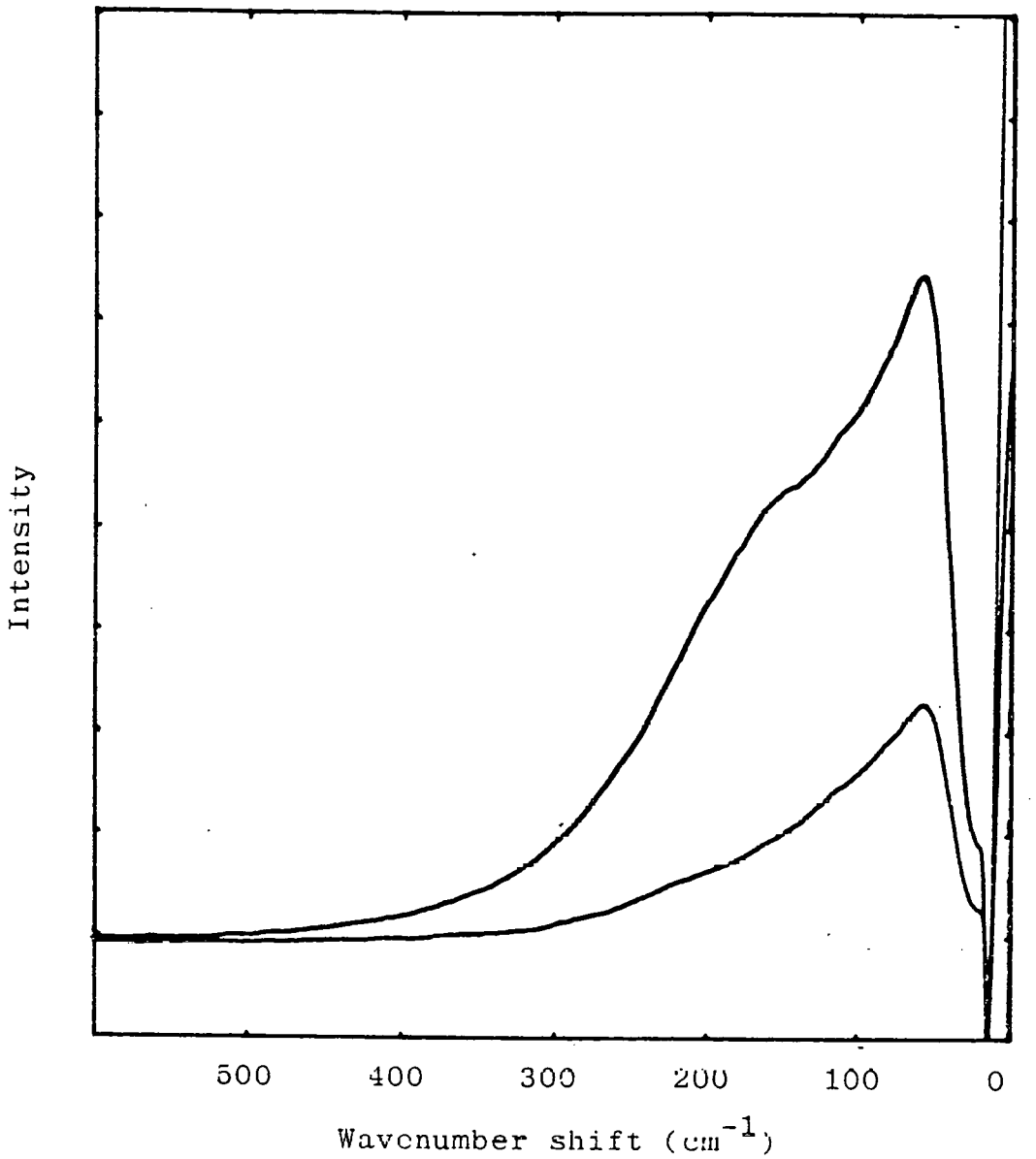

Fig. 4.23 Raman spectra of molten $CaCl_2$. T=800°C.

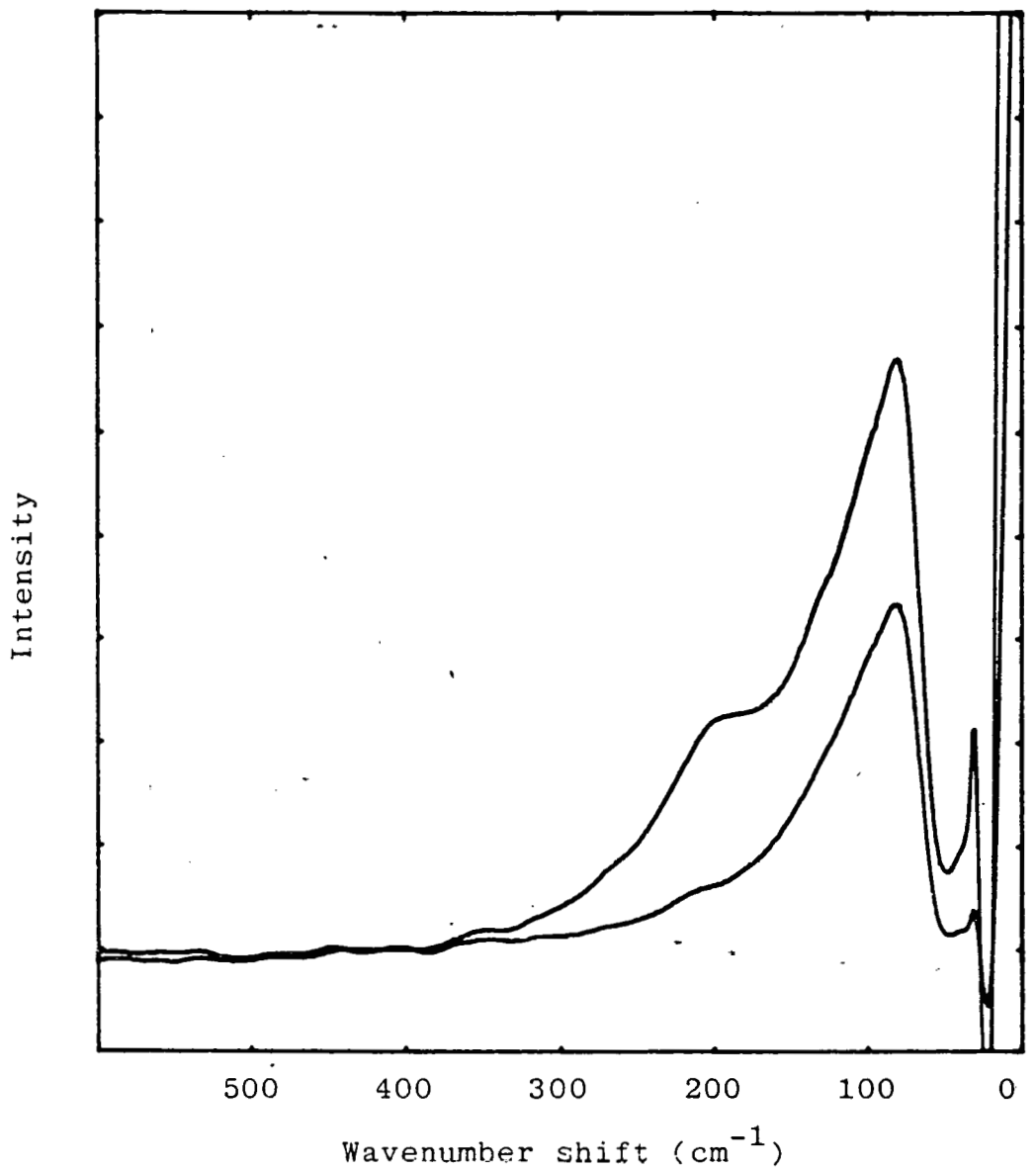

Fig. 4.24 Raman spectra of 33 mol.% $CaCl_2$ + 67 mol.% CsCl. T=840°C.

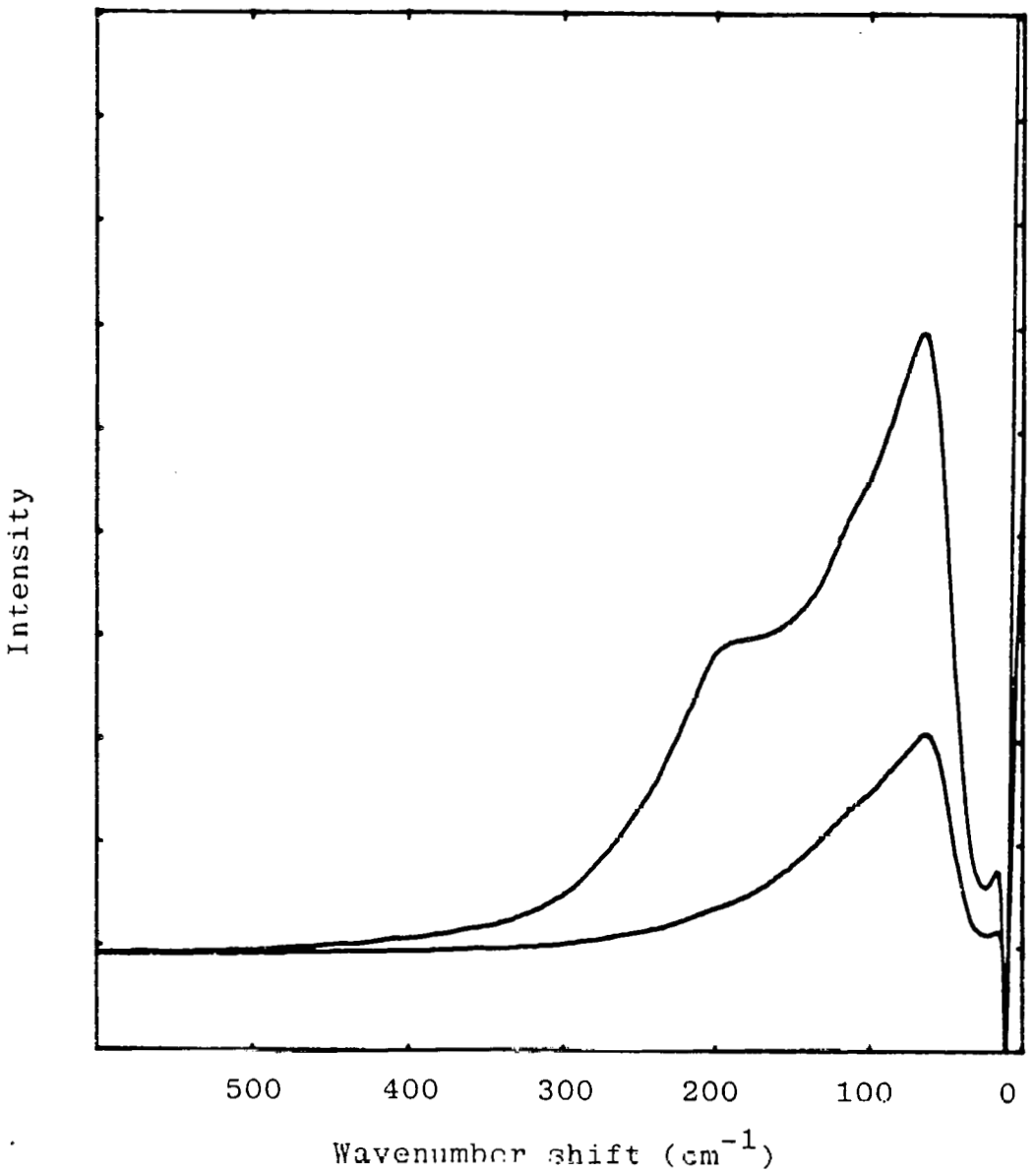

Fig. 4.25 Raman spectra of 33 mol.% $CaCl_2$ + 67 mol.% KCl. T=670°C.

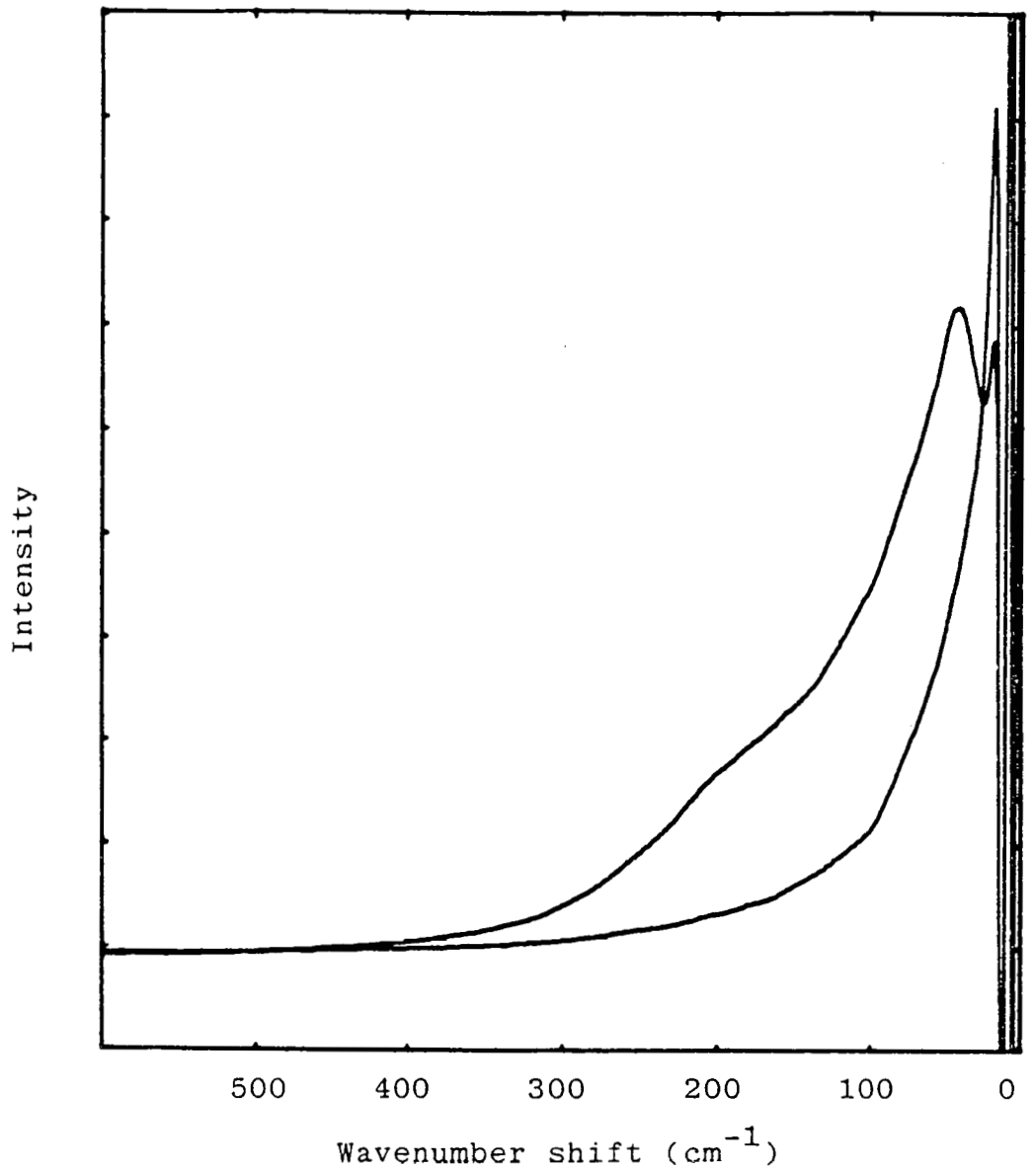

Fig. 4.26 Raman spectra of 33 mol.% $CaCl_2$ + 67 mol.% NaCl. T=670°C.

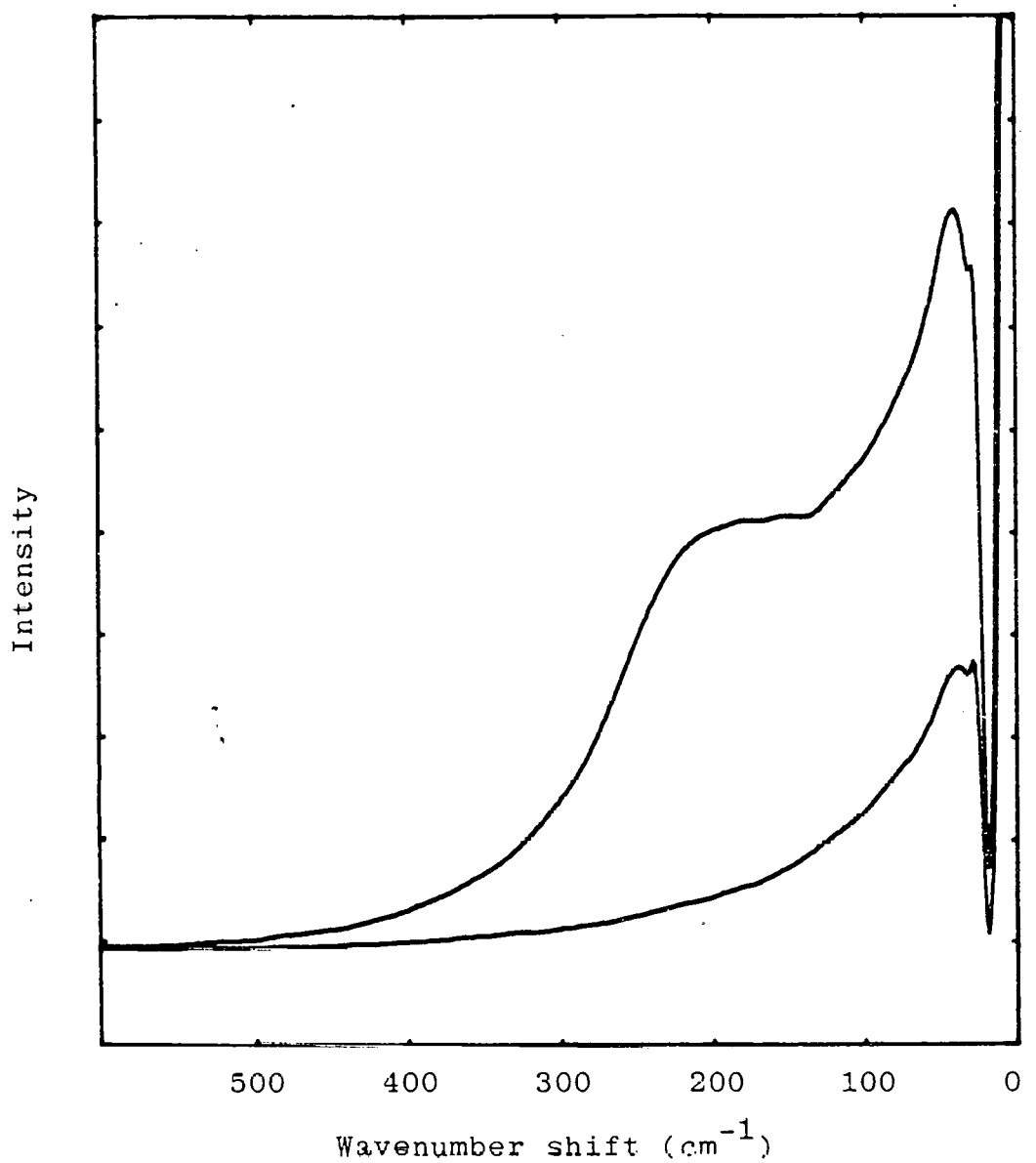

Fig. 4.27 Raman spectra of equimolar molten mixture of $MgCl_2$ + $CaCl_2$. T=720°C.

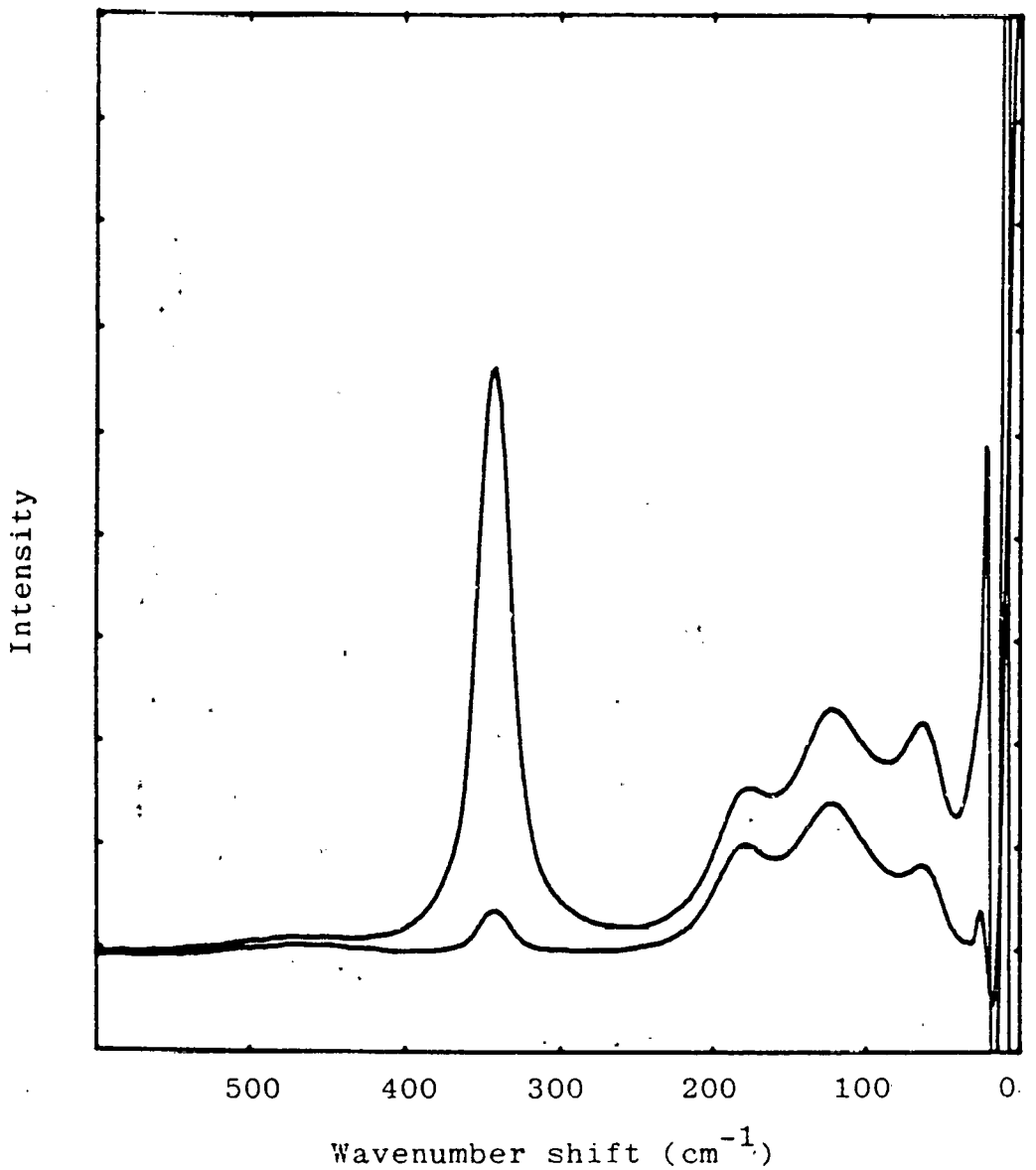

Fig. 4.28 Raman spectra of 25 mol.% $AlCl_3$ + 75 mol.% KCl. T=800°C.

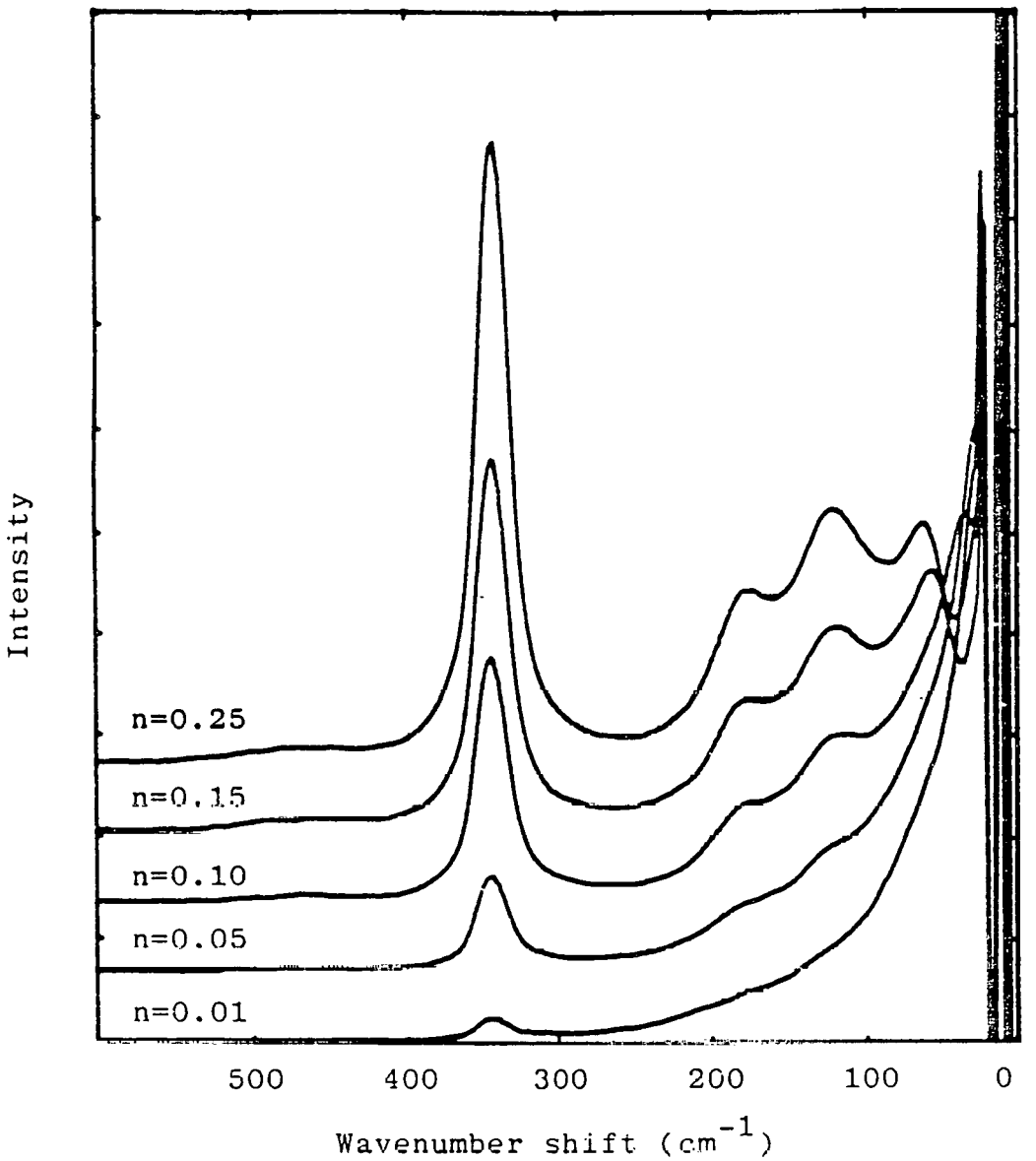

Fig. 4.29 Raman spectra of $nAlCl_3$ + (1-n)KCl.
(n= mole fraction of $AlCl_3$ in the melt)

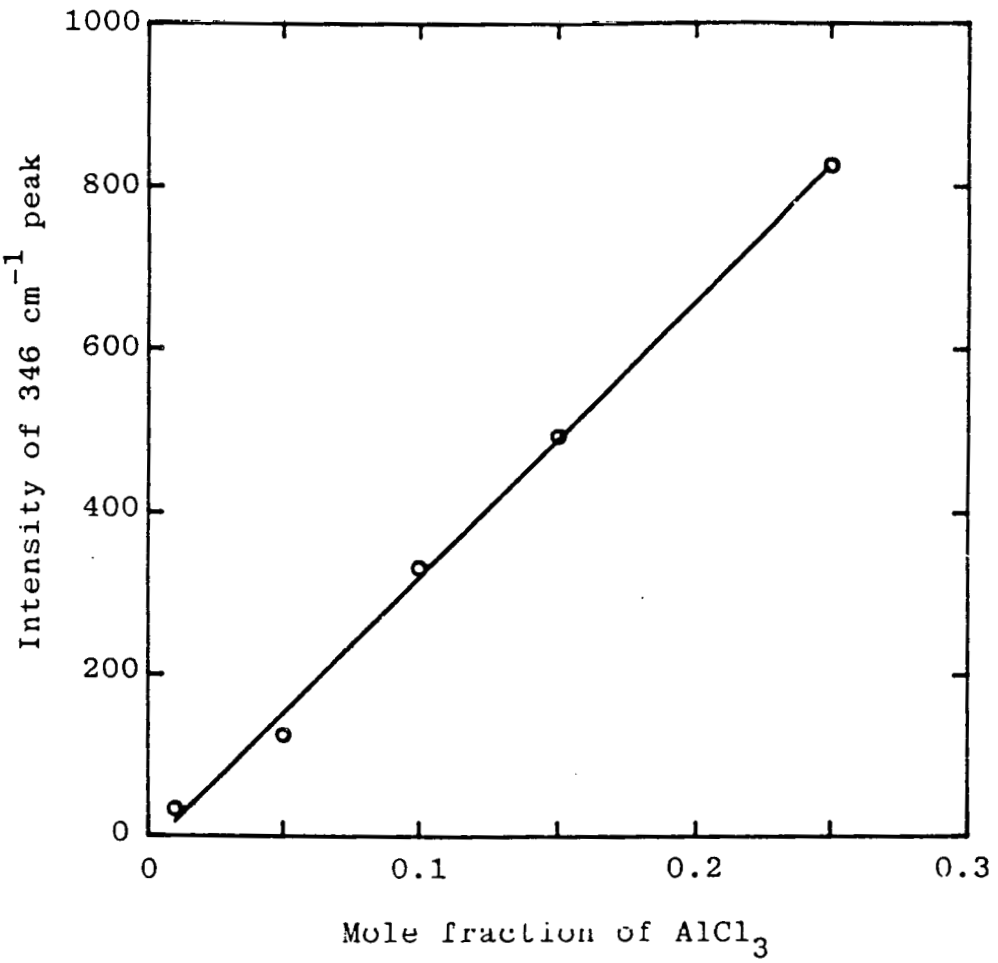

Fig. 4.30 A plot of peak intensity vs mole fraction of $AlCl_3$ in KCl melt. The peak intensity was normalized and measured from base line.

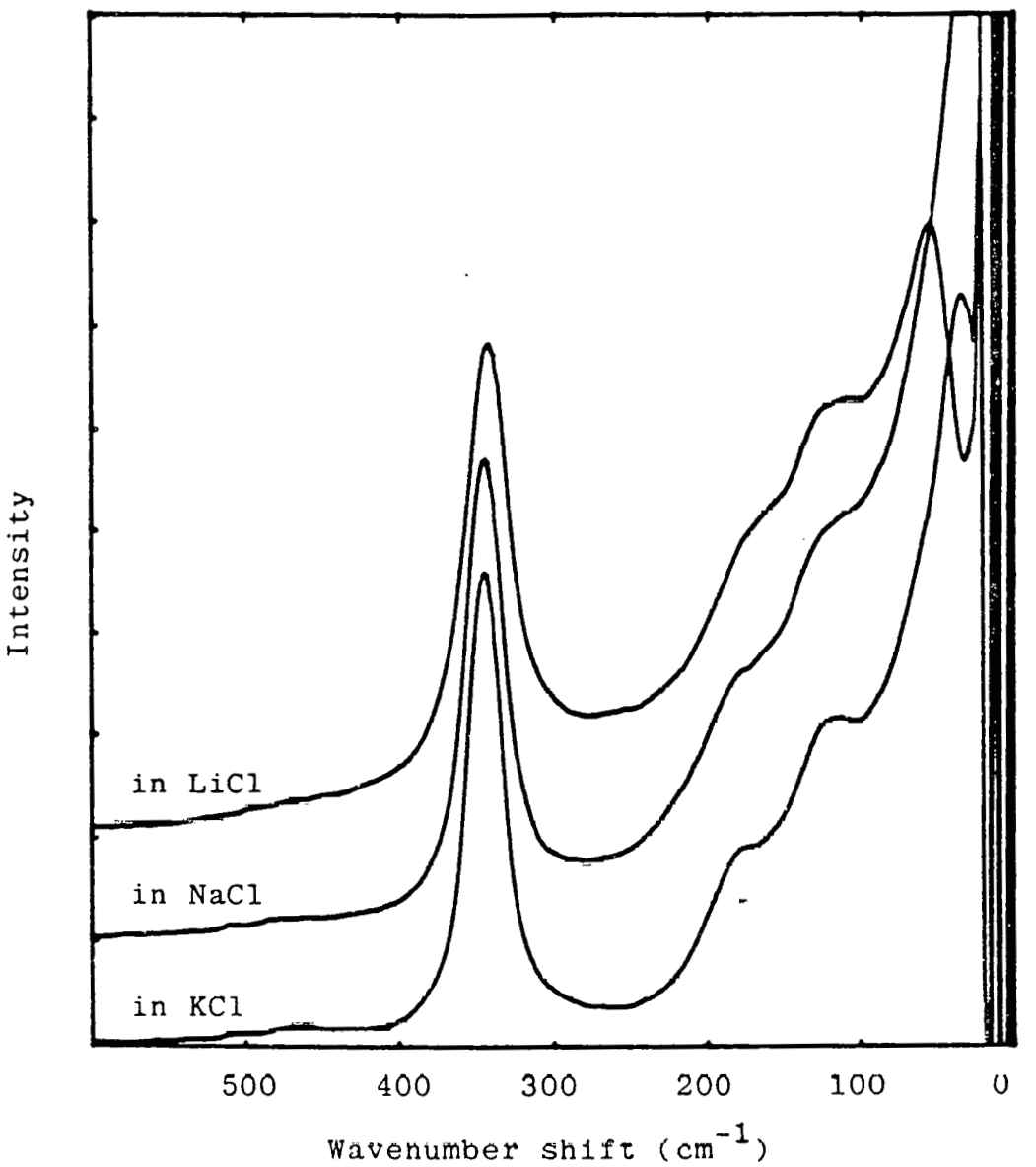

Fig. 4.31 Raman spectra of 10 mol.% $AlCl_3$ in different alkali chloride melts. T=800°C.

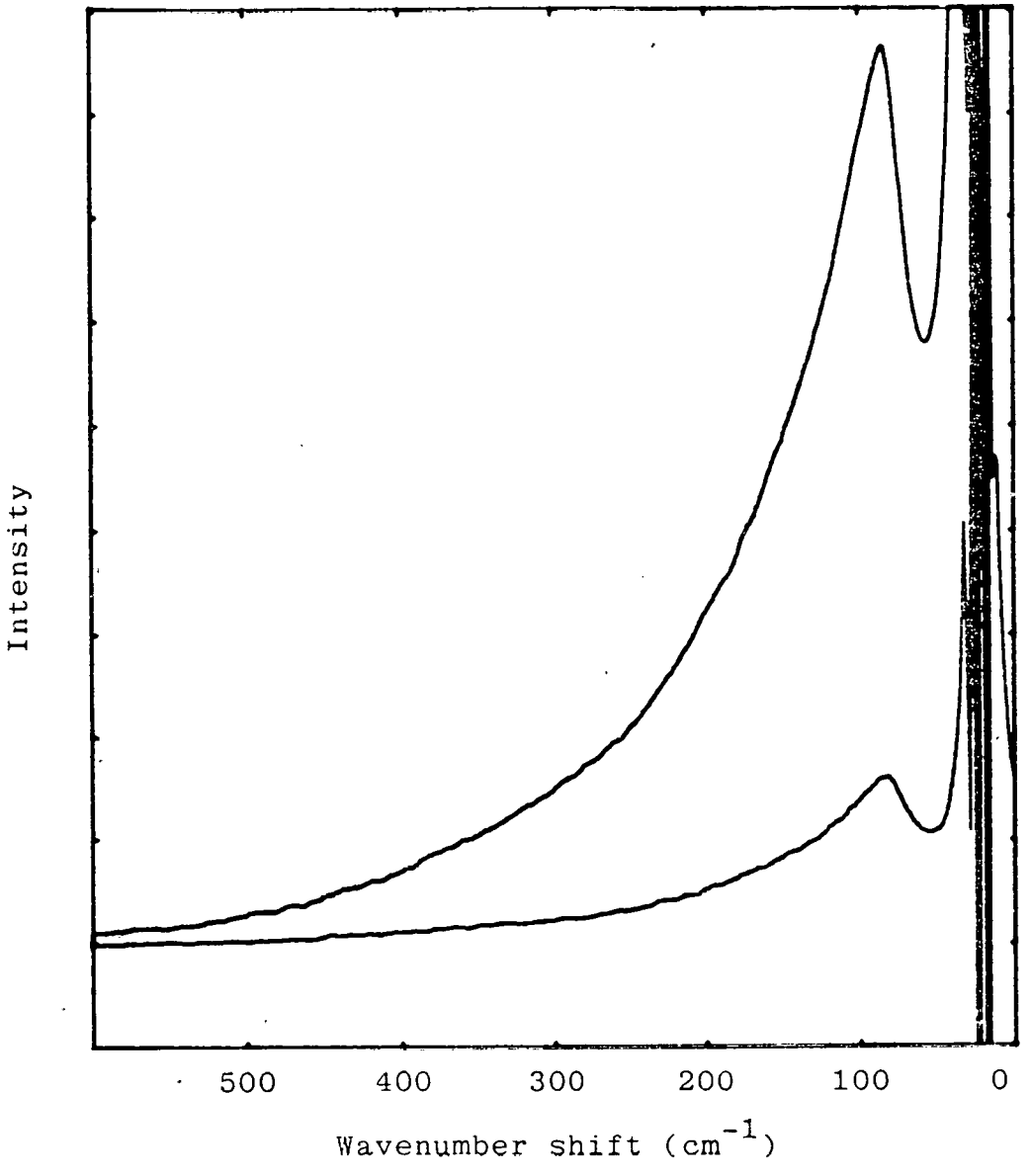

Fig. 4.32 Raman spectra of 45 wt.% LiCl + 55 wt.% NaCl. T=700°C.

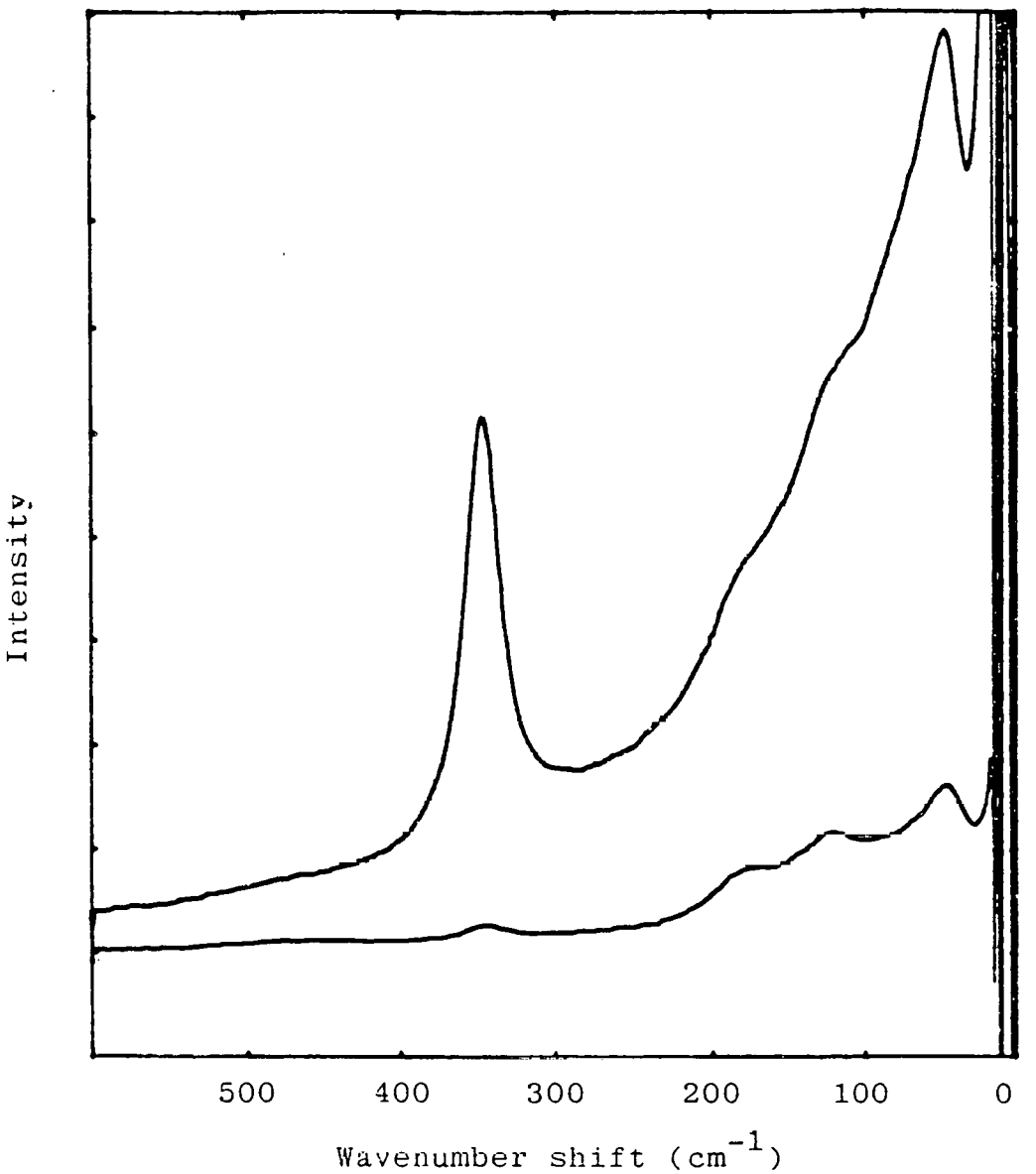

Fig. 4.33 Raman spectra of 10 wt.% $AlCl_3$ + 40 wt.% LiCl + 50 wt.% NaCl. T=610°C.

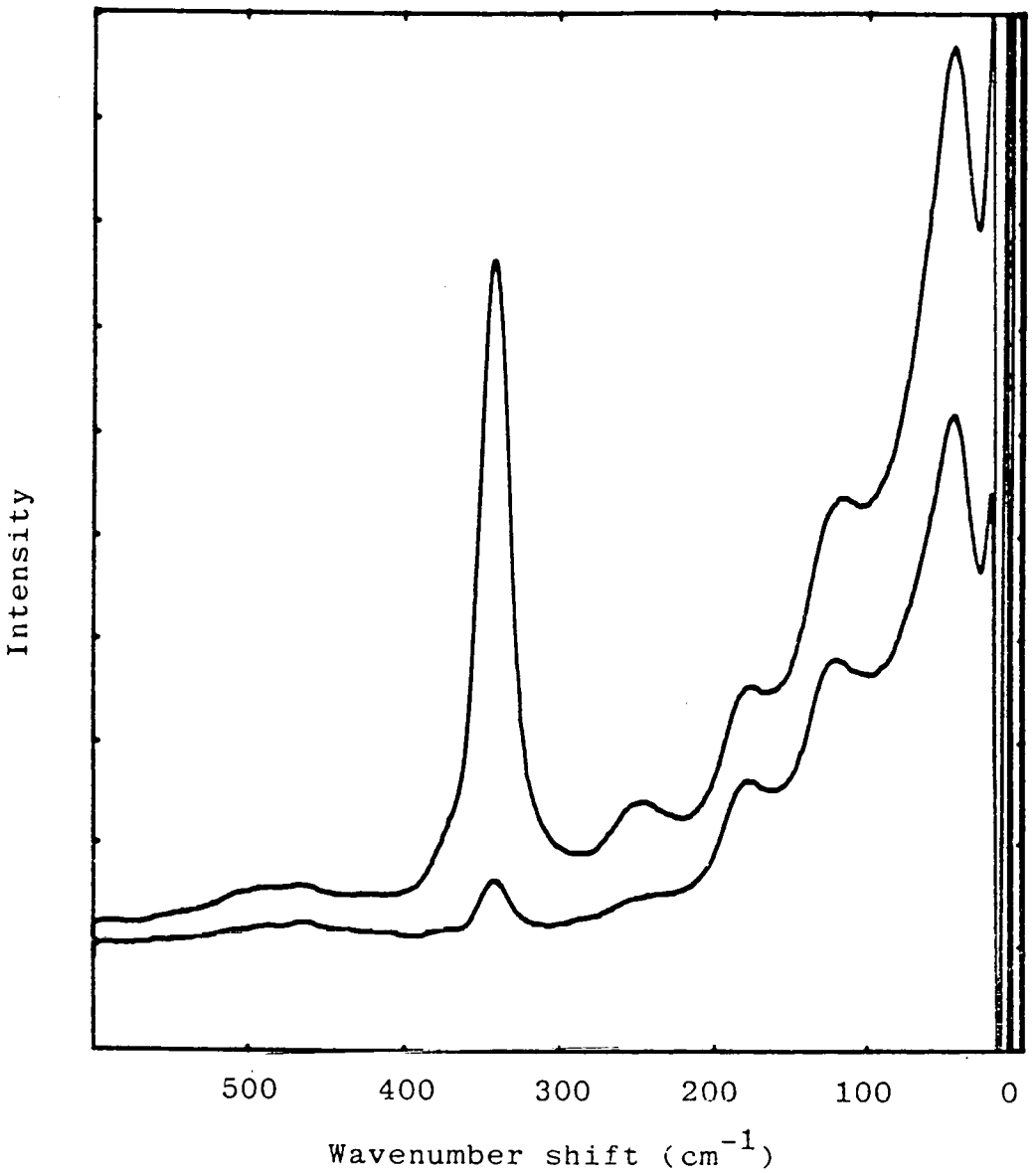

Fig. 4.34 Raman spectra of 10 mol.% $AlCl_3$ in CsCl melt. T=700°C.

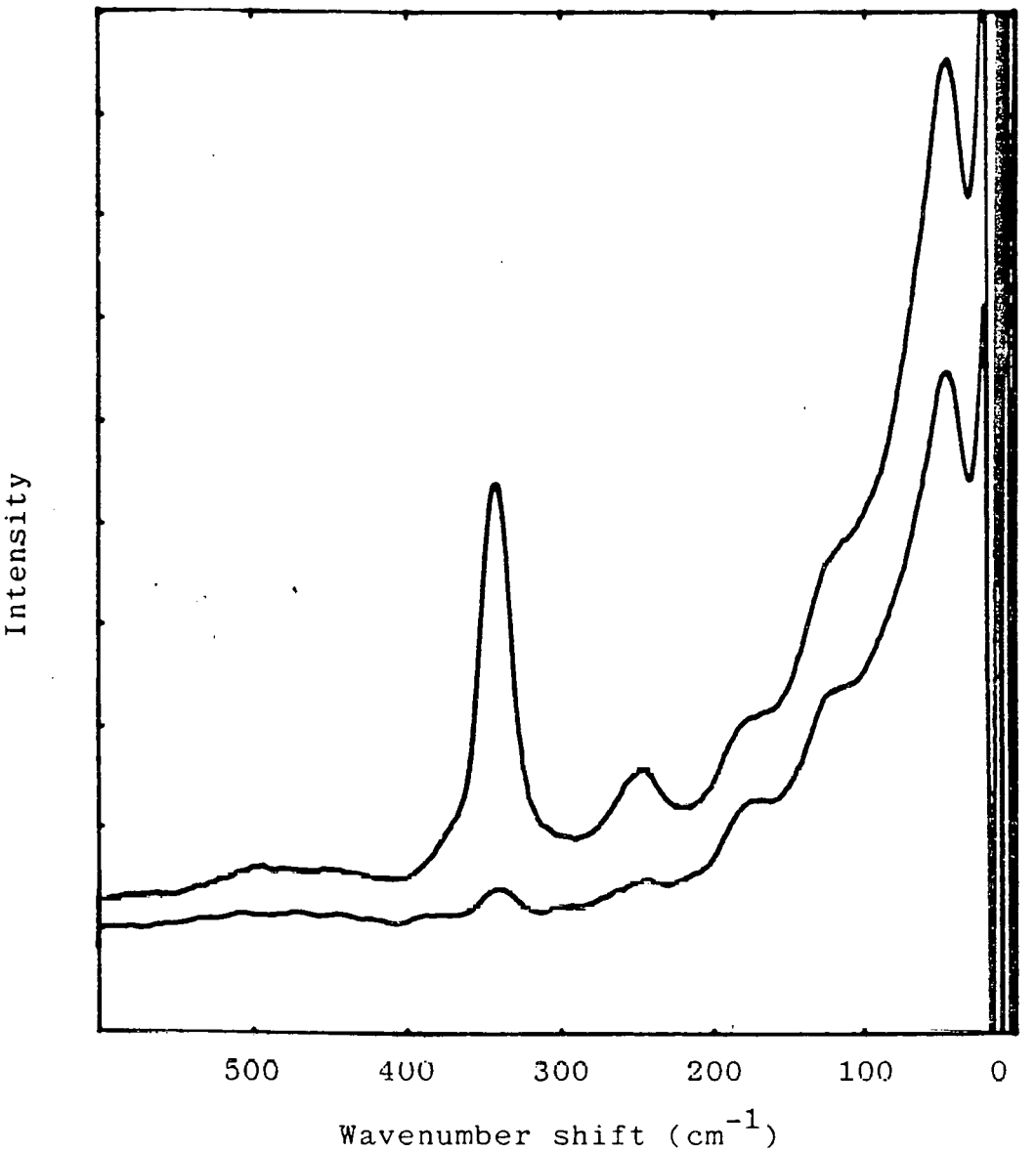

Fig. 4.35 (a) Raman spectra of 5 mol.% $AlCl_3$ + 95 mol.% CsCl. T=700°C.

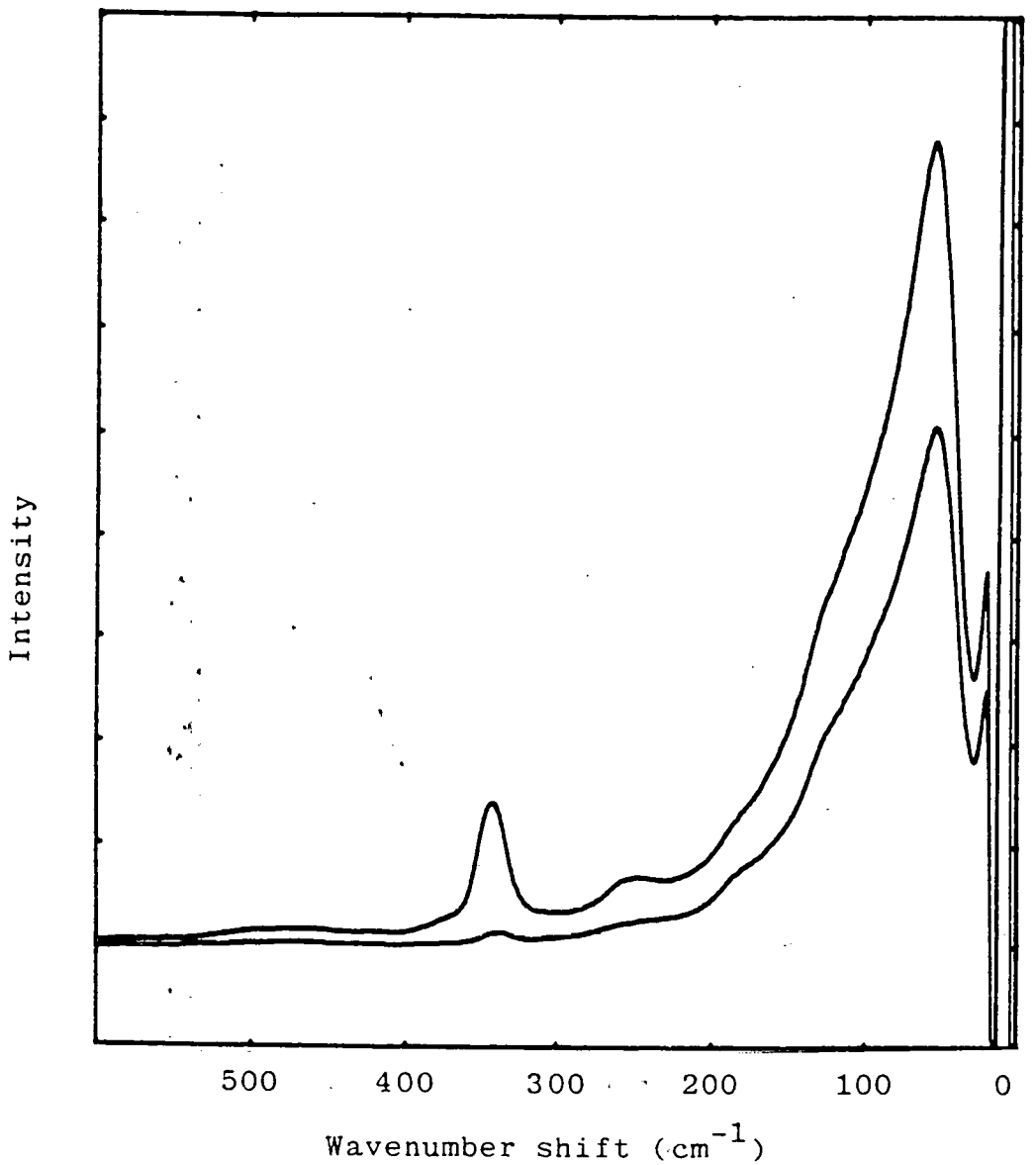

Fig. 4.35 (b) Raman spectra of .1 mol.% $AlCl_3$ + 99 mol.% CsCl. T=700°C.

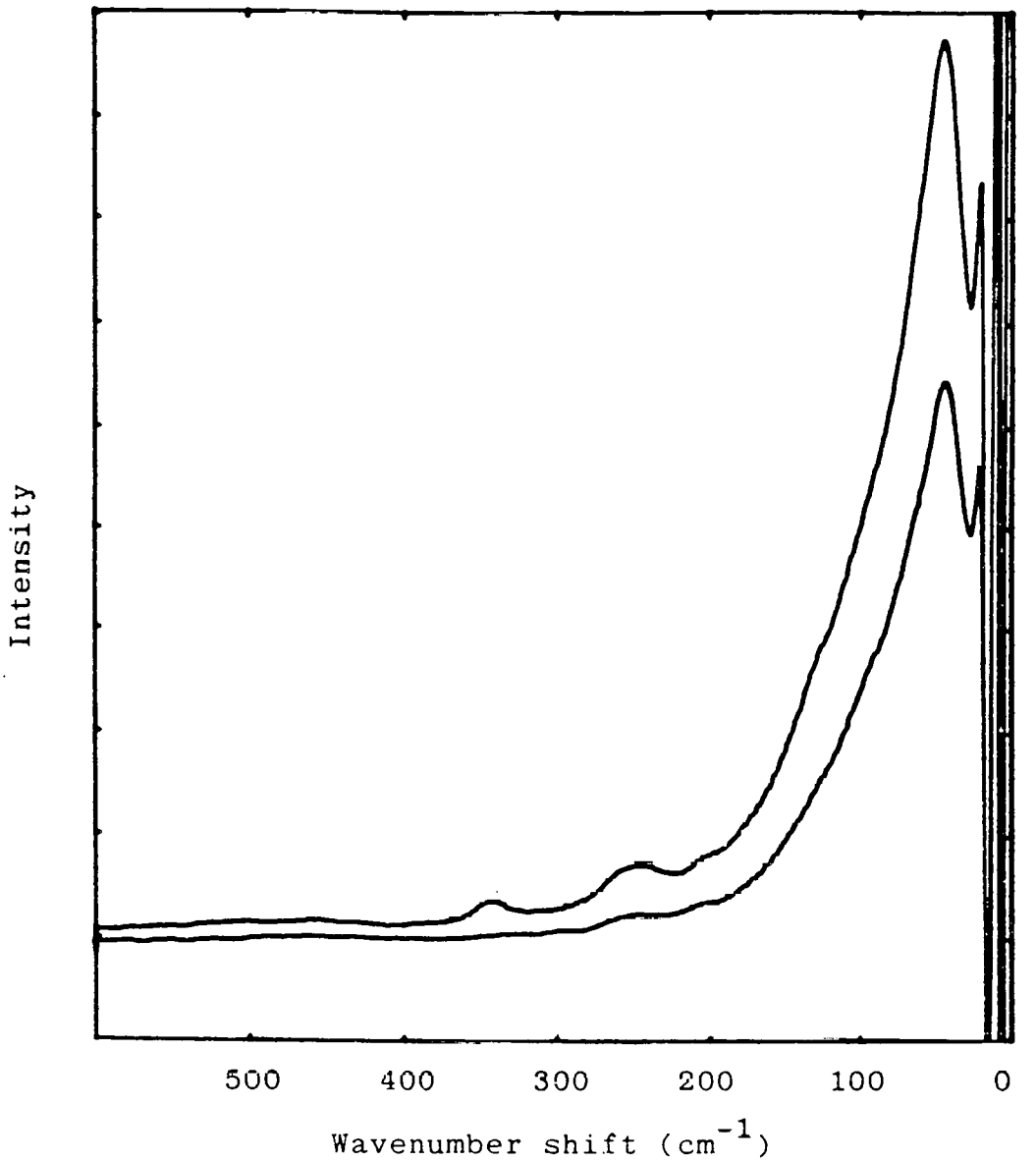

Fig. 4.35 (c) Raman spectra of 0.5 mol.% $AlCl_3$ + 99.5 mol.% CsCl. T=700°C.

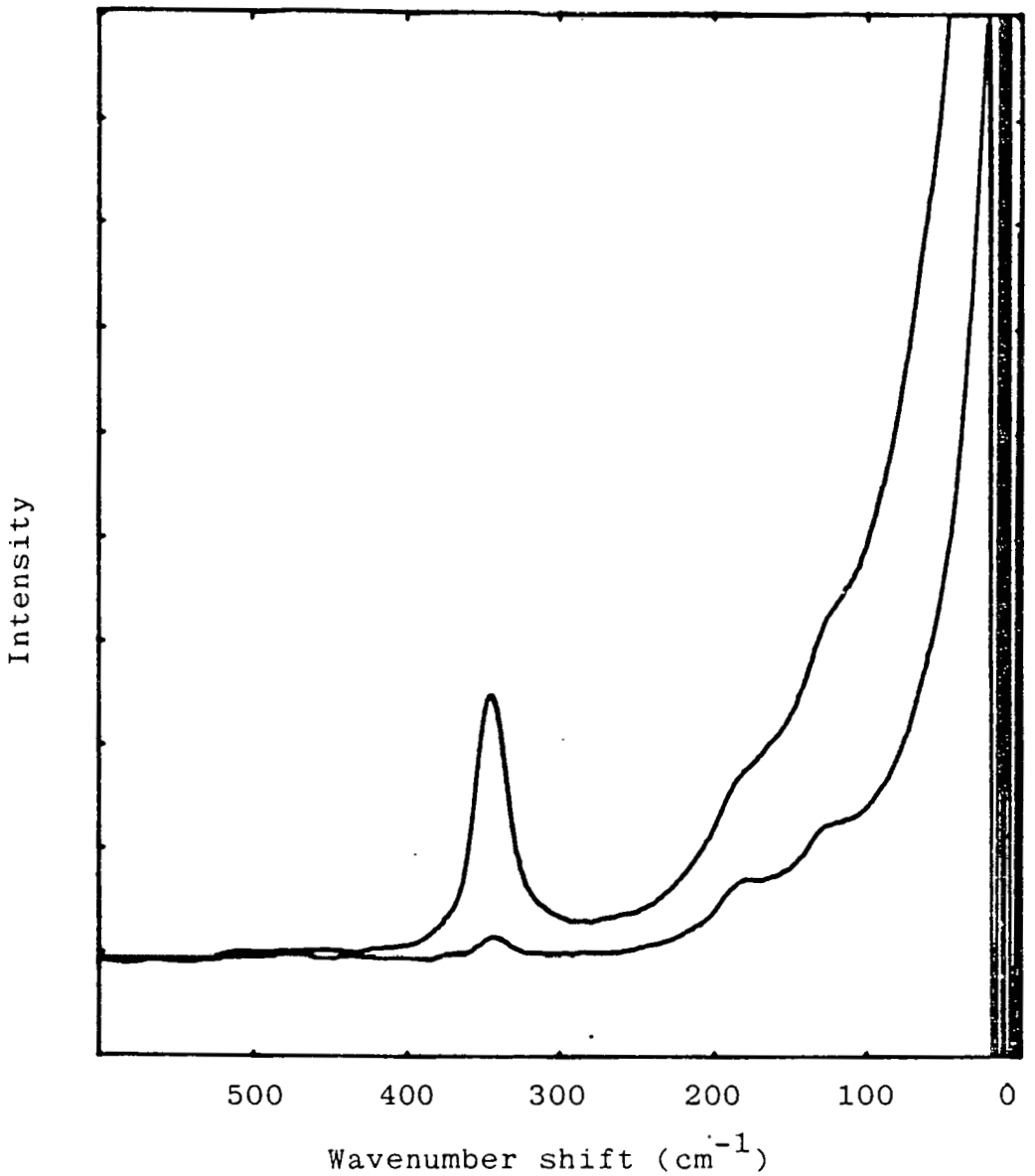

Fig. 4.36 (a) Raman spectra of 5 mol.% $AlCl_3$ + 95 mol.% KCl. T=800°C.

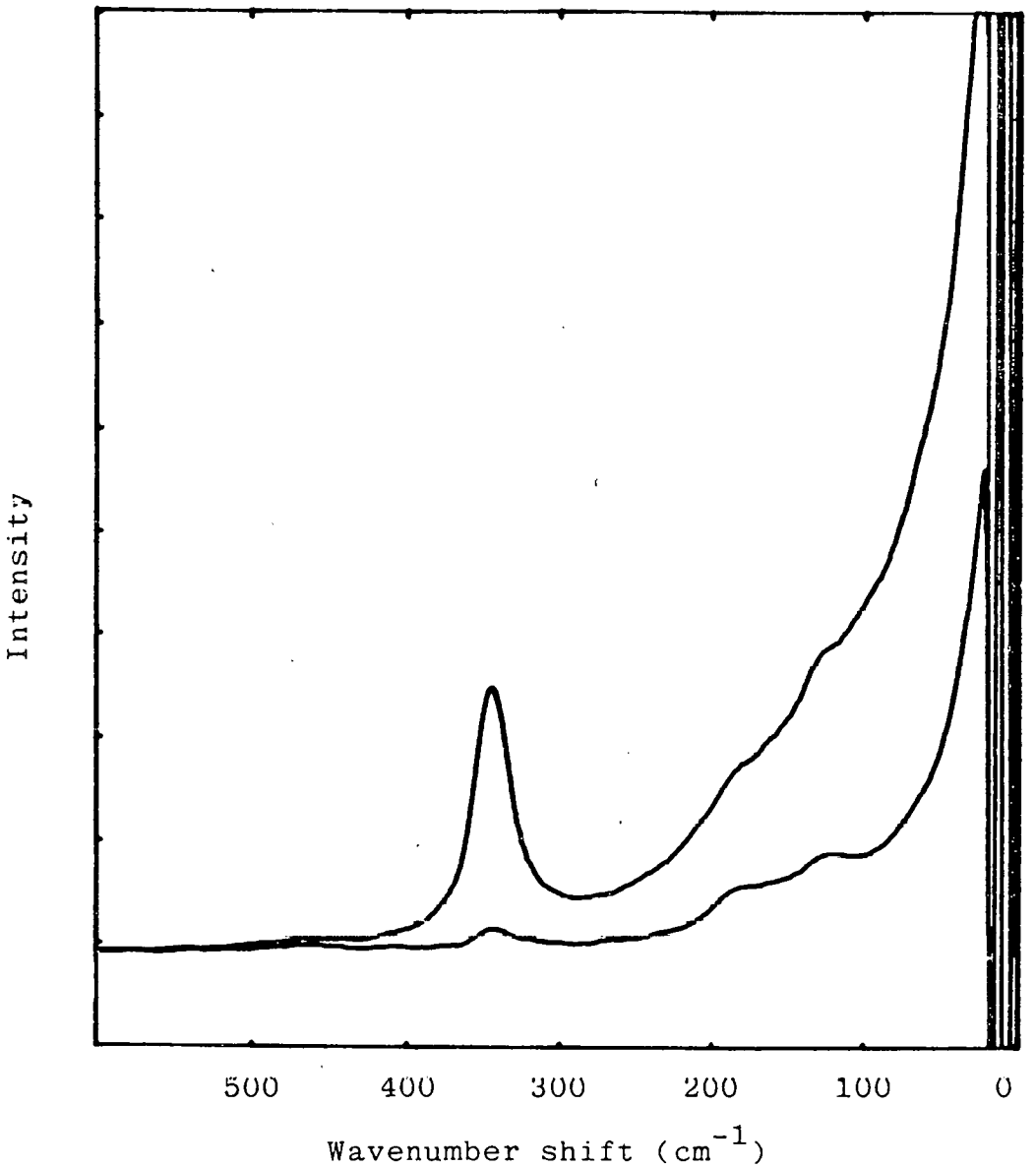

Fig. 4.36 (b) Raman spectra of 5 mol.% $AlCl_3$ + 95 mol.% NaCl. T-810°C.

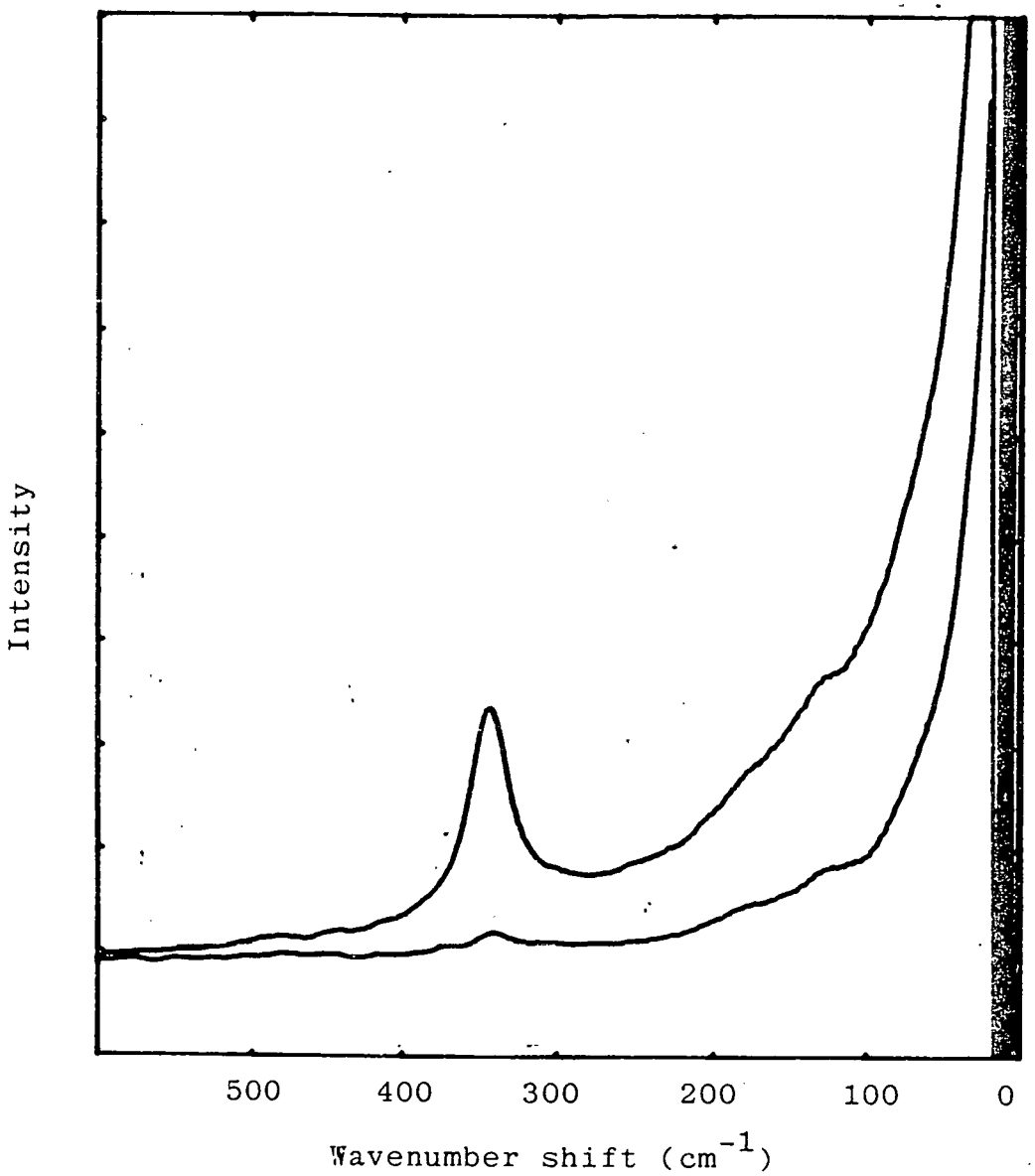

Fig. 4.36 (c) Raman spectra of 5 mol.% $AlCl_3$ + 95 mol.% LiCl. T=700°C.

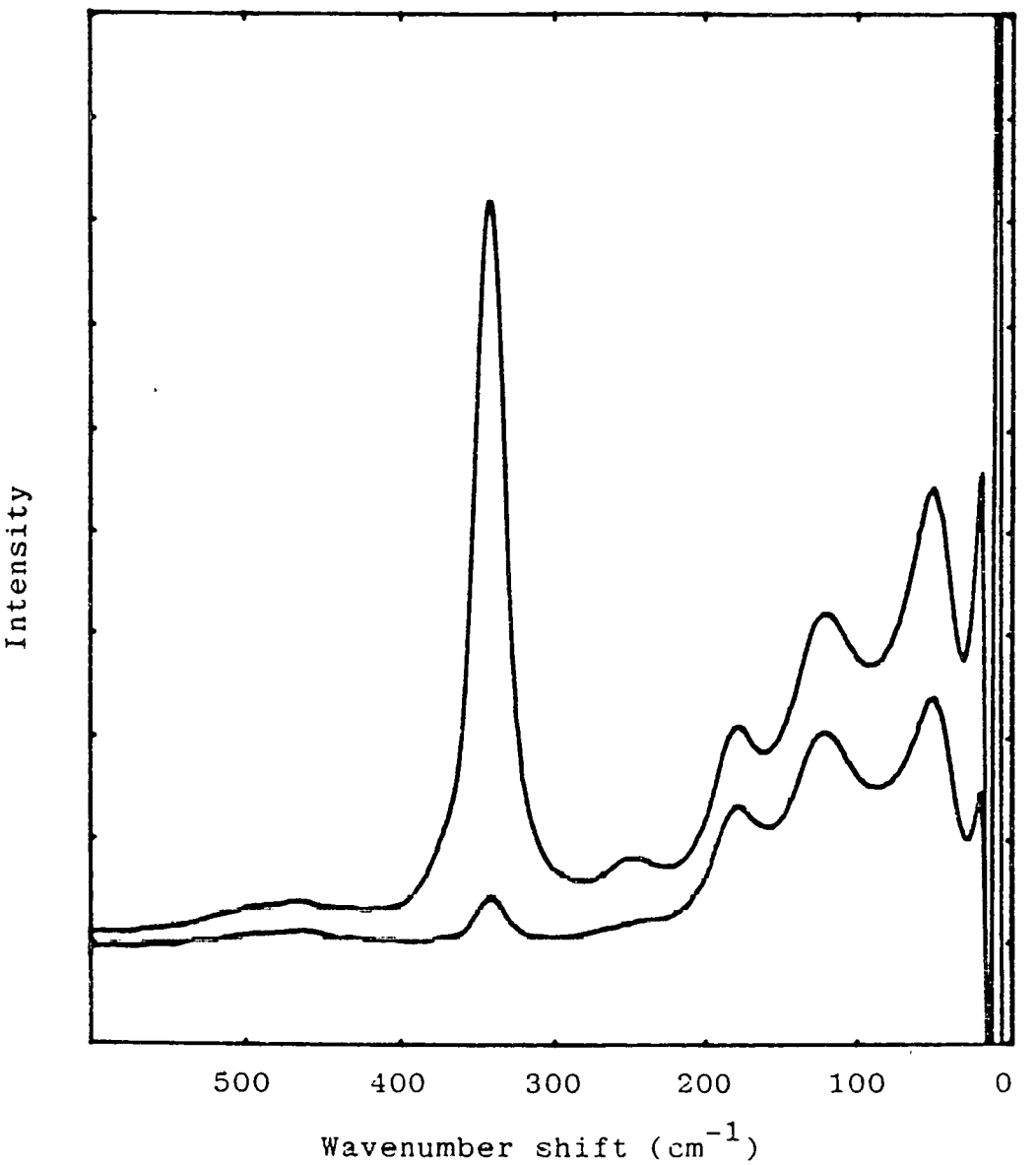

Fig. 4.37 (a) Raman spectra of 15 mol.% $AlCl_3$ + 85 mol.% CsCl. T=700°C.

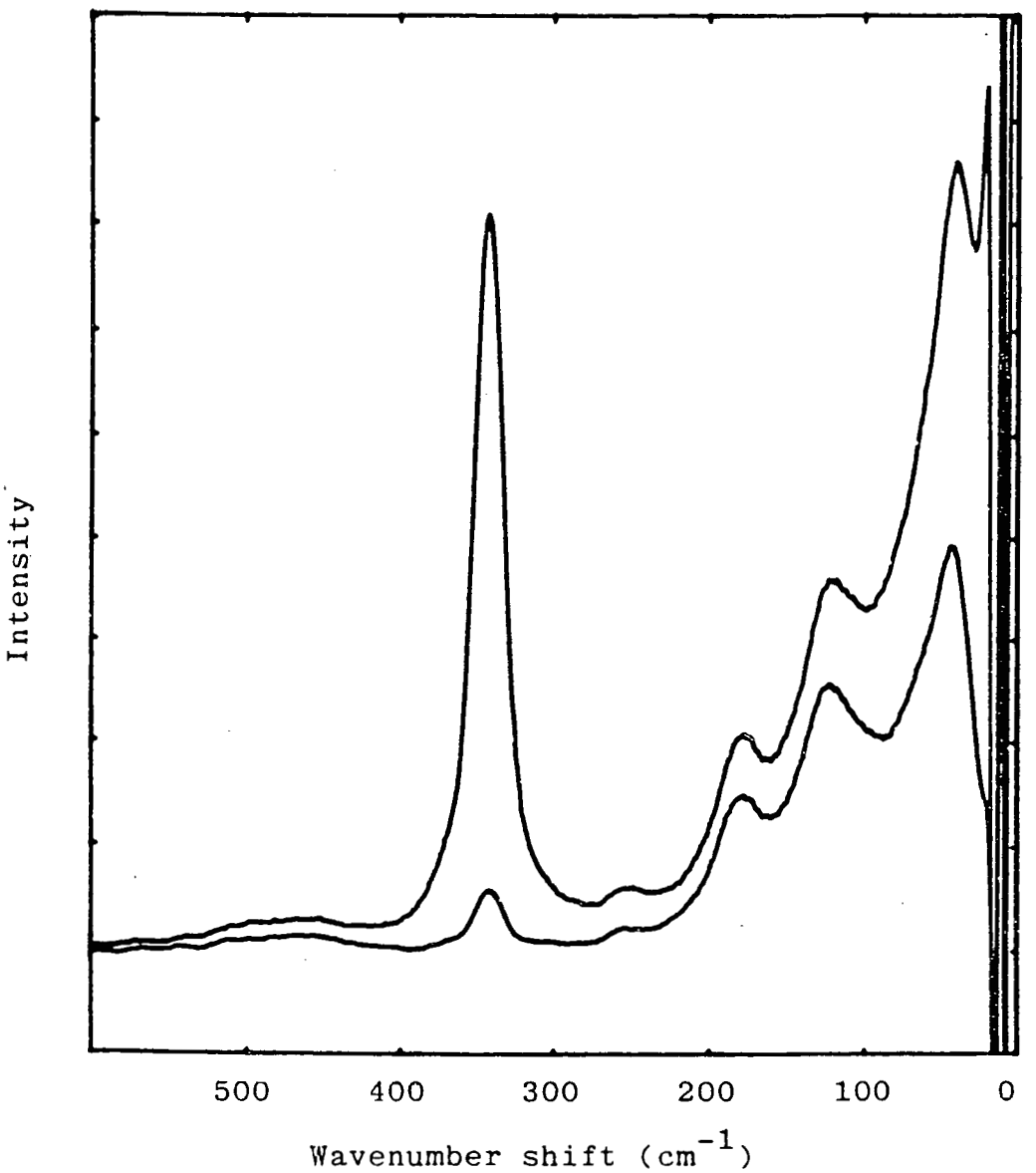

Fig. 4.37 (b) Raman spectra of 21 mol.% $AlCl_3$ + 79 mol.% CsCl. T=700°C.

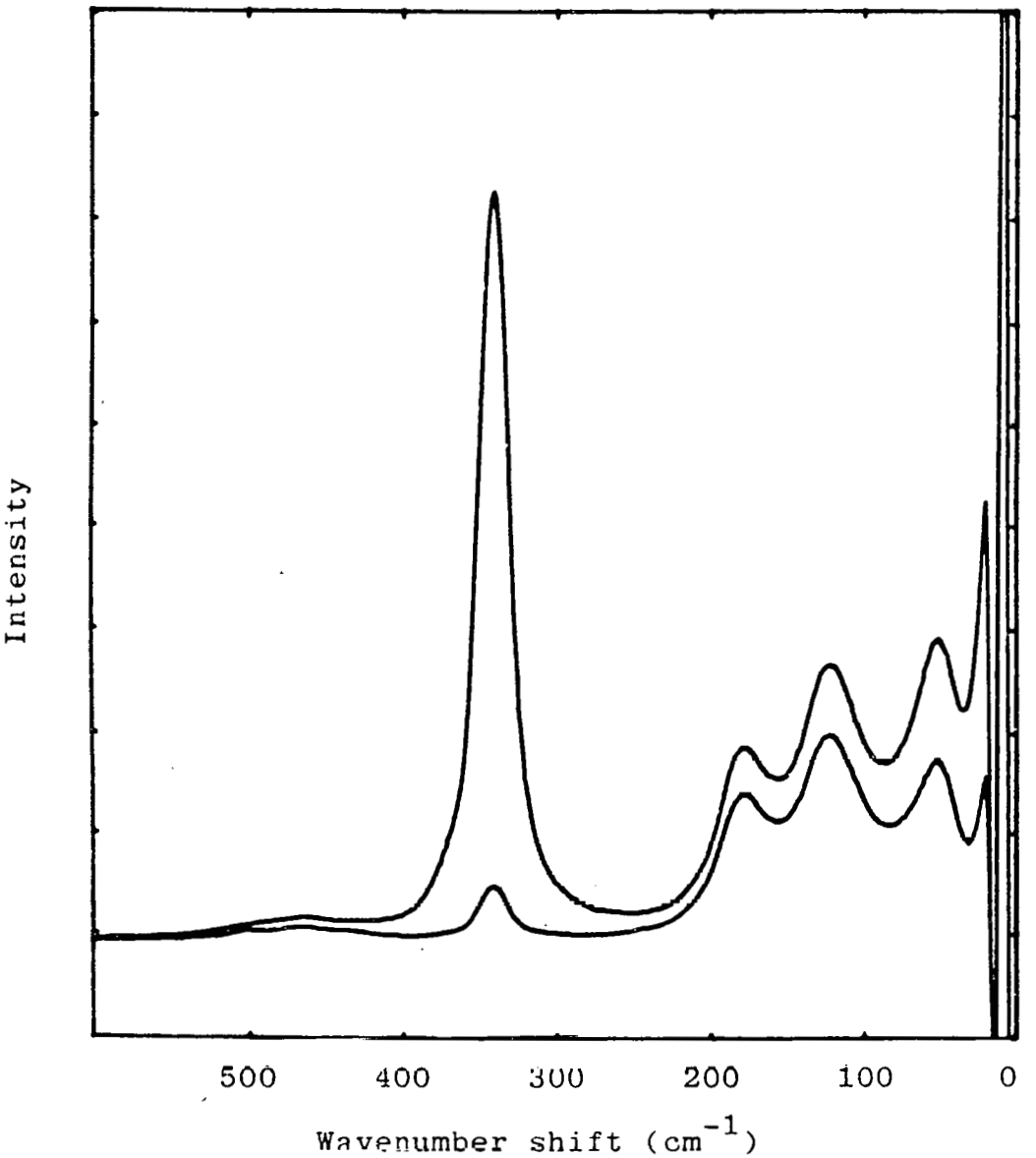

Fig. 4.37 (c) Raman spectra of 25 mol.% $AlCl_3$ + 75 mol.% CsCl. T=700°C.

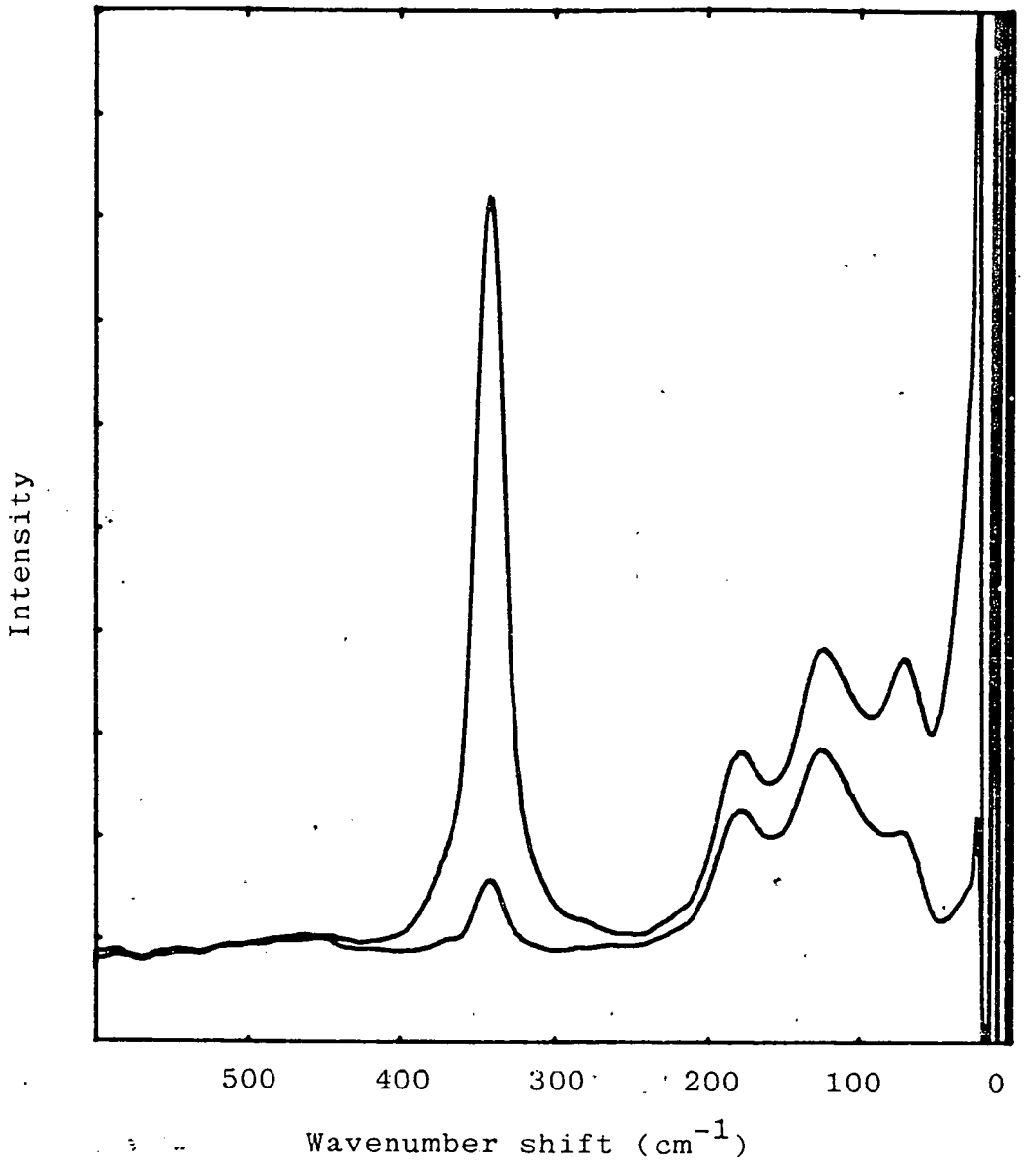

Fig. 4.37 (d) Raman spectra of 33 mol.% $AlCl_3$ + 67 mol.% CsCl. T=700°C.

4.3.2 Raman spectra during electrolysis

4.3.2.1 Melt clarity and Raman spectra

A. Before Electrolysis To see the effect of melt clarity on Raman spectra, a sequence of experiments was conducted on the electrolyte melts for aluminum and magnesium electrolysis.

The melts of potassium chloride, sodium chloride, and the molten mixtures of the two salts were very clean with high values of transmitted laser power. No appreciable Raman peaks were found for these melts, as expected.(Fig. 4.10,11,13)

The transmitted power of the mixture melt of sodium chloride and potassium chloride was lowered by about 45% with the addition of calcium chloride which was claimed, by Alfa Product, to be 99.99% pure and packed under argon. For Raman measurements, this salt had to be purified by the method including thionyl chloride treatment. Because of the low vapor pressure of $CaCl_2$ even at high temperature, however, subliming could not be conducted on this salt. At the solid state, an extended period of $SOCl_2$ treatment was applied to this salt (about 3 days at 600°C). The purified $CaCl_2$ by this method caused no dropping of laser transmitted power when it was added to the clean mixture of NaCl and KCl. Raman measurement of the molten mixture of $CaCl_2$, KCl, and NaCl in the weight ratio of 6:18:65 showed no appreciable peaks, as observed earlier in Fig. 4.21.

Upon addition of magnesium chloride, the Raman lines appeared as shown in Fig. 4.22, with the same clarity of the supporting electrolyte. It is believed that this clarity is due to the preparation of salts by the use of thionyl chloride. It was also learned that, for analytical measurements, even the salts claimed to be high grade must be purified. The melt composition was 11 wt.% $MgCl_2$, 6 wt.% $CaCl_2$, 18 wt.% KCl, and 65 wt.% NaCl. Pre-electrolysis was conducted in this melt at a temperature of 750°C.

Pre-electrolysis was conducted at 1.6 V, which is higher than that for the decomposition of H_2O but lower than that for the electrodeposition of Mg. The electrodes were glassy carbon (1/8 in. dia.). To prevent mixing of the deposits with the bulk melt, the cathode was shrouded by a 3/8 in. dia. fused quartz tubing which was one-end closed and had 2 holes on the side for melt circulation. The current density was almost constant at the value of 1.8 mA/cm^2 throughout 10-hour long pre-electrolysis. This constant low current density tells that the salts prepared in this research by the method described earlier are pure enough for this kind of analytical research. During pre-electrolysis, Raman spectra were measured. It was observed that the $MgCl_4^{2-}$ peak became weaker as time passing, with no change in peak position (Fig. 4.38), though the transmittance was almost constant throughout the pre-electrolysis.

The same sequential experiments were conducted on the electrolyte melt for aluminum chloride electrolysis. The melts of NaCl, LiCl, and

the mixtures of NaCl-LiCl and $AlCl_3$-NaCl-LiCl were clean, and for them Raman spectra were measured (Fig. 4.9,10,14,32,33). Pre-electrolysis was conducted on the melt of 5 wt.% $AlCl_3$ - 42 wt.% LiCl - 53 wt.% NaCl at 700°C. The electrodes were 1/8 in. dia. glassy carbon. To prevent mixing of the deposits with the bulk melt, the cathode was shrouded by a 3/8 in. dia. quartz tubing with 2 holes on the side and one-end closed, as in the same way for magnesium experiment. No current reduction was observed after 10 hours long pre-electrolysis at 1.6 V. Although the clarity did not appear to be changed, the aluminum chloride Raman peak at 349 cm^{-1} continued to diminish in height without change in wave-number.(Fig. 4.39)

The vaporization of magnesium chloride or aluminum chloride was not suspected to be the only reason since any appreciable condensate of magnesium chloride or of even highly volatile aluminum chloride could not be located above the melt. Furthermore, the reduction rate in peak intensity was almost constant although the vaporization has to be less as time passing because of the lower activity in the melt at the lower concentration.

The reduction in intensity of Raman peaks in extremely clean melts has been reported privately by Prof. G. N. Papatheodorou, Dept. of Chemical Engineering, University of Patras, Patras, Greece. He observed a similar phenomenon in melts he had made ultrapure by resublimation. The decrease of Raman intensity was believed to be related to the total charge passed through the cell. Should cleanliness of highly electrolyzed melts be associated with loss of Raman spectra, collection of

spectra close to the electrodes was thought to be complicated because of the higher current densities in these regions. Furthermore, focusing of the laser beam became difficult when the melt was too clear.

B. During Electrolysis Raman spectra of magnesium electrolysis have been recorded at different current densities up to 130 mA/cm^2 (Fig. 4.40). Electrolysis was conducted galvanostatically on the system of 11 wt.% $MgCl_2$ - 6 wt.% $CaCl_2$ - 18 wt.% KCl - 65 wt.% NaCl at 750°C, which resembles the industrial composition. Raman spectra were measured at the position close to the glassy carbon cathode. By focusing the laser beam and by using the round glassy carbon as cathode, it was possible to make the laser beam pass through the surface region of the cathode in the melt. Raman measurement was conducted before and during electrolysis. There was a decrease in peak height of the Mg-Cl line without a shift in position as current density increases. The total equivalent charge was 6688 coulombs, based on the $MgCl_2$ content in the melt, and the total charge passed was about 1000 coulombs when the measurement was finished, which means that the concentration of $MgCl_2$ was above 9 wt.% during the entire experiment. Therefore, the peak decrease in the spectra was thought to indicate that the laser beam passed the boundary region of the cathode.

An experiment identical to that conducted on $MgCl_2$ was performed in the $AlCl_3$ system. Electrolysis was conducted on the melt of 10 wt.% $AlCl_3$ - 40 wt.% LiCl - 50 wt.% NaCl at 700°C at different current densities. $AlCl_3$ content was 3 grams which is of 6512 coulombs equiva-

lent, and the experiment was conducted before 900 coulombs of total charges had passed. Other experimental conditions were the same as in $MgCl_2$ experiment above. Fig. 4.41 shows the Raman results. One can observe that the maximum peak at 349 cm^{-1} decreases as current density increases.

This kind of experiment was extremely difficult to perform in such a way as to maintain sufficient melt clarity to detect a proper Raman spectrum, because the melts became milky from particulates generated by the electrolysis and colored from what seemed to be dissolved chlorine. These particles were extremely fine and almost smoke-like, and they strongly scattered the laser light. However, no appreciable change in the Raman spectra was observed.

From the fact that transmitted power decreased to several percent from an initial value of about 75% before electrolysis, it was possible to determine that the intensity decrease in the Raman spectrum was also due to a simple decrease in the intensity of the exciting radiation because of the blocking effect of the particulates. Although it was difficult to quantify the blocking effect of the particulates on Raman signal, Raman peak heights in Fig. 4.40 and 41 clearly show the trends in current density variation in the surface region of the cathode.

4.3.2.2 Smoke-like particle generation during electrolysis

As described in section 4.3.2.1, the electrolyte became milky from

the particulates generated during electrolysis. These particles were evident when the laser beam passed through the melt since they strongly scattered the light as in Fig. 4.42. Fig. 4.42 (a) shows the laser beam passing through the melt. The shorter glassy carbon electrode was the cathode and the long electrode was the glassy carbon anode shrouded with fused quartz tubing. The melt composition was 10 wt.% $AlCl_3$ - 40 wt.% LiCl - 50 wt.% NaCl, and the temperature was 700°C. When electrolysis started in a potentiostatic mode at a potential of 1.90 V between the electrodes, the smoke-like cloud was observed right underneath the cathode (Fig. 4.42 (b)). The density of the cloud became higher with continued electrolysis (Fig. 4.42 (c)). After some time, the cloud could be observed in the entire cell, and no more Raman observation was possible because the particles scattered the laser beam very strongly. (Fig. 4.42 (d))

From the experiments on aluminum and magnesium electrolysis, it was evident that the particles were always formed during electrolysis, and they were coming from the cathode in the form of smoke. They were observed on such cathode materials as graphite, glassy carbon, and titanium diboride. It was also observed that they were generated even at lower potential than the equilibrium decomposition potential of aluminum chloride or magnesium chloride. Upon electrolysis, they seemed to be denser at the cathode and at the bottom of the cell, becoming full of the cell with continued electrolysis.

The particles disappeared quickly when argon gas saturated with $SOCl_2$ was bubbled through the melt, but it took long to remove them

without bubbling. It was observed that the anode region in the cell was free of these particles during electrolysis, possibly due to the high concentration of Cl_2.

These scattering particles were thought to be different from the streamers since they were generated even under the theoretical decomposition potential of $AlCl_3$ or $MgCl_2$, and they were invisible unless illuminated by strong light like a laser beam. Raman measurements did not show any difference to suggest that they may not be Raman active. From the fact that they were observed only during electrolysis, it was thought that they might be related to current losses. Further research is required to identify the nature of the fine particles and to find any relation to current efficiency.

Through these experiments, it was proved that $SOCl_2$ has great clarifying capabilities for preparation of spectral grade melts. To our knowledge this is the first use of thionyl chloride in these systems.

The color of the melt inside the anode shroud was found to become yellow by the chlorine evolution during electrolysis. It was also observed that the color of the melt turned yellow-green when $SOCl_2$ was bubbled through the melt. Raman measurements of the colored melt did not show any appreciable change in the spectra, suggesting that the nature of the coloration of the electrolyte may not be identified by Raman spectroscopy. The color disappeared by sparging with argon. These experiments showed that gas solubilities in these melts were much higher than expected.[90,91] These observations suggested either that

the gas solubility data in the literature are wrong, or that gas solubilities can greatly exceed the equilibrium values.

4.3.2.3 Streamers occurrence during electrolysis

Streamers (or metal fogging) were clearly observed in this research. The streamers were observed at higher potentials than the equilibrium decomposition potential of $AlCl_3$ or $MgCl_2$. The streamers were different from the smoke-like particles in that they could be seen to bare eyes without any strong light, and they heavily attacked the fused quartz cell to change the color of the cell to brown.

The photographs in Fig. 4.43 show the development of streamers in $AlCl_3$ electrolysis cell. The electrolyte was 10 wt.% $AlCl_3$ - 40 wt.% LiCl - 50 wt.% NaCl, and the temperature was 700°C. Electrolysis was conducted potentiostatically at a potential of 2.3 V between the anode and the cathode. In Fig. 4.43, the glassy carbon in the center of the cell served as cathode, and the other on the left was anode which was shrouded by a fused quartz tubing. The photograph in Fig. 4.43 (a) was taken when electrolysis just started. Chlorine gas bubbling may be observed at the anode. After 10 seconds, a weak streamers stretching downward in the cell could be seen at the tip of the cathode (Fig. 4.43 (b)). In Fig. 4.43 (c), the streamers can be clearly observed, and they appeared to flow to the bottom of the cell. Fig. 4.43 (d) shows the same cell as in (a), but it may be observed the tiny aluminum droplets at the surface of the cathode. The cell became dark because of the

streamers with continued electrolysis, and no more Raman measurements or observation of the cell were possible.

In magnesium electrolysis, the streamers were further evident than those in aluminum electrolysis. Fig. 4.44 (a) is a photograph of the development of the streamers, taken after 1 minute of electrolysis. The composition of the electrolyte was 11 wt.% $MgCl_2$, 6 wt.% $CaCl_2$, and 18 wt.% KCl, 65 wt.% NaCl. Electrolysis was conducted galvanostatically at a current density of 100 mA/cm^2 at a temperature of 750°C. On the left is a 1/4 in. graphite cathode; on the right is a 1/8 in. graphite anode shrouded with fused quartz tubing. Streamers have begun to emanate from the cathode. Chlorine gas bubbles can be seen on the anode. In Fig. 4.44 (b), the development of the streamers can be clearly observed. Fig. 4.44 (c) shows the same cell as Fig. 4.44 (a) but after approximately 5 minutes of electrolysis at a current density of 100 mA/cm^2. It is evident that the streamers emanating from the cathode have grown over essentially the entire breadth of the cell. This photograph also shows the appearance of tiny droplets of magnesium on the tip of the cathode. Chlorine bubbles are seen to continue evolving on the anode. About 10 minutes after the on-set of electrolysis, the electrolyte became so cloudy that it was not possible to observe the electrolysis cell (Fig. 4.44 (d)).

It is well known that many metals dissolve to some extent in their own molten halide salts. If the dissolution is considered, dissolved magnesium is reported to exist as subchloride in the form of $MgCl$[93] or Mg_2Cl_2,[94] which may be Raman active. But attempts to measure Raman

spectra of the streamers have yielded nothing, suggesting the streamers may not be Raman active. However, the streamers may not be thought as the metal dissolution if one considers the fact that the solubility of excess magnesium in its chloride has been reported less than 1 mol.%.[95]

In an attempt to understand the nature of the streamers, a magnesium chloride mixed with calcium and alkali chloride melt in proportions representative of a magnesium electrolysis melt was prepared and analyzed by Raman spectroscopy. Addition of magnesium metal ribbon, transported in an inverted graphite crucible, into the chloride melt resulted in the generation of particles and reduced the transmitted laser power even without electrolysis. The cell resembled Fig. 4.44 (d). The streamers appeared to emanate clearly from the magnesium metal. The same phenomena were observed with the exposure of aluminum metal to the melt of $AlCl_3$-NaCl-LiCl. All the attempts to identify these particles by Raman spectroscopy were unsuccessful.

Electrolysis had no effect on this phenomenon. However, chlorine gas was observed to have the capability of clarifying the melt. The tests were conducted on the electrolyte of 5 wt.% $AlCl_3$ - 53 wt.% NaCl - 42 wt.% LiCl. Upon exposure of molten aluminum to the melt, transmitted laser power dropped from 180 to 80 mW. With the production of chlorine gas at the bare anode at 2.1 V, the transmitted power returned to the original value of 180 mW within 20 minutes. Passage of thionyl chloride also clarified the melt. Thionyl chloride can chlorinate aluminum or magnesium metal, oxides, or subchlorides, but chlorine gas can not

chlorinate the oxide at this temperature. The fact that chlorine gas clarified the melt suggested that the particles were not oxides. This is not in agreement with that of Wendt and Reuhl[96] since they thought them to be oxides.

In summary, the streamers could be clearly observed in the $AlCl_3$ and $MgCl_2$ electrolysis cells. Even though they may not be Raman active, the particles composing the streamers would not be suspected to be aluminum oxide or magnesium oxide since the chlorine gas would have no effect on them were that the case. It might be also said the streaming is not solely the result of electrolysis.

4.3.2.4 Raman spectra in the cathodic boundary layer

Attempts were made to penetrate the cathode boundary layer to determine if species other than trivalent aluminum exist. It was estimated that, for a 10 wt.% $AlCl_3$ solution, the boundary layer, under diffusive mass transfer control conditions, is approximately 800 μm thick when the current density is 100 mA/cm^2.(Appendix 1) Because the diameter of the laser beam can be reduced to 400 μm by careful focusing, it was thought that Raman spectra could be measured for the cathodic boundary layer. It was observed that the dependence of Raman peak intensities on the current density was the indication that the laser beam passed through the surface region of the cathode.(Fig. 4.41,42)

To confirm that the laser beam can penetrate the boundary layer, a

somewhat different experiment was conducted. Fig. 4.45 shows Raman spectra taken for aluminum chloride electrolysis conducted under different conditions from those described up to this point. In this case the melt contained not 10% $AlCl_3$, but only 1% $AlCl_3$ in the supporting electrolyte, NaCl:LiCl 50:40 by weight as before. The point of this experiment was to test the sensitivity of Raman spectroscopy to reduced concentrations of $AlCl_3$. Curves (a) and (b) were measured in the bulk electrolyte at the beginning of the experiment and after passing 400 coulombs of charge. The total equivalent charge was 650 coulombs, based on the $AlCl_3$ content in the melt. While the intensity of the 349 cm^{-1} peak decreases, its presence is still evident even in curve (b), where the total content of $AlCl_3$ at the time of measurement was less than 0.4 weight percent. Curve (c) was measured in the cathode boundary layer only after 30 coulombs of charge had passed. The principal $AlCl_4^-$ peak cannot be found. This confirms that the laser beam indeed penetrated the cathode boundary layer.

An electrolysis experiment was conducted on the Alcoa Smelting Process electrolyte. The temperature was low, 610°C, so that the cell would produce solid crystalline aluminum. This would serve two purposes. First, the electrode/electrolyte interface would be much less mobile and thus easier to follow with the incident laser beam. This point is important for studying the local chemistry inside the cathode boundary layer. Secondly, if the scattering particles observed in earlier electrolysis are finely dispersed aluminum droplets, conducting electrolysis at temperatures at which the product is solid aluminum is one way of reducing the quantity of these particles in the melt. The

result, however, did not show any difference from the original spectra except the reduced intensity, as in the Fig. 4.45. Tests at a temperature of 680°C also gave rise to the same featureless results.

In an attempt to get the boundary layer more easily, a molten tin cathode was tried, because; (a) molten tin does not react with glass, (b) molten tin alloys with aluminum metal, and (c) the shape in the electrolyte is a hemisphere. More importantly, in this system the electrolyte density becomes higher as the concentration of $AlCl_3$ decreases.[95,96] This inhibits buoyancy driven convection and allows the boundary layer to grow. Electron microscopy confirmed that the cell was producing aluminum which alloyed with tin. However, Raman measurements did not show any appreciable new peaks corresponding to the other species. The same featureless Raman results were obtained with a cathode consisting of molten aluminum metal contained in an alumina tube with a 1/8 in. diameter hole near the bottom.

Clark and Woodcock[82] measured the Raman spectrum of molten KCl and found that spectrum has the quasi-exponential form centered on zero frequency. It was also reported recently that the high-frequency regions of the spectra of the ionic melt can be described by an exponential.[72] With this knowledge, some efforts were made to generate the base line curves, because subtracting this base line from the Raman spectrum was hoped to reveal the weak Raman signals. In some systems such as $AlCl_3$ - ACl attempts were successful, but in general it was not easy to generate exact base line curves because of the difficulty in locating regions free of Raman peaks in the spectra.

Even with these various efforts, the presence of other species could not be detected. Although the existence of the subvalent form has been justified on theoretical grounds, scant experimental evidence is available with regard to the stability of the subvalent species of aluminum in either liquid or solid phases. If such species exist, it is believed that they exist only for kinetic reasons (created faster than they can be discharged at high currents). For example, if change of valence from +3 to +1 is rapid, but the change from +1 to 0 (neutral metal) is slow, then the lower valent form would exist in the boundary layer, under high current electrolysis.

In summary, the subvalent species could not be identified during aluminum deposition from $AlCl_3$-LiCl-NaCl melt by Raman spectroscopy. If they exist, they are thought to be undetectable by the instrumentation employed. To try to detect the presence of these species, cyclic voltammetry (Chap. 5) was conducted on the same system.

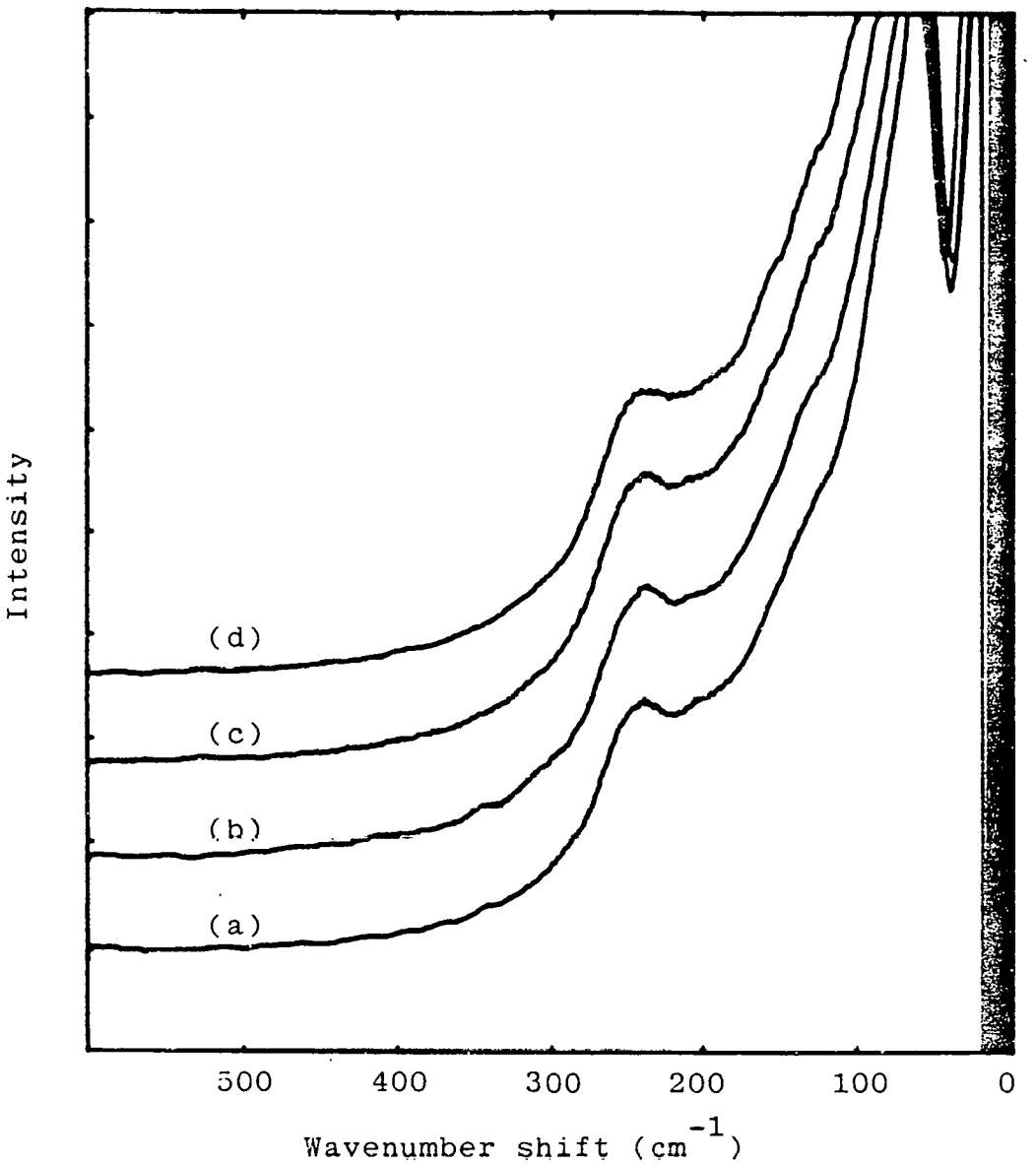

Fig. 4.38 Raman spectra of 11 wt.% $MgCl_2$ - 6 wt.% $CaCl_2$ - 18 wt.% KCl - 65 wt.% NaCl measured during pre-electrolysis at 1.6 V. T=750°C. (a) Before electrolysis; (b) After 1 hour; (c) After 5 hours; (d) After 10 hours.

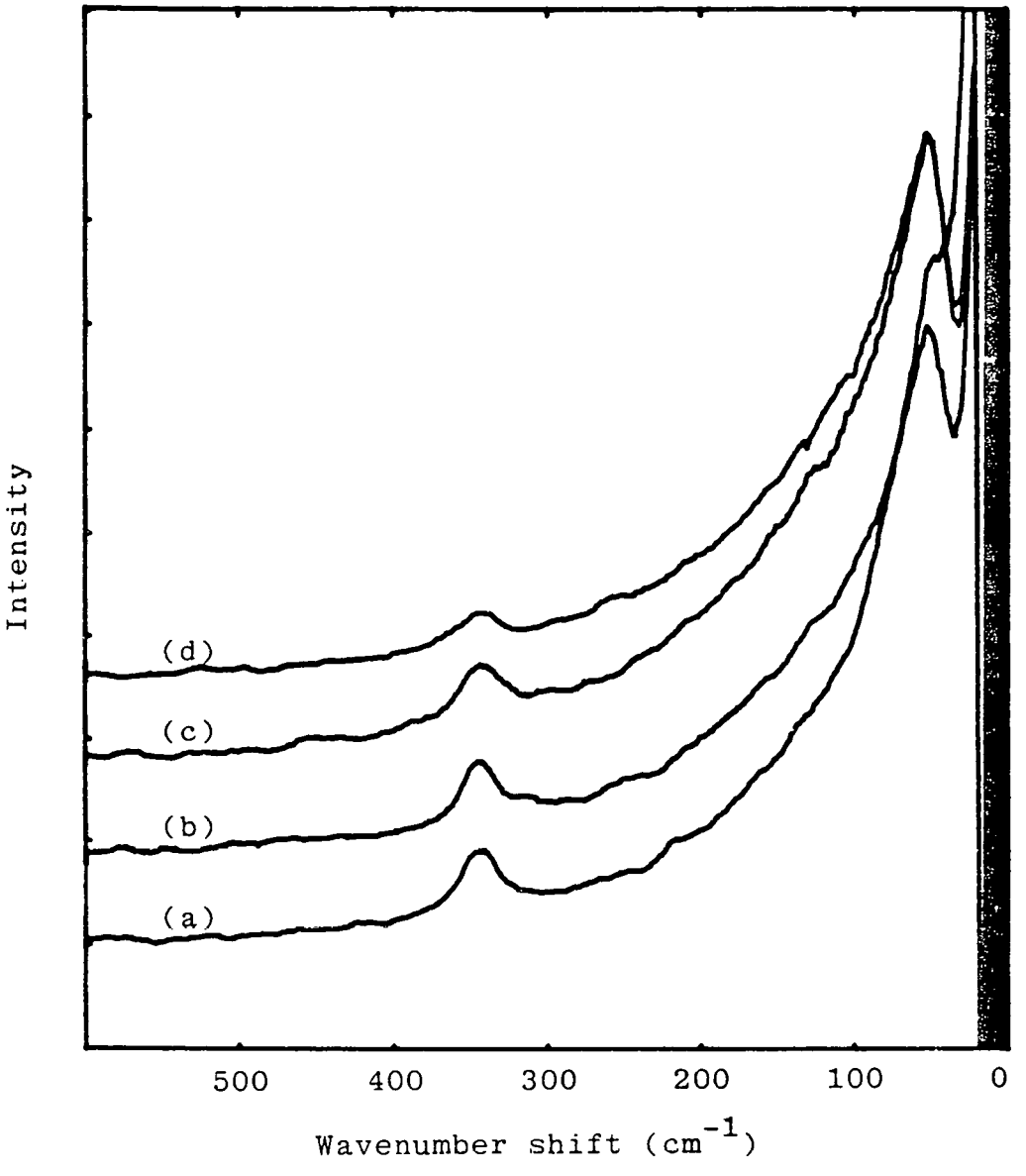

Fig. 4.39 Raman spectra of 5 wt.% $AlCl_3$ - 42 wt.% LiCl - 53 wt.% NaCl measured during pre-electrolysis at 1.6 V. (a) Before electrolysis; (b) After 1 hour; (c) After 4.5 hours; (d) After 10 hours.

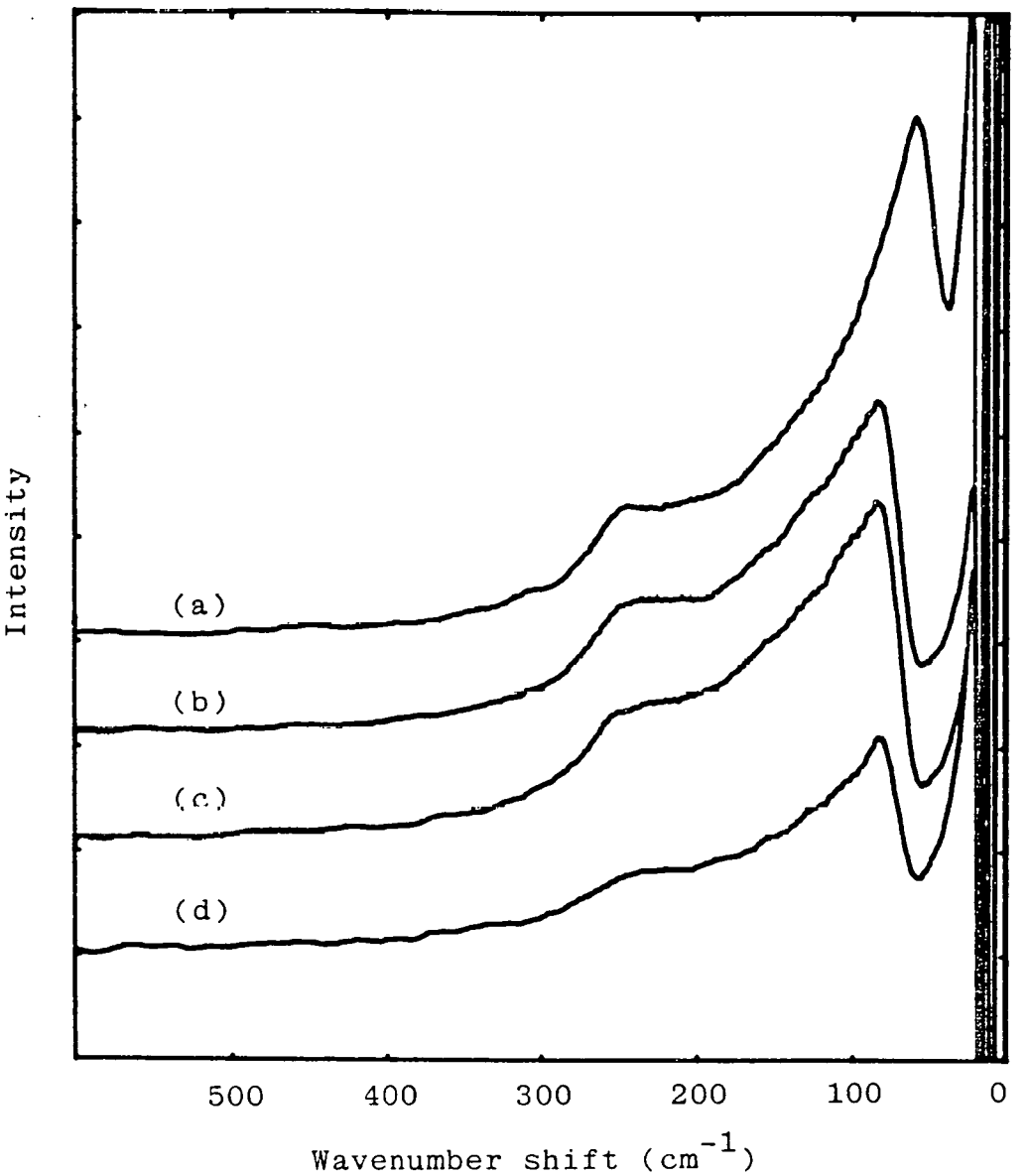

Fig. 4.40 Raman spectra of 11 wt.% $MgCl_2$ - 6 wt.% $CaCl_2$ - 18 wt.% KCl - 65 wt.% NaCl measured during electrolysis at different current densities. T=750°C. (a) No current; (b) 30 mA/cm^2; (c) 90 mA/cm^2; (d) 150 mA/cm^2.

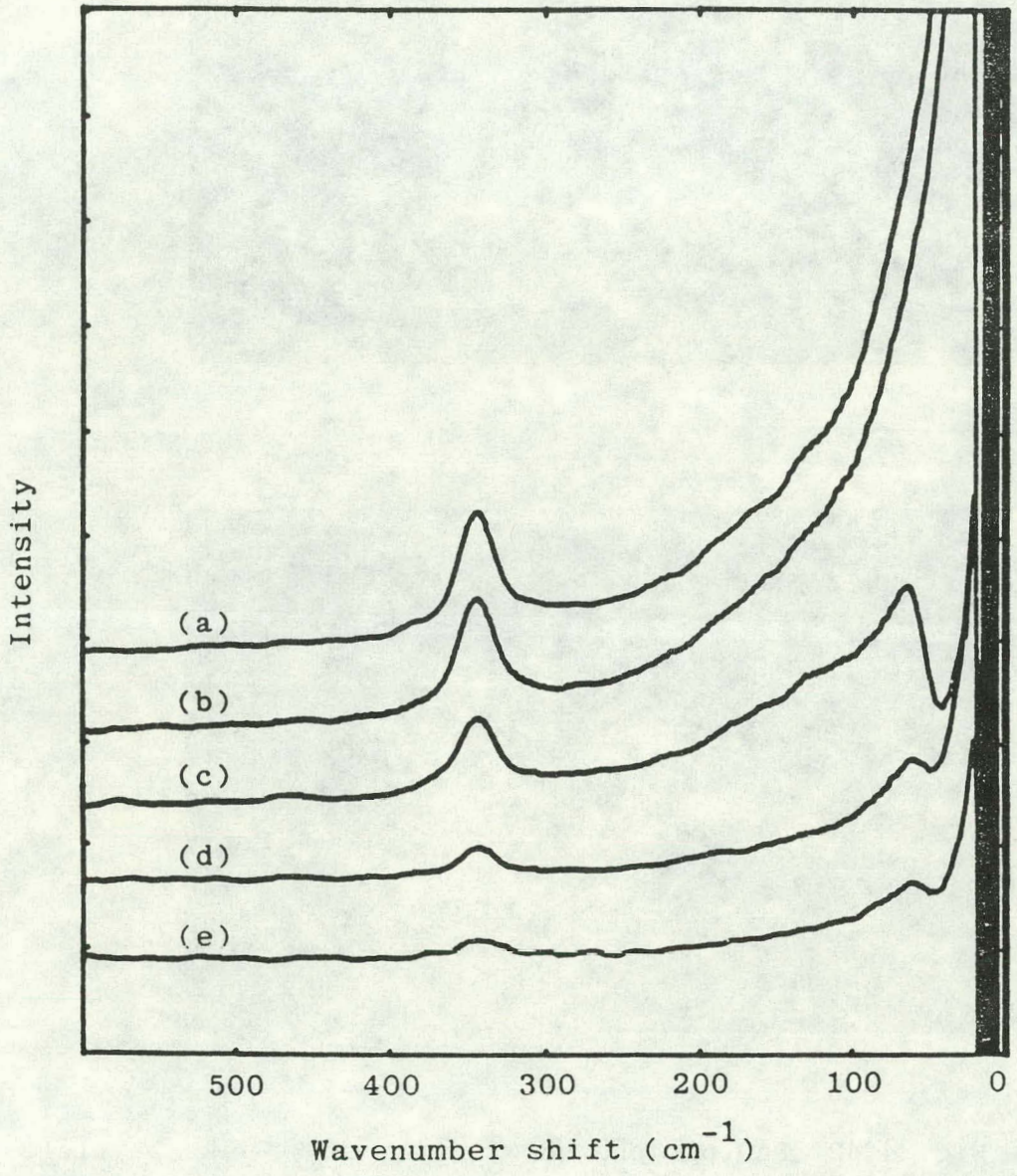

Fig. 4.41 Raman spectra of 10 wt.% $AlCl_3$ - 40 wt.% LiCl - 50 wt.% NaCl measured during electrolysis at different current densities. T=700°C. (a) No current; (b) 3 mA/cm^2; (c) 30 mA/cm^2; (d) 60 mA/cm^2; (e) 90 mA/cm^2.

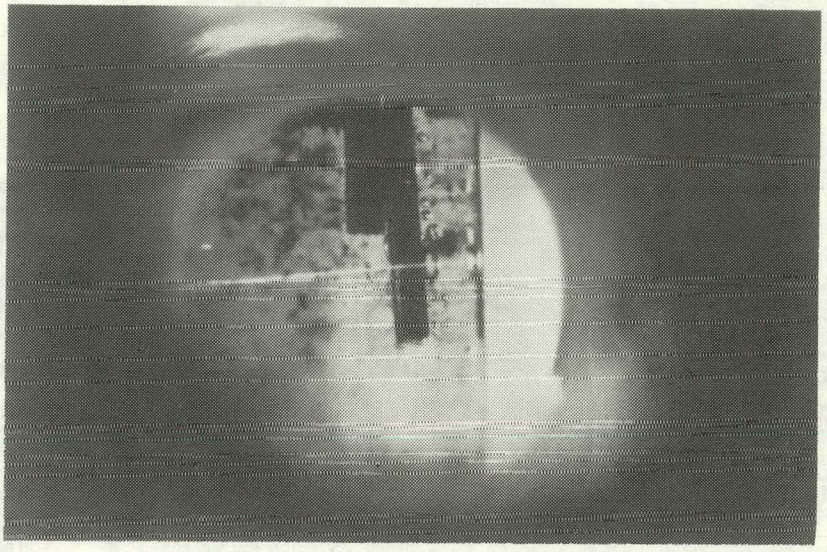

(a)

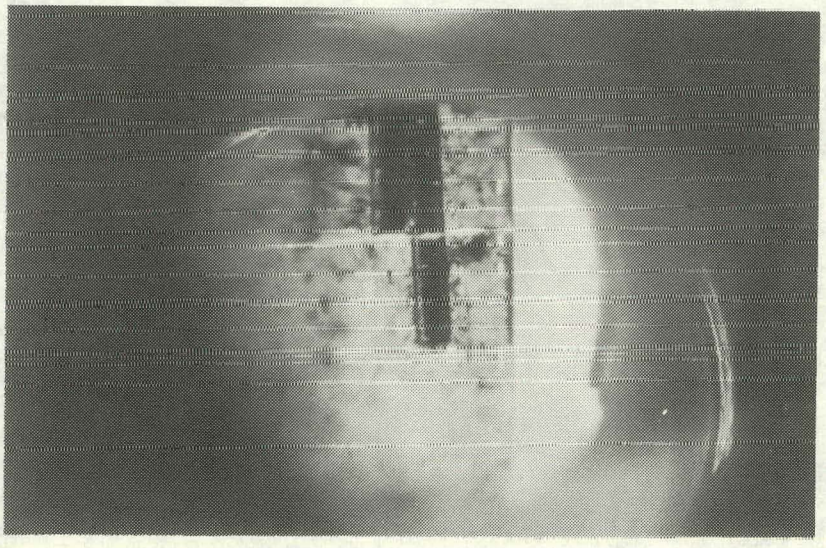

(b)

Fig. 4.12 Photographs showing the smoke-like particle generation during electrolysis of 10 w/o $AlCl_3$ - 40 w/o LiCl - 50 w/o NaCl at 1.9 V. T=700°C.
(a) Before electrolysis; (b) After 1 min.;
(c) After 2 min.; (d) After 5 min.

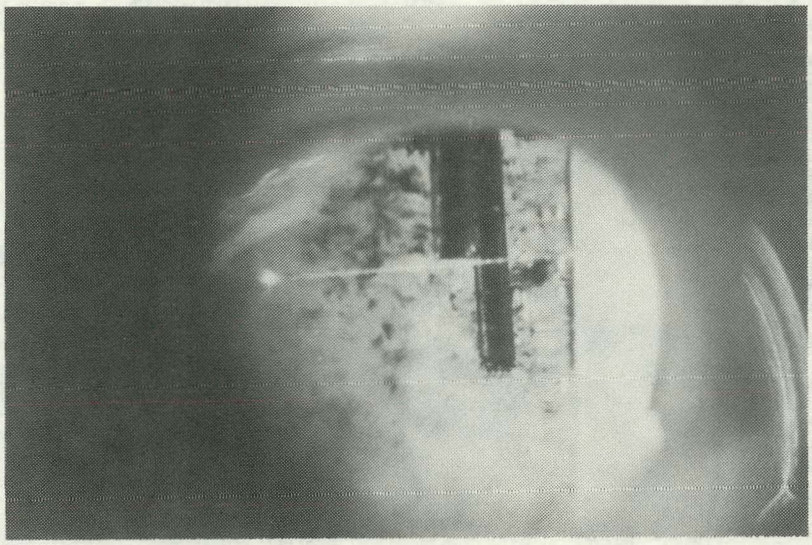

(c)

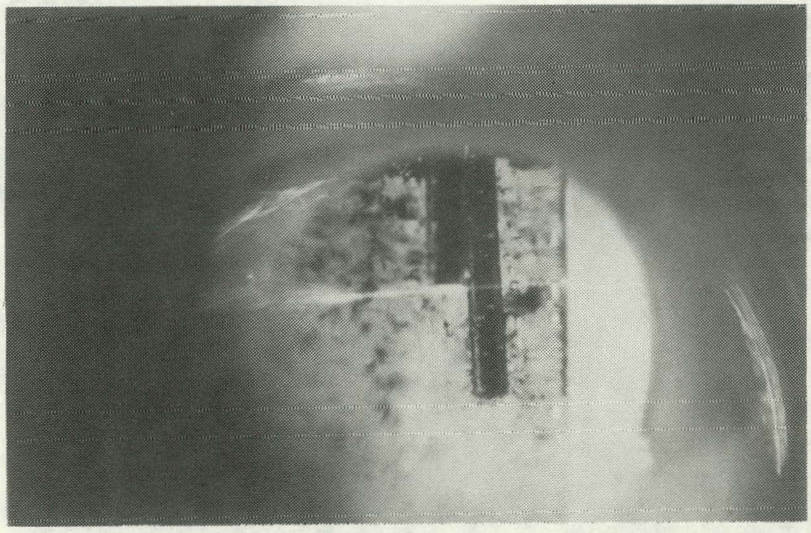

(d)

Fig. 4.42 continued.

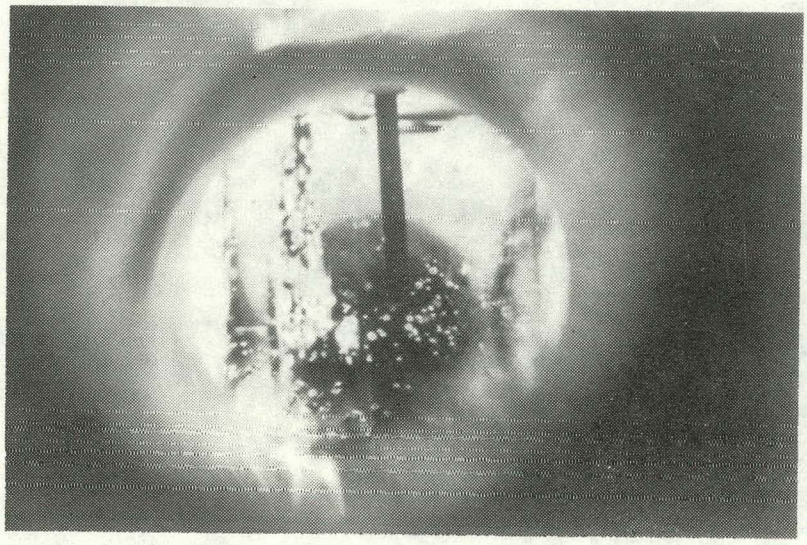

(a)

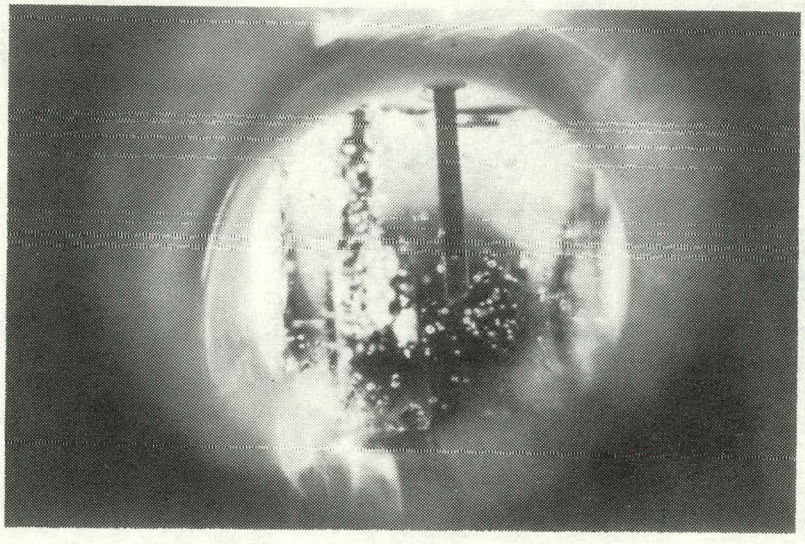

(b)

Fig. 4.43 Streamer development during $AlCl_3$ electrolysis. Electrolyte; 10 wt.% $AlCl_3$ - 40 wt.% LiCl - 50 wt.% NaCl. V = 2.30 V. T=700°C. (a) When electrolysis started; (b) After 10 sec; (c) After 30 sec; (d) After 10 min.

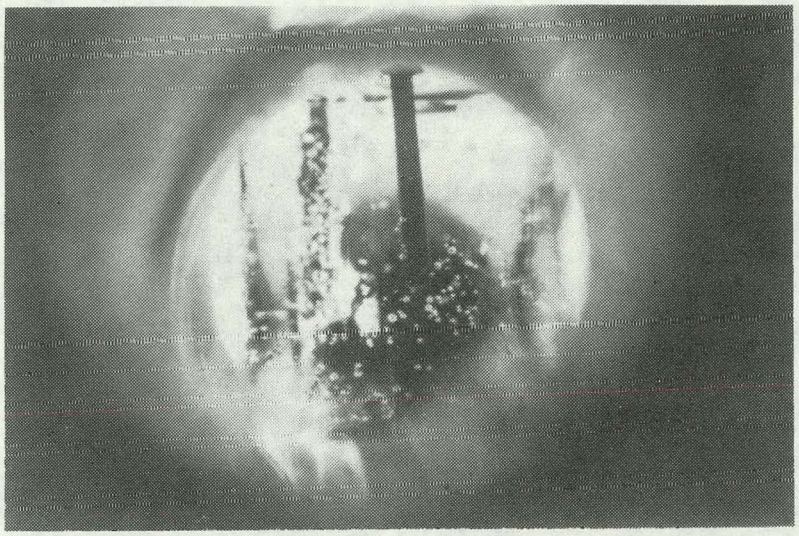

(c)

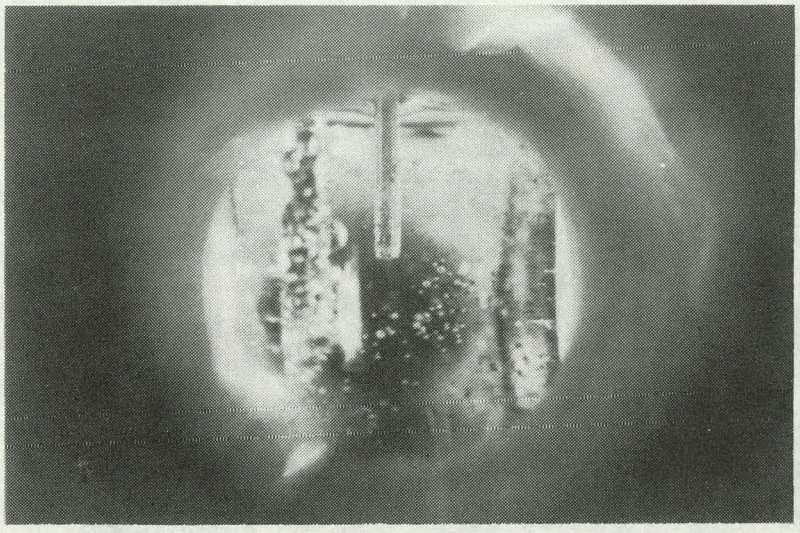

(d)

Fig. 4.43 continued.

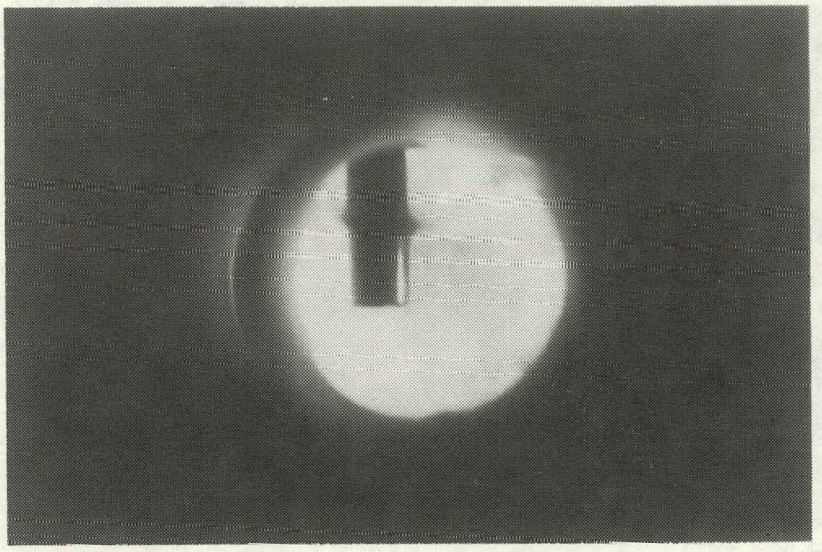

(a)

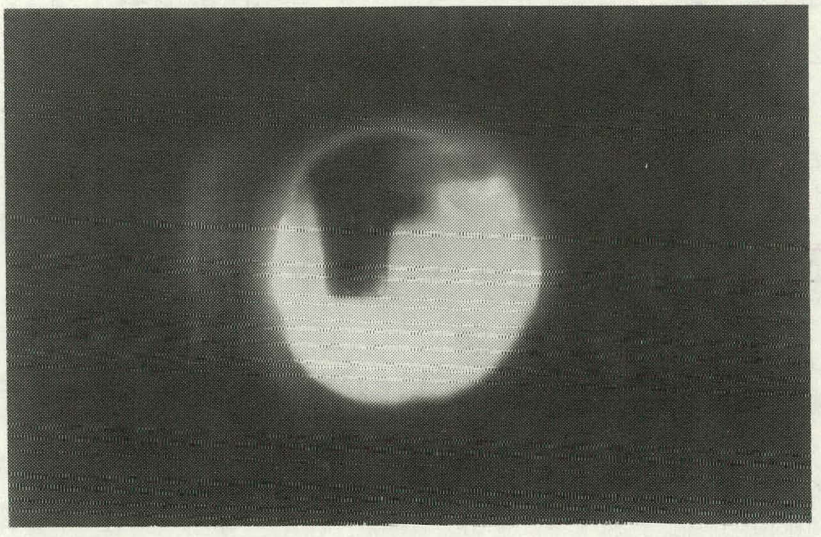

(b)

Fig. 4.44 Streamer development during $MgCl_2$ electrolysis. Electrolyte: 11 wt.% $MgCl_2$ - 6 wt.% $CaCl_2$ 18 wt.% KCl - 65 wt.% NaCl. T=750°C. i=100 mA/cm^2. (a) After 1min.; (b) After 2 min.; (c) After 5 min.; (d) After 10 min.

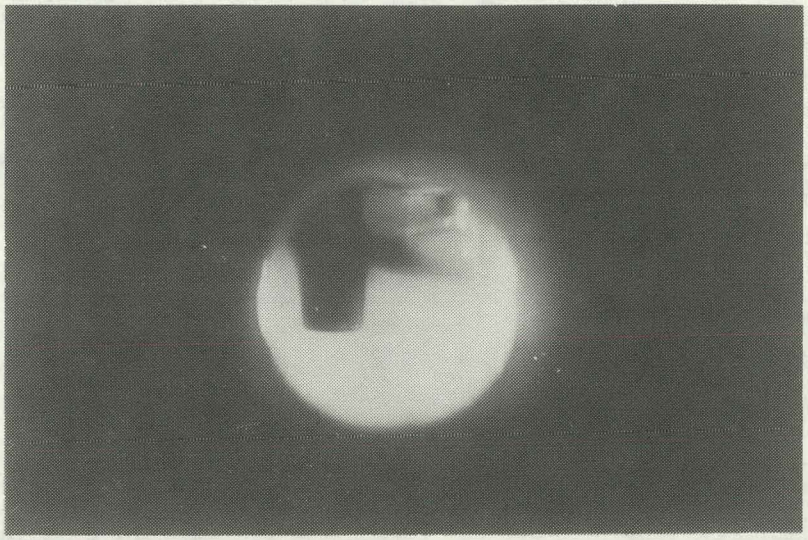

(c)

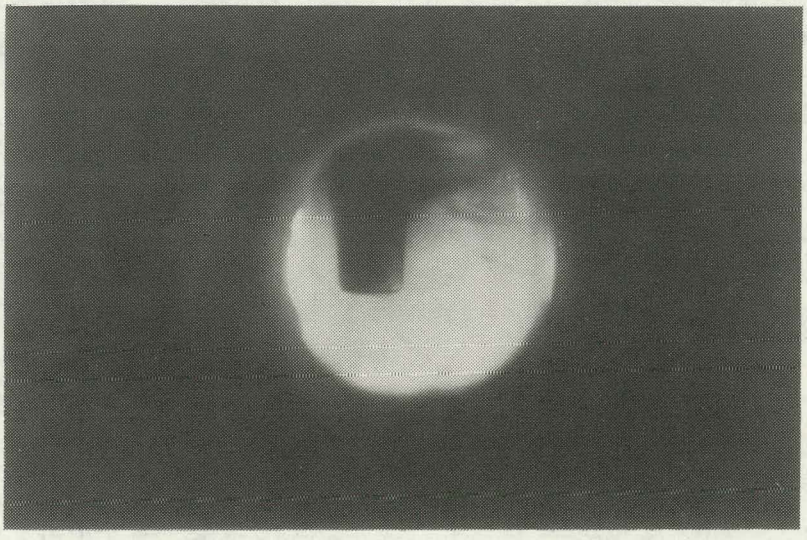

(d)

Fig. 4.44 continued.

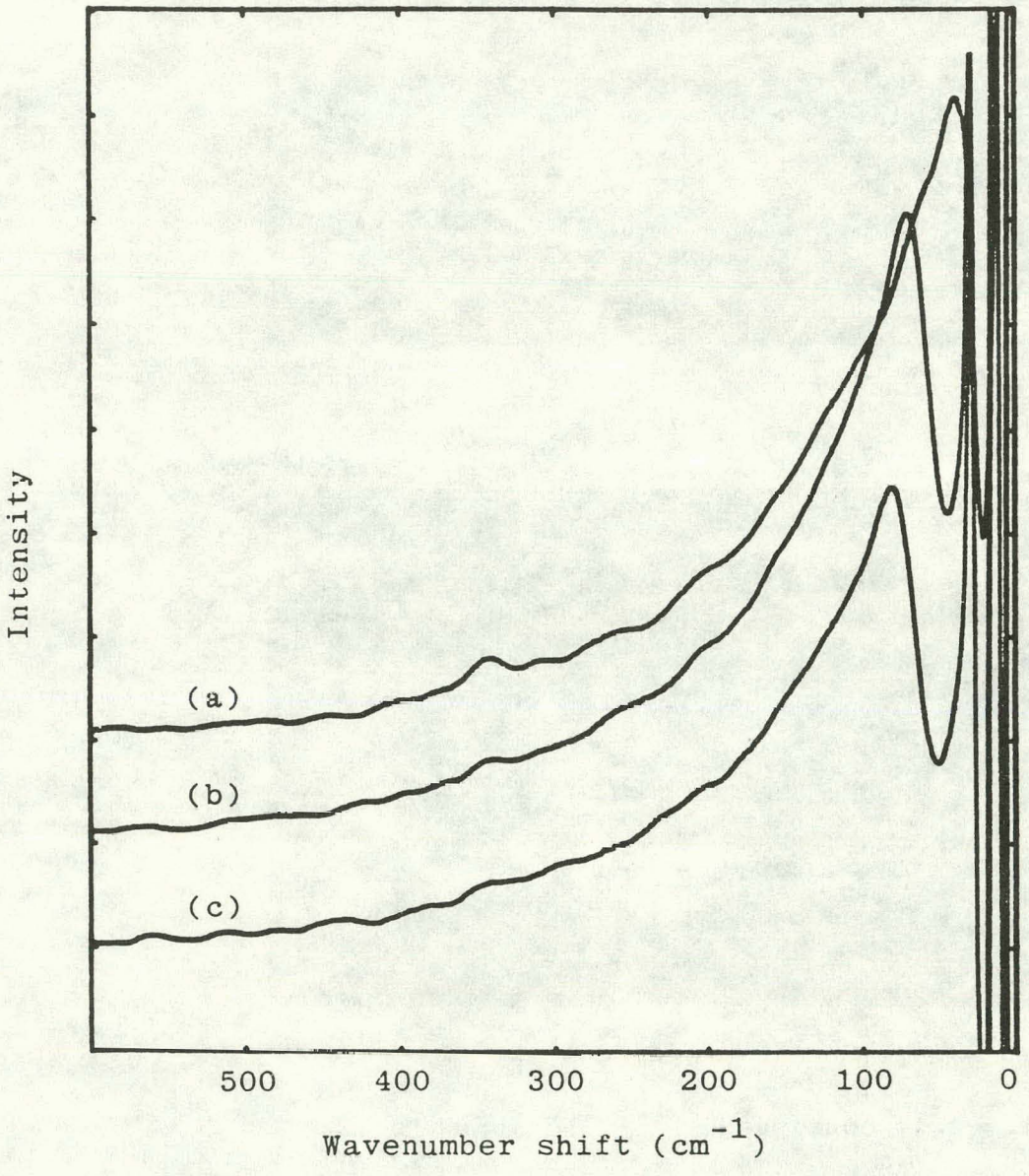

Fig. 4.45 Raman spectra of 1 wt.% $AlCl_3$ in the supporting electrolyste(NaCl:LiCl = 50:40 by weight). T=620°C. Total equivalent charge based on $AlCl_3$ content was 650 coulombs. (a) Before electrolysis; (b) After 400 coulombs of charge passed; (c) At the cathode boundary layer after 30 coulombs of charge passed.

5. ELECTROCHEMICAL STUDIES

The process of reduction of metal from molten salt media may be described as consisting of 3 different steps; the diffusion of the metal complex ion, the dissociation of the complex to metal cation and anion like chlorine ion, and the discharge of metal ion. For example, aluminum reduction from chloride melt can be described as following scheme.[99,100]

Diffusion : $AlCl_4^-$(electrolyte) → $AlCl_4^-$(electrode)

Homogeneous reaction : $AlCl_4^- = Al^{3+} + 4Cl^-$

Charge transfer : $Al^{3+} + 3e^- = Al$

Each step may be divided into still more elementary steps. The overall reduction rate is controlled by the slowest step which can be determined by electroanalytical methods such as voltammetry.

Voltammetry may be described as the electrochemical analysis in which a potential is imposed on an electrochemical cell and the resulting current response is measured. The current-potential curves can provide insight into the extent of the reversibility of an electrode reaction. Furthermore, this technique investigates the electrode processes and yields information about the reduction steps and the number of electrons involved.

There have been reported the voltammetric studies of aluminum reduction kinetics in chloride melts. Some work has been done on the system of acidic chloroaluminate melts at low temperatures,[42,101-106] and many other studies have been conducted on the deposition of aluminum from basic melts at high temperatures.[6,19,43,99,100,107-111] Most results agree on that the reduction reaction is mass transfer controlled, but there have been many reports that charge transfer step has to be considered.[6,42,43,101,103]

Less voltammetric research has been conducted on magnesium chloride system. The electrolyte has usually been the solutions of $MgCl_2$ with NaCl or KCl, or both. There has been general agreement that the deposition of magnesium is diffusion controlled.[37-39] There have been no reports of voltammetric study on systems resembling industrial electrolytes.

Cyclic voltammetry has been known as the most effective and versatile electroanalytical technique available for the mechanistic study of electrode processes.[112] It is well suited for revealing the steps in the overall reaction, determining reversibility, and identifying new species which appear as a result of combined electrochemical and chemical steps. The effectiveness of cyclic voltammetry derives from its capability to rapidly observe redox behavior over a wide range of electrode potential. The purpose of using voltammetry in the present research was to try to obtain information about the generation of short-lived species in the chloride cells. These are in effect kinetic

entities, present only during electrolysis at high current densities, and undetected by Raman spectroscopy. Cyclic voltammetry was conducted on the systems of magnesium chloride and aluminum chloride in their supporting electrolytes.

5.1 Fundamentals of Cyclic Voltammetry

Cyclic voltammetry consists of cycling the potential of an electrode which is immersed in an unstirred solution, and measuring the resulting current. A cyclic voltammogram, a display of current (vertical axis) versus potential (horizontal axis), is obtained by measuring the current at the working electrode during the potential scan. The triangular potential excitation signal sweeps the potential of the electrode between two values. The resulting current may be considered as the response signal to the potential excitation signal.

A typical cyclic voltammogram obtained in this research is shown in Fig. 5.1 for a silver working electrode in an electrolyte containing 2.2 wt.% $MgCl_2$ as electroactive species in a supporting electrolyte which contained $CaCl_2$, KCl, and NaCl at the weight ratio of 6:18:65. The initial potential E_i (a) with respect to the reference electrode is chosen to avoid any electrolysis of $MgCl_2$ when the E_i is imposed on the working electrode. The potential is then scanned negatively, as indicated by arrows. When the potential is sufficiently negative to reduce Mg^{2+}, cathodic current flows as indicated at (b), due to the electrode process,

$$Mg^{2+} + 2e^{-} \rightarrow Mg.$$

The electrode becomes a sufficiently strong reductant to reduce Mg^{2+}. The cathodic current increases rapidly (b → c) until the concentration of Mg^{2+} at the electrode surface approaches zero, and the current peaks at (c). The current then decays (c → d) as the solution surrounding the electrode is depleted of Mg^{2+} due to its electrolytic reduction to Mg.

The scan direction is switched to positive for the reverse scan (d). When the electrode becomes a sufficiently strong oxidant, Mg on the electrode is oxidized by the following electrode process (d → e).

$$Mg \rightarrow Mg^{2+} + 2e^{-}$$

The anodic current increases until the surface concentration of Mg approaches zero and the current peaks (e). The current then decays as the solution is depleted of Mg (e → f).

The important parameters of a cyclic voltammogram are the magnitudes of the peak currents, i_{pa} and i_{pc}, and the potentials at which the peaks occur, E_{pa} and E_{pc}. The position and shape of a given peak are dependent upon such factors as scan rate, electrode material, solution composition, and the concentration of reactants.

The major theoretical work on the cyclic voltammetry has been done on aqueous systems, but most of the concepts could be applied to the

molten salt systems. The basic equations for cyclic voltammetry relate the peak current (i_p) and the corresponding potential (E_p) to the electrochemical rate constant (k_s) at the standard potential (E°), the Tafel slope (b), the concentration (C), and the scan rate (v). Depending on the charge transfer reaction and the reduction product, the resulting equations are different. For a simple cathodic charge transfer under reversible conditions (O + ne = R), the peak current i_{pc} is given by the relation

$$i_{pc} = 0.4463\ (nF)^{3/2} A\ \left(\frac{Dv}{RT}\right)^{1/2} C$$

where n = number of electrons involved in the reduction,

F = Faraday constant,

A = area of the working electrode, cm^2,

v = scan rate, V/s,

C = concentration of the bulk species, mol/cm^3,

D = diffusion coefficient of the electroactive species, cm^2/s.

and others have their usual meanings. Either the number of electrons taking part in the reaction, the diffusion coefficient, or the concentration of electroactive material may be evaluated from measurement of the peak current in the reversible region if the other two quantities are independently obtainable.

The peak potential E_p for a reversible process is related to the

polarographic half-wave potential $E_{1/2}$ by the expressions

$$E_{pc} = E_{1/2} - 1.11 \frac{RT}{nF}$$

$$E_{pa} = E_{1/2} + 1.11 \frac{RT}{nF}$$

where the polarographic half-wave potential ($E_{1/2}$) is related to the standard electrode potential E° by the following equation.

$$E_{1/2} = E^\circ - \frac{RT}{nF} \ln \frac{f_{red}}{f_{ox}} \left(\frac{D_{ox}}{D_{red}} \right)^{1/2}$$

$$\simeq E^\circ$$

Under irreversible conditions, i.e., when the rate of the reverse reaction is negligible throughout the potential region studied, distinctly different equations apply. The peak current is given as

$$i_{pc} = 2.99 \times 10^5 \, n \, (\alpha N)^{1/2} \, A \, D^{1/2} \, C \, v^{1/2}$$

where α = transfer coefficient,

N = number of electrons in the rate-determining step in the process.

The peak potential for the irreversible process is also given by a different expression from that for the reversible process.

$$E_{pc} = E^\circ - \frac{RT}{\alpha NF}\left\{0.780 + 0.5 \ln\left(\frac{D(ox)\ \alpha\ N\ F\ v}{RT}\right) - \ln k_s\right\}$$

or with the expression of Tafel slope, $b(=2.303RT/\alpha NF)$,

$$E_{pc} = E^\circ - b\left\{0.52 - 0.5 \log(b/v) - \log k_s + 0.5 \log v\right\}$$

where k_s is the heterogeneous rate constant.

For quasi-reversible reactions, the responses virtually approach those of the reversible reactions at low scan rates, while they resemble those of the irreversible reactions at high scan rates. The potential difference between cathodic and anodic peaks, ΔE_p, or the dependence of the potential of the peak on scan rate may be used as tests for the reversibility of the reaction.

All the above considerations have been based on the assumption that the reaction product is soluble either in the solvent or in the electrode (e.g. liquid cathode). If the product is insoluble (for example, solid deposit), different equations may have to be applied. Diagnostic criteria for different reactions are shown in Table 5.1.

Table 5.1 Diagnostic Criteria For Charge Transfer Reactions[105]

1. Reversible Charge Transfer

E_p : Independent of v

$E_{pc} - E_{pa}$ = 2.22RT/nF (V) and independent of v

$i_p/v^{1/2}$: independent of v

i_{pc}/i_{pa} = 1

2. Quasi-reversible Charge Transfer

E_p shifts with v

$E_{pc} - E_{pa}$ = 2.22RT/nF (V) at low v,
but increases with v

$i_p/v^{1/2}$: virtually independent of v

i_{pa}/i_{pc} = 1 only for α=0.5

* As v increases, the response approaches those for the irreversible charge transfer.

3. Irreversible Charge Transfer

E_p shifts cathodically by a factor of
1.151RT/αnF (V) for 10-fold increase in v.

$i_p/v^{1/2}$: constant with v

* There is no current on the reverse scan.

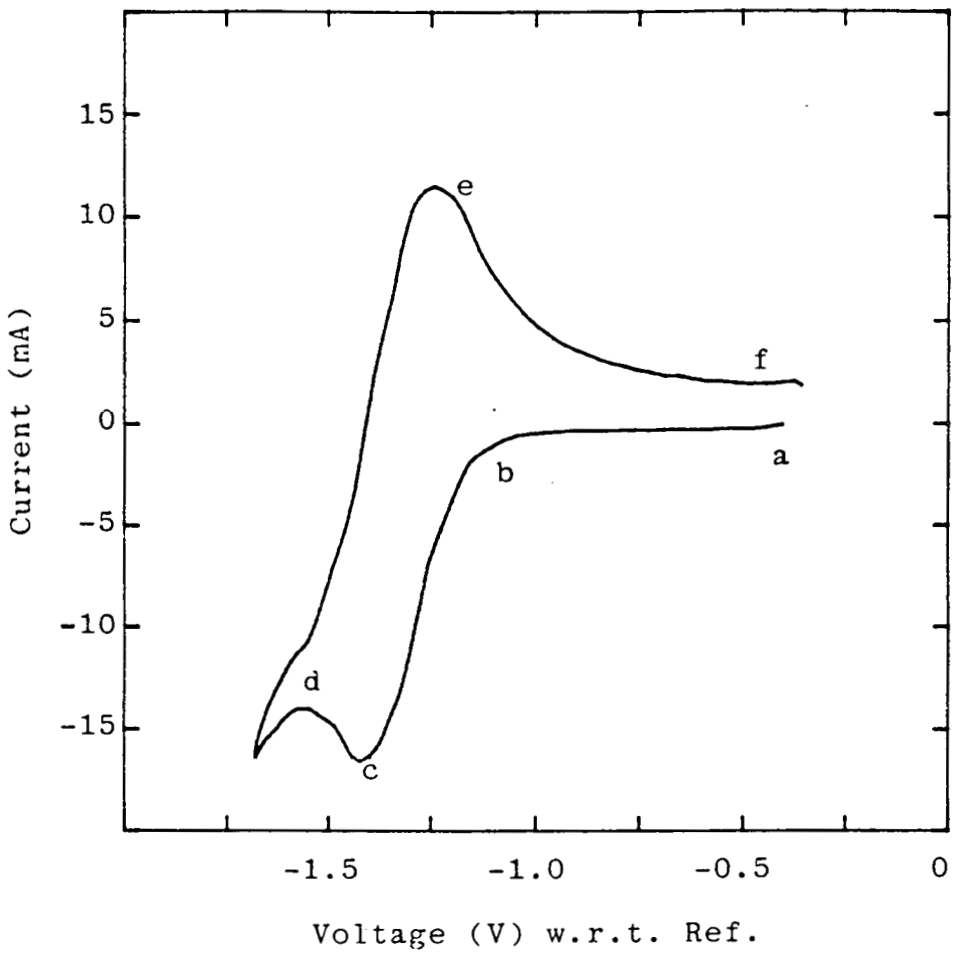

Fig. 5.1 A typical cyclic voltammogram of 2.2 wt.% $MgCl_2$ in $CaCl_2$ - KCl - NaCl mixture melt in the weight ratio of 6:18:65. Working electrode: Silver. Area: 0.08 cm^2. T=800°C. v=0.2 V/s.

5.2 Experimental

Experiments were conducted in the same furnace as that described in Raman Scattering Studies section. The only difference was the size which was increased to accommodate the bigger electrolysis cells. The windows were of great help for checking the electrode position or for observing the occurrences in the electrolyte. The working condition of the furnace was chosen to eliminate the thermal convection in the cell by calibrating the furnace for uniform temperature at the window level. The salts were purified by the method described earlier.

The cell for cyclic voltammetry was made of fused quartz (52 mm O.D.). The stainless steel cap has 7 fittings, 2 gas ports, and one 3/8 in. O.D. tube which accessed the cell by means of a 3/8 in. valve. (Fig. 5.2) The fittings were used for a thermocouple, a reference electrode, cathode and anode for pre-electrolysis, and a counter electrode and two working electrodes for voltammetry. Due to the detachability, the valved tube allowed melt composition to be regulated and sampled as well as to introduce a new electrode, all without interruption of the experiment.

Working electrodes were made from different solid substances such as platinum, gold, silver, tungsten, and pyrolytic graphite. The electrodes were usually sealed with an fused quartz tubing so that only controlled area can be exposed to the solution. The shapes of wire and flag were also used as working electrode, when the sealing was diffi-

cult. The area of the working electrode was made much smaller than that of the counter electrode so that the counter electrode might not be polarized to an appreciable extent, and thus, the cell current could reflect the reaction at the working electrode. The counter electrode consisted of 3 mm diameter glassy carbon one end of which was ground to a point so that the gas evolution during measurement could be smooth and cause minimal disturbance of the electrolyte.

Reference electrodes used the asbestos fiber as the diaphragm and were prepared in the following steps. The asbestos wick (7 mm long) is inserted into the one end of the 7 cm-long 8 mm-diameter fused quartz tubing which was made 2 - 3 mm by pulling in the flame. The tube with the asbestos wick is heated to burn away any cotton threads and the binders in the asbestos. The tube is squeezed onto the asbestos in the extent that it can hold the wick tightly, but not completely seal the end. The tip is checked for small leaks by testing with a Tesla coil after evacuation. The well-made tip has a small leak at the asbestos fiber, and a fine blue spark can be seen going from the Tesla coil into the tip. Tips with no leak or big leak cannot show these spark. This tubing is joint to 6 mm diameter quartz tubing. A 1 mm diameter silver wire is used for the reference electrode. One end of this wire is coiled to give a large surface area Ag/Ag^{+} exchange reaction when the wire is dipped in the melt. The electrolyte for the reference electrode is charged in the glove box filled with dry argon gas. For the $MgCl_2$ study, the electrolyte for the reference electrode was a solution of AgCl (5 weight percent) in the supporting electrolyte for magnesium electrolysis, i.e., $CaCl_2$-KCl-NaCl in the ratio of 6:18:65 by weight,

and a solution of AgCl/NaCl/LiCl (5:53:42 by weight) for $AlCl_3$ electrochemistry,

For pre-electrolysis, a platinum plate (4 mm x 8 mm) or a glassy carbon rod (1/8 in. diameter) served as cathode, and as anode, glassy carbon rod usually was used. As a working electrode, silver, gold, glassy carbon, tungsten, titanium diboride, or platinum has been tried.

Measurements were conducted with a Potentiostat/Galvanostat, PAR Model 173, and a Universal Programmer, PAR Model 175. Slow scan responses were recorded by a X-Y recorder, Hewlett Packard 7004B X-Y, while fast responses were recorded and stored with a Digital computer, DEC MINC 23. The FORTRAN programs for the measurements are shown in the Appendix 2.

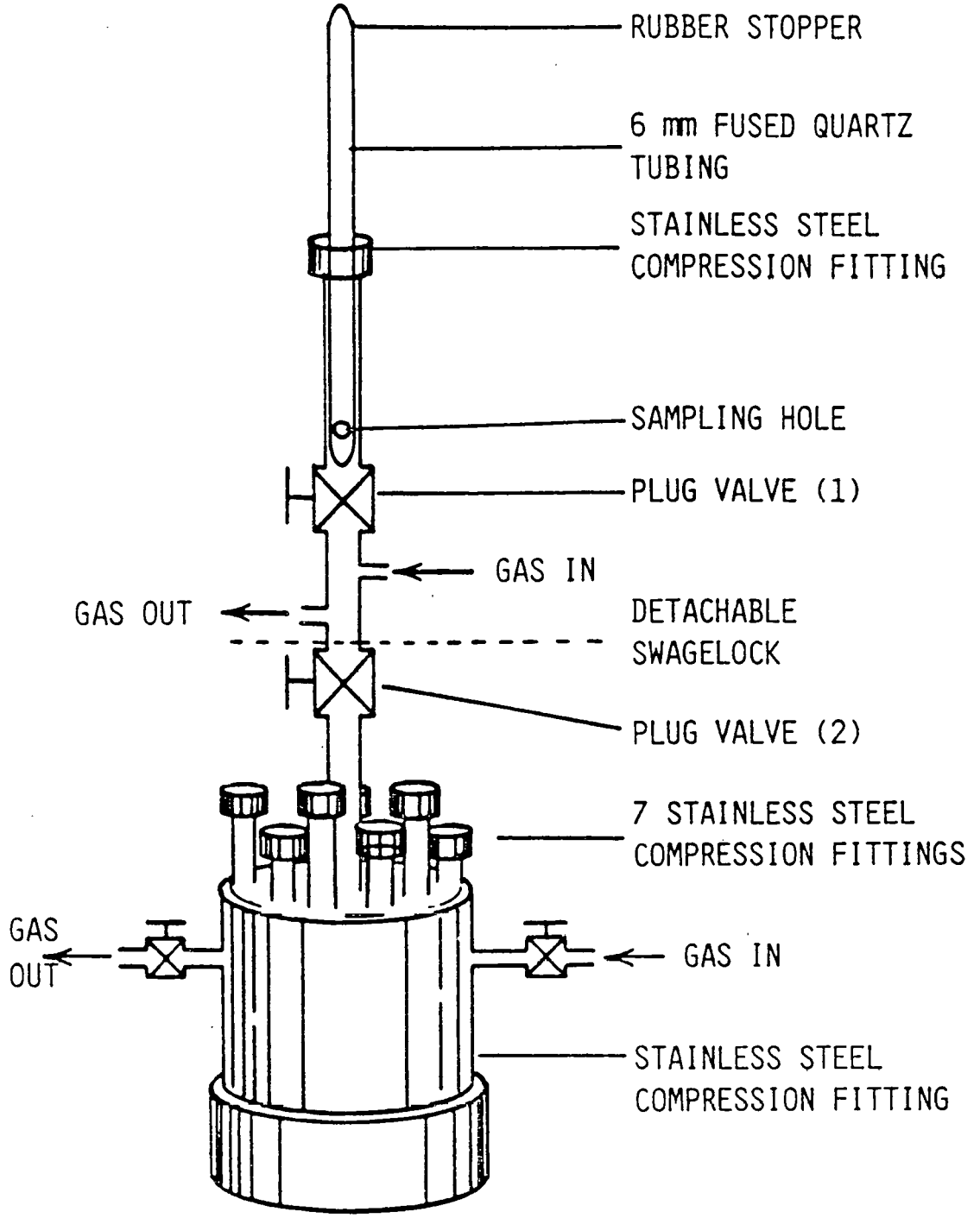

Fig. 5.2 Schematic of cell cap for voltammetric study. The detached valve(1) is connected to the valve(2) after purging the connection tube with argon gas.

5.3 Results and Discussion

5.3.1 Mg^{2+} reduction in $MgCl_2$-$CaCl_2$-KCl-NaCl melt

The electrochemical behavior of the solvent electrolyte was first examined. The standard decomposition potentials of pure $MgCl_2$, NaCl, and AgCl at 750°C were calculated as about -2.49,[9] -3.25,[113] and -0.84 V,[114] respectively. These values were calculated for pure liquid states, and thus, they are not representative of the true decomposition potentials in the solution. The decomposition potentials in the solution at the compositions considered in this research could not be found in the literature. For the determination of the scan range, however, these values may be accepted. Fig. 5.3 shows the voltammogram of the molten $CaCl_2$-KCl-NaCl mixture in the weight ratio of 6:18:65 which resembles the composition of the industrial supporting electrolyte.

In Fig. 5.3, the voltage on the abscissa shows the potential of the working electrode (in this case, tungsten) with respect to the reference electrode. The reference electrode was silver wire immersed in the molten mixture of AgCl-$CaCl_2$-KCl-NaCl (5:6:18:65 by weight). Since the voltage range of interest for $MgCl_2$-$CaCl_2$-KCl-NaCl electrolyte lies up to -1.65 V with respect to silver reference electrode, the voltammogram in Fig. 5.3 was generated by scanning up to -1.75 V at a scan rate of 50 mV/s. The residual current was very low (less than 1 mA) in the potential range of magnesium deposition, and it did not

decrease with pre-electrolysis. The cathodic current started to increase at the voltage of about -1.7 V, which was thought to be due to the electrolysis of Na^+. It was supported by the fact that the anodic charge was very low compared to the cathodic charge indicating sodium dissolution in the melt. The low residual current clearly demonstrates that the developed purification method using $SOCl_2$ provides materials suitable for this kind of electroanalytical studies without further purification.

Fig. 5.4 shows a typical cyclic voltammogram for the deposition of magnesium at silver working electrode at 750°C from a melt containing 2.2 weight percent of $MgCl_2$. The solvent melt composition was $CaCl_2$-KCl-NaCl in the weight ratio of 6:18:65. The reference electrode was the same as that described above. The scan rate was 0.4 V/s and the area of the working electrode was 0.08 cm^2. The well defined trace shows clearly the reduction and oxidation processes. The fact that the current does not increase sharply in Fig. 5.4 with the onset of reduction is consistent with the formation of a soluble reaction product which is expected under the circumstances, since magnesium alloys with silver under these conditions. The cathodic wave was found to obey the Heyrovsky-Ilkovic relationship (Fig. 5.5), which confirms the soluble product.[115]

The value of the potential difference between peak potentials for the cathodic and reoxidation processes was observed to be greater than expected for a simple reversible process. The equation given by Nicholson and Shain[116] predicts 98 mV for 2 electron process, while

Fig. 5.4 shows about 182 mV which is close to 196 mV for 1 - electron process. However, the scan rate had essentially no effect on the difference in the peak potentials, and the ratios of anodic peak current to the cathodic current were not unity.(Fig. 5.6) These observations are in conformity with the quasi-reversible process. Thus, it may be too early to state that there is a monovalent species being reduced at the working electrode. This observation was in good agreement with literature.[37,117]

Fig. 5.7 shows a cyclic voltammogram obtained for the deposition of magnesium at platinum working electrode from the same melt described in the previous paragraph. The scan rate was 0.1 V/s and the area of the working electrode was 0.08 cm^2. The voltammogram in Fig. 5.7 is characteristic of the strong adsorption of the reduction product. The weak peak at -1.2 V on the reduction curve and the strong peak at -0.82 V on the oxidation curve are thought to be representative of the adsorption.[112,118,119] Furthermore, in the case of a platinum working electrode, the cathodic peak potential shifted to more cathodic values as the scan rate increased, whereas the anodic peak potential remained unchanged(Fig. 5.8), resulting in much greater value of the difference in the peak potentials than that in the case of silver electrode. With working electrode of glassy carbon, no sharp cathodic peak could be observed.(Fig. 5.9) Instead, a broad wave followed by a sharp increase in the current on the reduction curve and several peaks on the oxidation curve were generated. This observation was in good agreement with the literature[39] which explained them by the deposition of magnesium and sodium. The bumps at -1.5 V and -0.5 V on the oxidation curve were

explained by oxidation of pure sodium and the sodium penetrating the carbon electrode, respectively. The monovalent species could not be detected at platinum or glassy carbon working electrodes.

The cathodic peak current vs (scan rate)$^{1/2}$ plots were linear and within experimental error, passed through the origin (Fig. 5.10,11). This confirmed that the magnesium reduction process was diffusion controlled in the experiments as conducted.

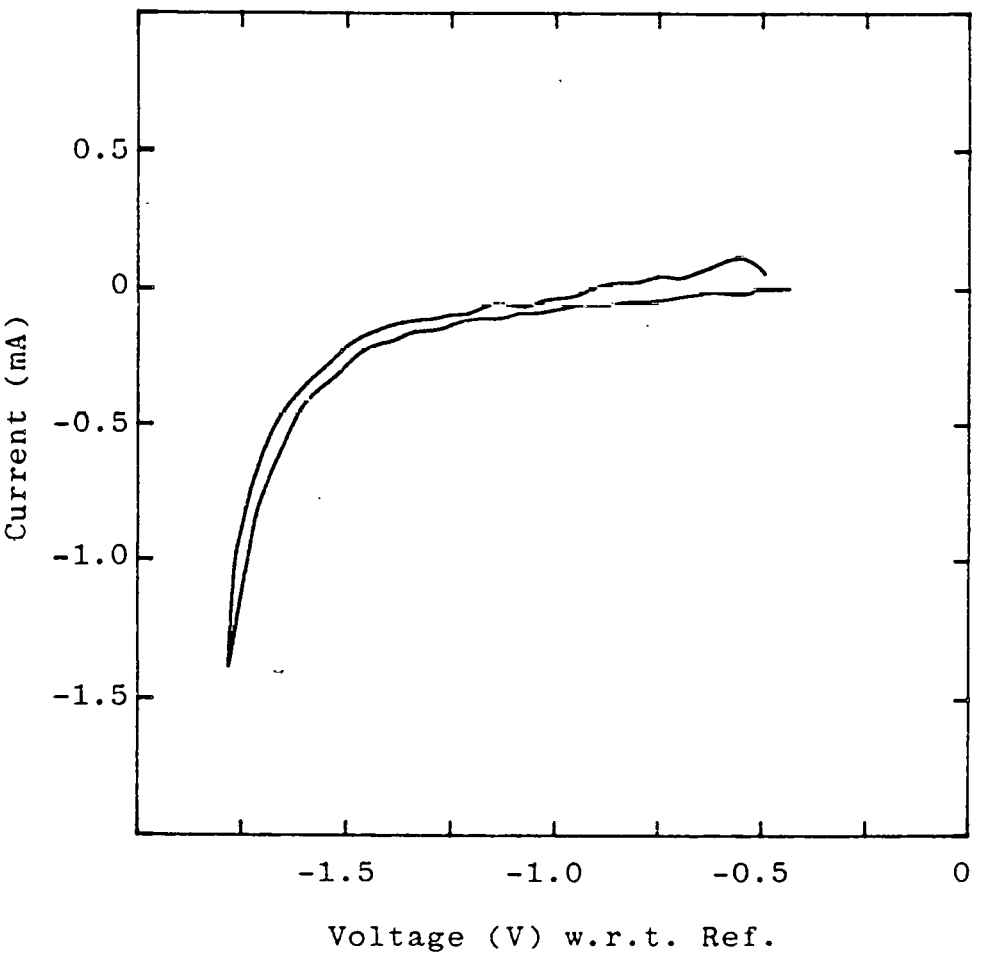

Fig. 5.3 Residual current in the $CaCl_2$-KCl-NaCl mixture melt in the weight ratio of 6:18:65. Working electrode: Tungsten. Area: 0.0242 cm^2. T=750°C. v=0.05 V/s.

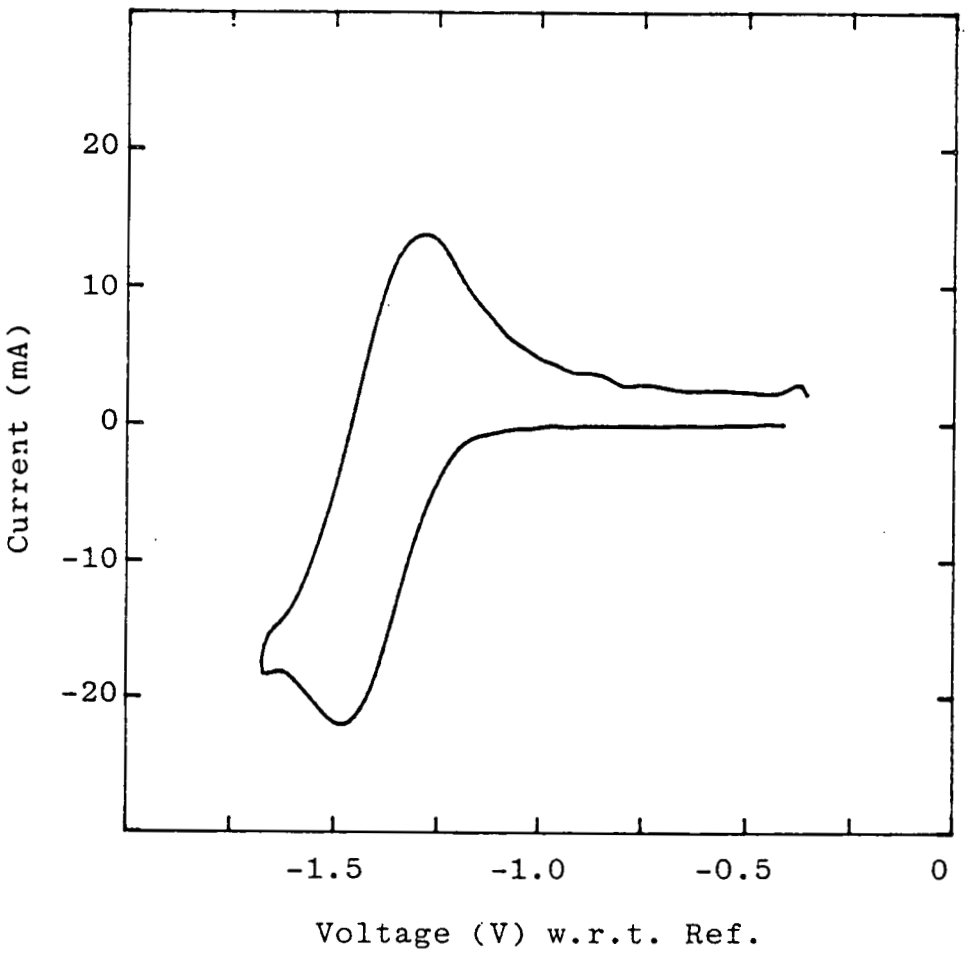

Fig. 5.4 Voltammogram of 2.2 wt.% $MgCl_2$ in the molten $CaCl_2$-KCl-NaCl mixture in the weight ratio of 6:18:65. Working electrode: Silver. T=750°C. Area: 0.08 cm^2. v=0.4 V/s.

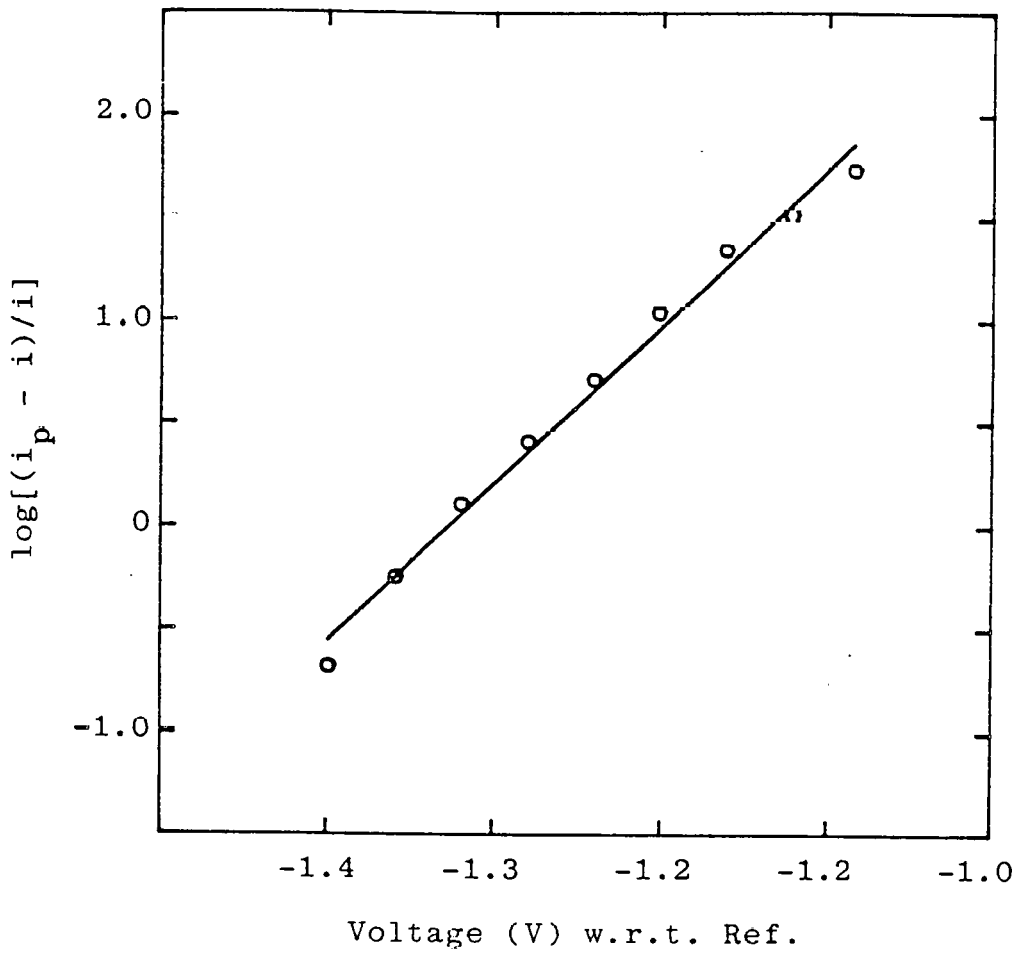

Fig. 5.5 A plot of $\log[(i_p - i)/i]$ vs V on the reduction wave for the Mg^{2+} reduction at silver working electrode. $MgCl_2$ content: 2.2 wt.% in the molten $CaCl_2$-KCl-NaCl mixture in the weight ratio of 6:18:65. Area: 0.08 cm^2. T=750°C. v=0.4 V/s.

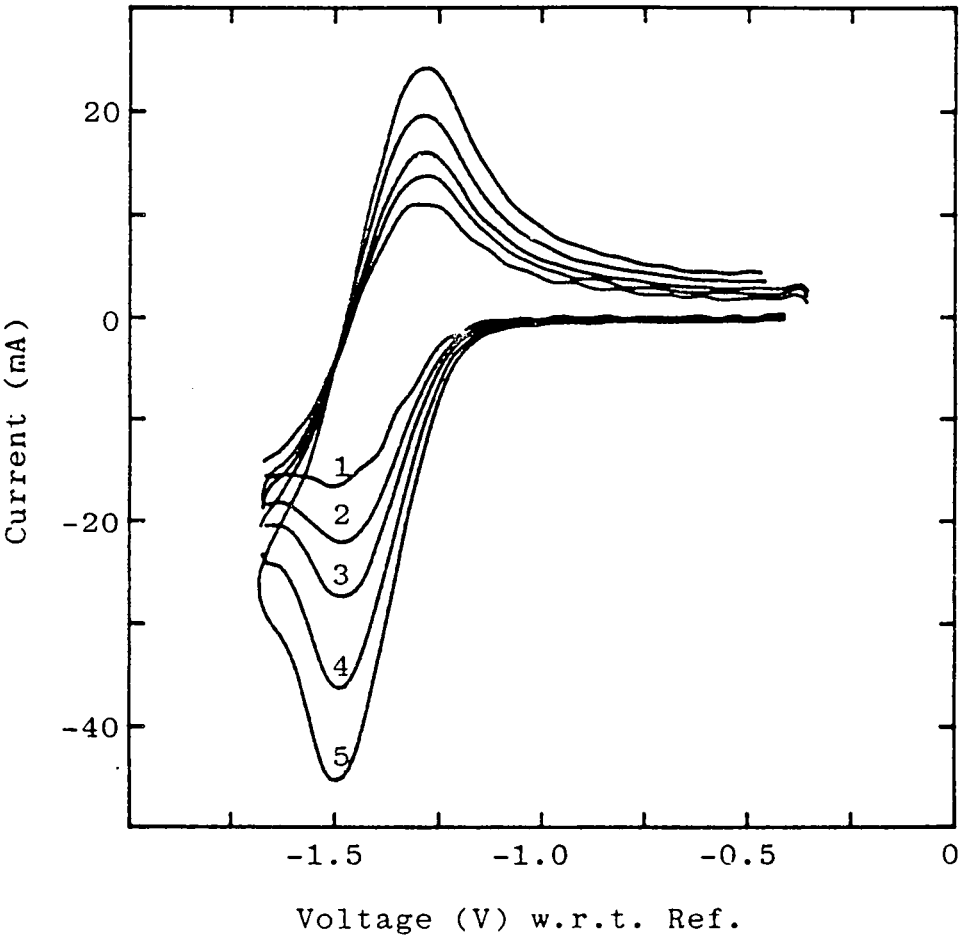

Fig. 5.6 Cyclic voltammograms at different scan rates for 2.2 wt.% $MgCl_2$ in the molten $CaCl_2$-KCl-NaCl mixture in the weight ratio of 6:18:65. Working electrode: Silver. Area: 0.08 cm^2. T=750°C. (1) 0.2 V/s; (2) 0.4 V/s; (3) 0.6 V/s; (4) 1.0 V/s; (5) 1.5 V/s.

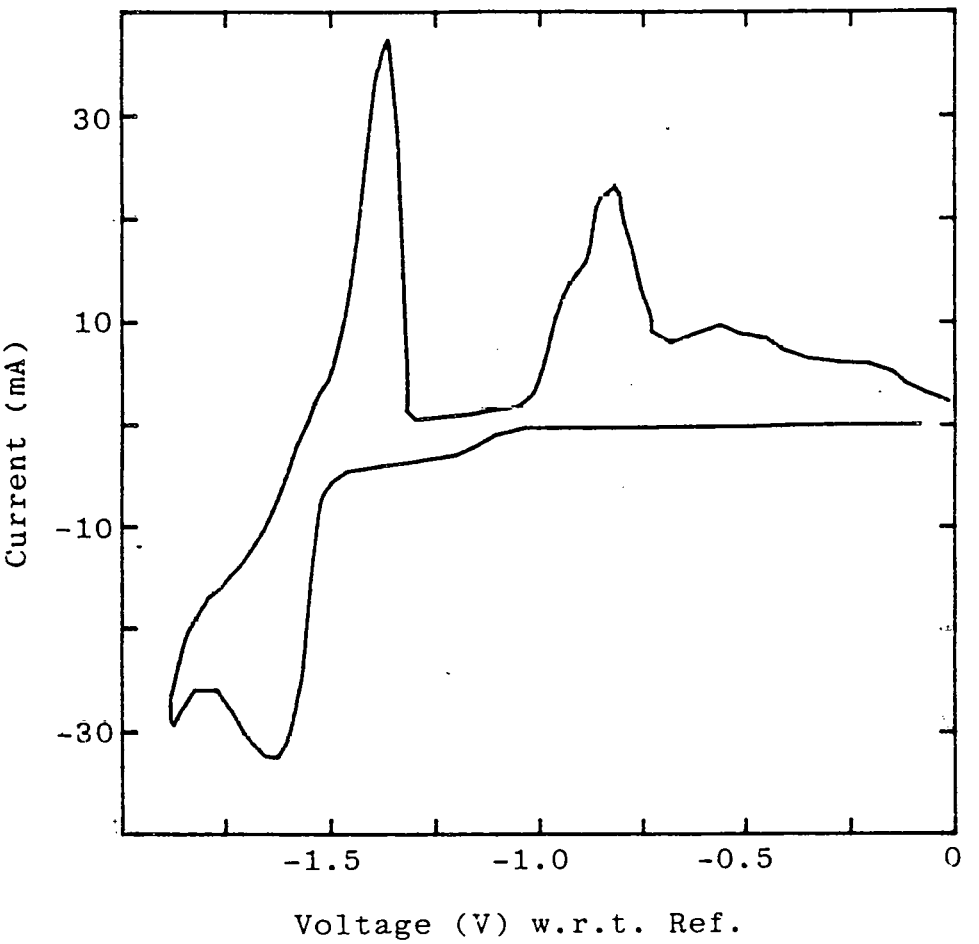

Fig. 5.7 Cyclic voltammogram of 2.2 wt.% $MgCl_2$ in the molten $CaCl_2$-KCl-NaCl mixture in the weight ratio of 6:18:65. Working electrode: Platinum. Area: 0.08 cm^2. T=750°C v=0.1 V/s.

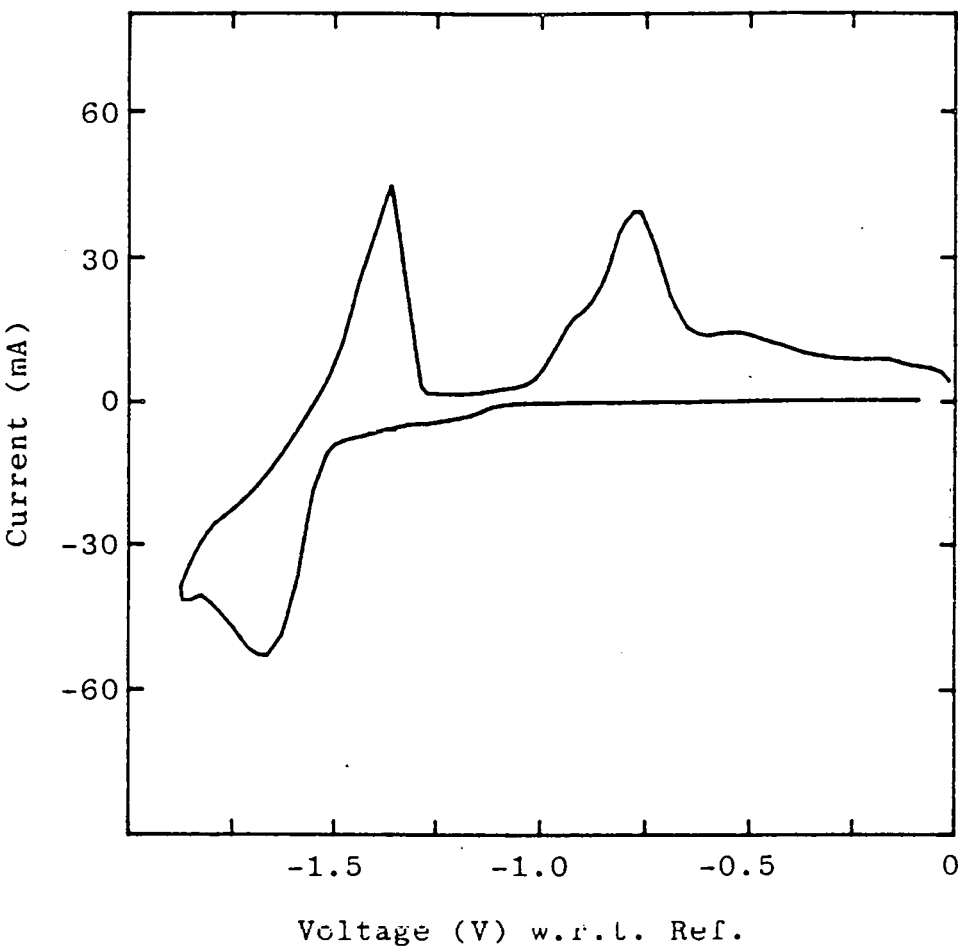

Fig. 5.8 Cyclic voltammograms at different scan rates for 2.2 wt.% $MgCl_2$ in the molten $CaCl_2$-KCl-NaCl mixture in the weight ratio of 6:18:65. Working electrode: Platinum. Area: 0.08 cm^2. T=750°C. (a) v=0.3 V/s.

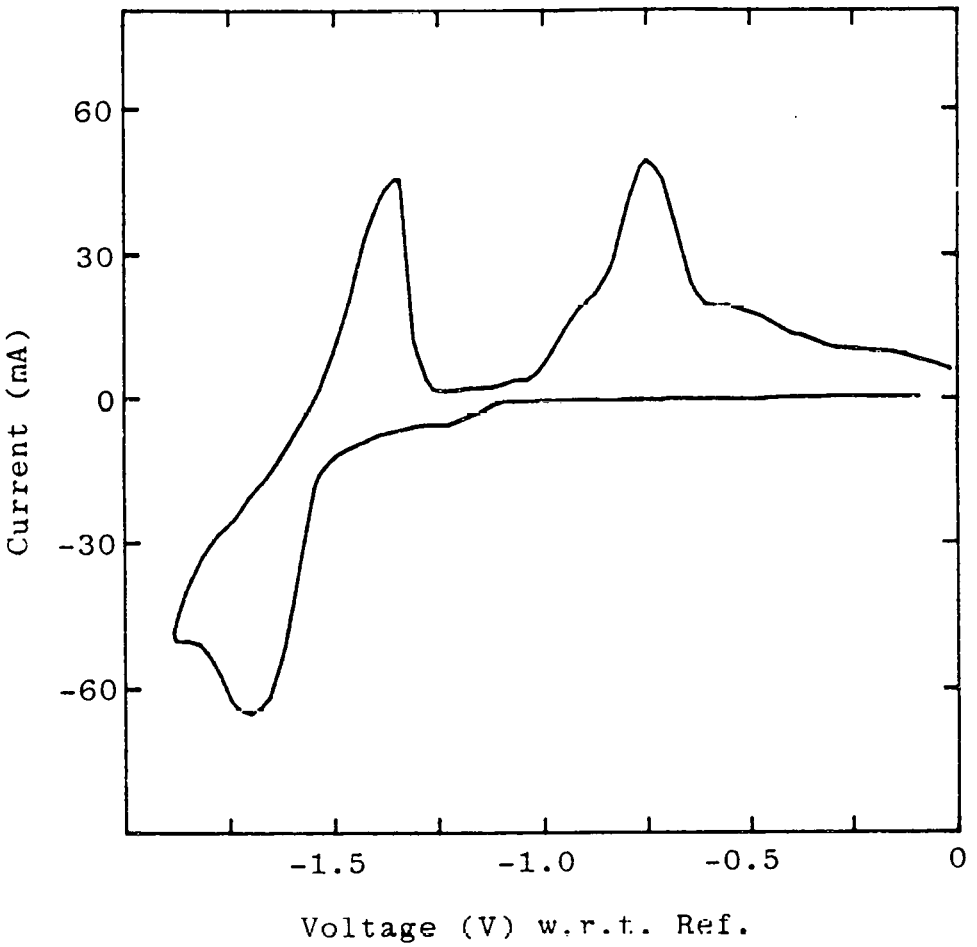

Fig. 5.8 (b) v=0.5 V/s.

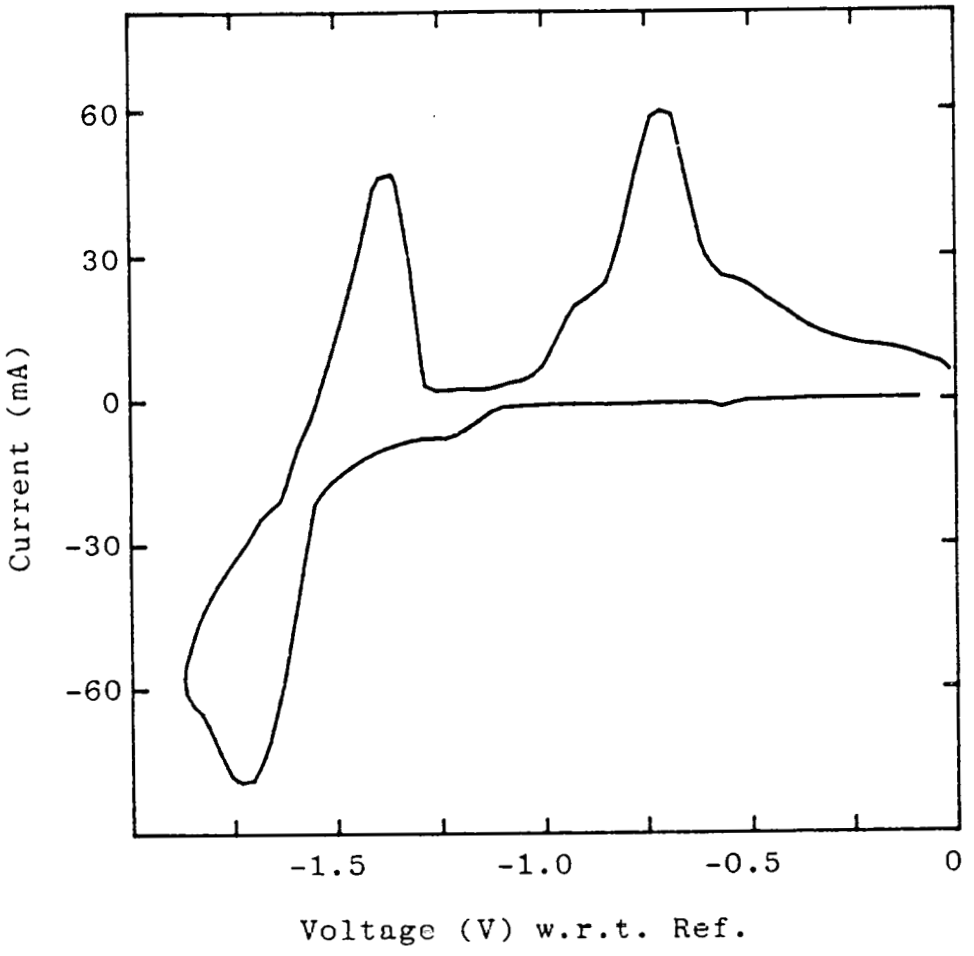

Fig. 5.8 (c) v=0.8 V/s.

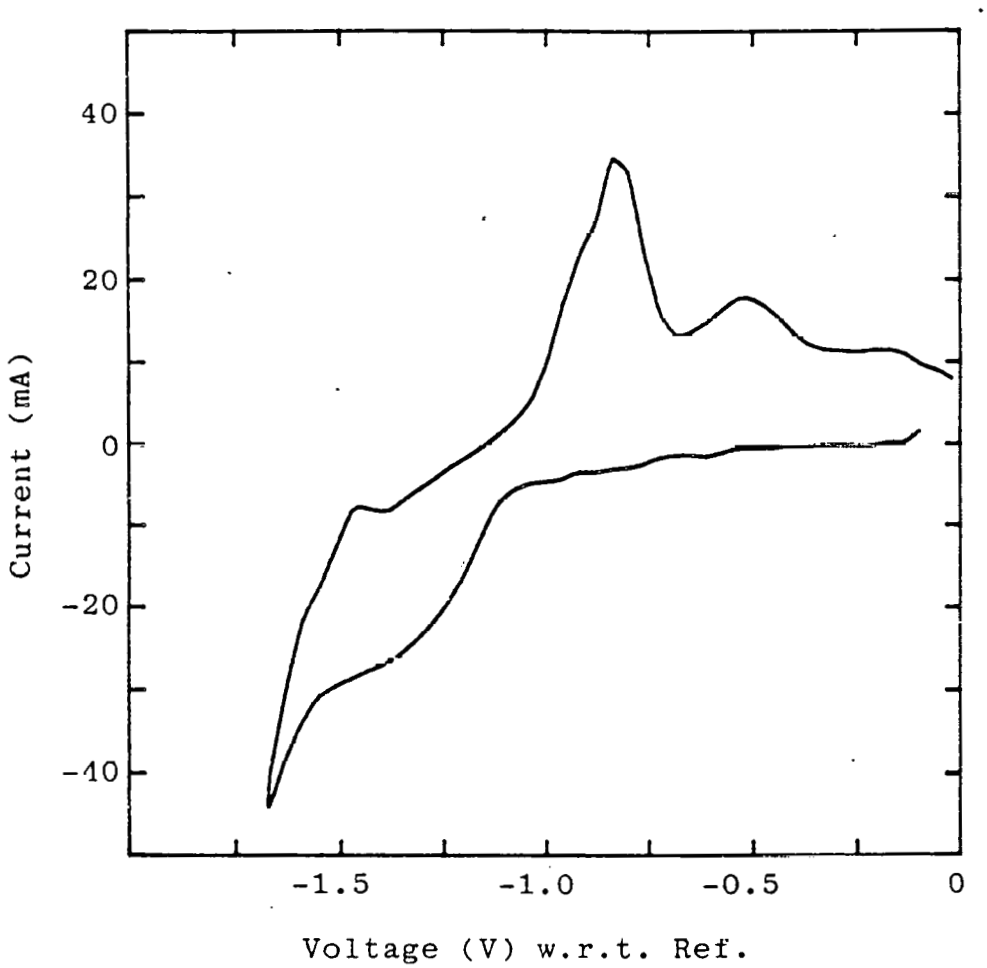

Fig. 5.9 Cyclic voltammogram at glassy carbon electrode for 2.2 wt.% $MgCl_2$ in the molten $CaCl_2$-KCl-NaCl mixture in the weight ratio of 6:18:65. Area: 0.542 cm^2 T=750°C. v=0.1 V/s.

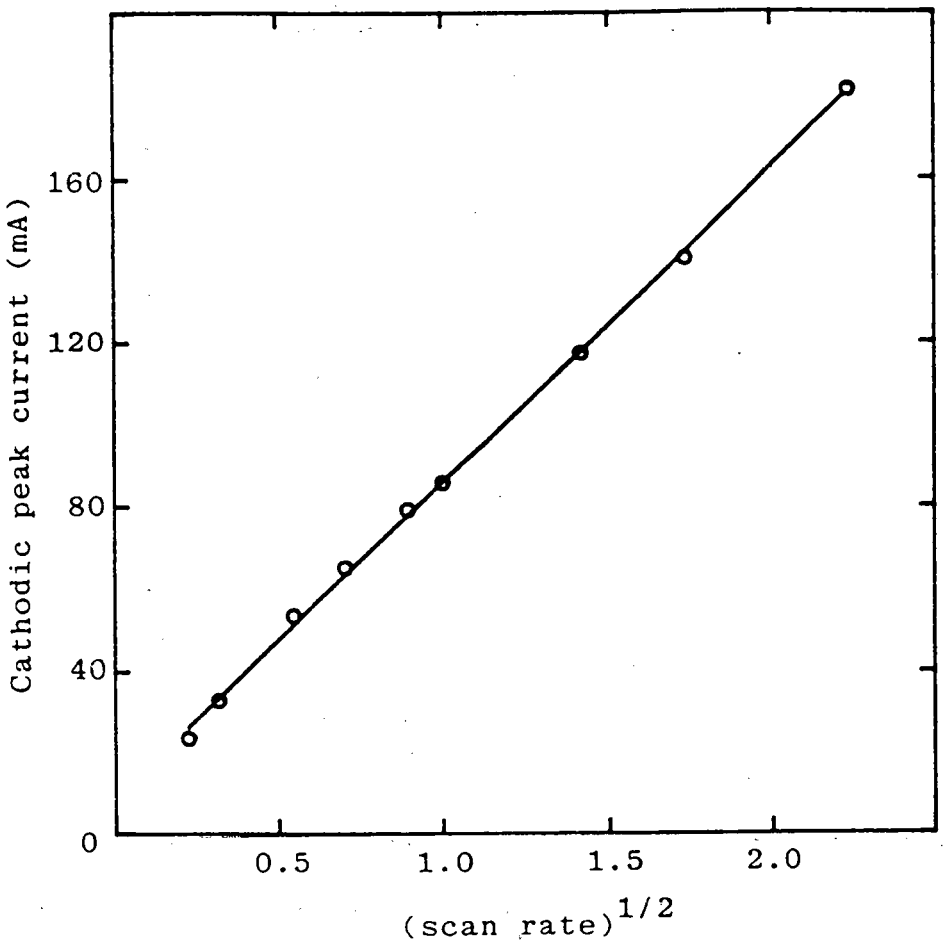

Fig. 5.10 A plot of the cathodic peak current vs (scan rate)$^{1/2}$ for Mg^{2+} reduction at silver electrode. $MgCl_2$: 2.2 wt.% in the molten $CaCl_2$-KCl-NaCl mixture in the weight ratio of 6:18:65. T=750°C. Area: 0.08 cm^2.

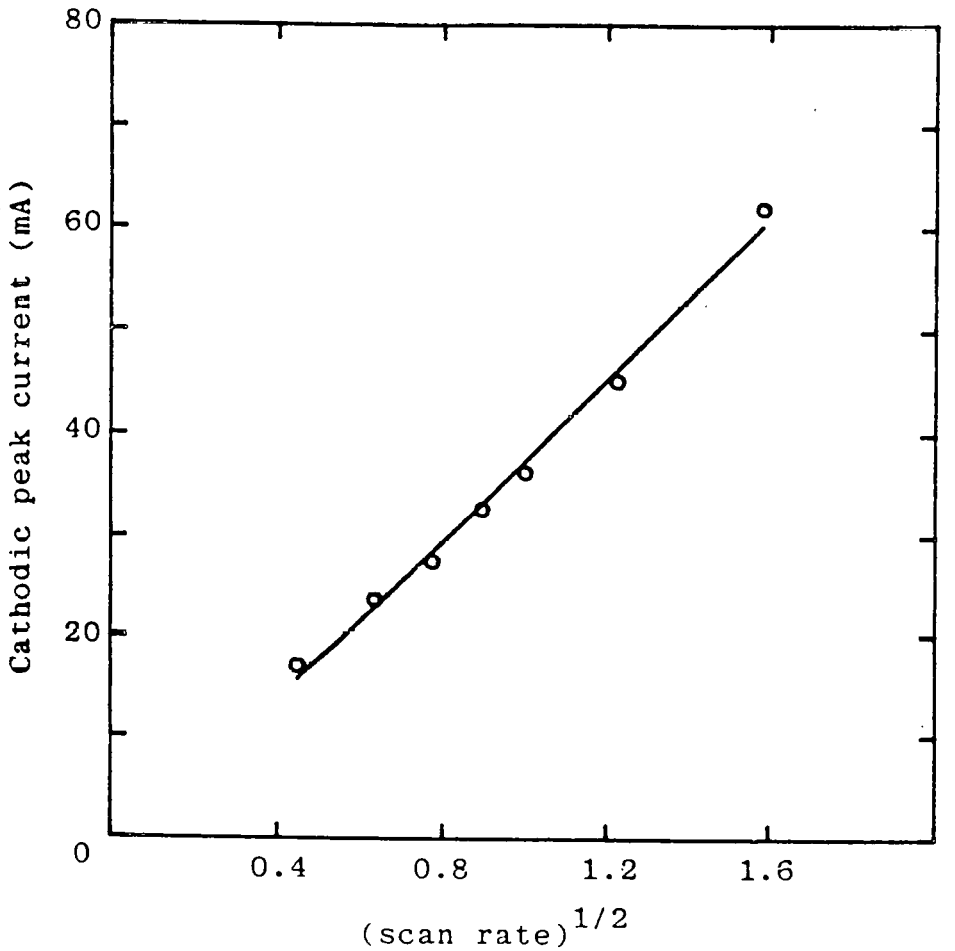

Fig. 5.11 A plot of the cathodic peak current vs (scan rate)$^{1/2}$ for the reduction of Mg^{2+} at platinum electrode. $MgCl_2$: 2.2 wt.% in the molten $CaCl_2$-KCl-NaCl mixture in the weight ratio of 6:18:65. T=750°C A=0.08 cm^2.

5.3.2 Al^{3+} reduction in $AlCl_3$-LiCl-NaCl melt

The voltammetric study was also conducted on Al deposition from $AlCl_3$-LiCl-NaCl melt. Fig. 5.12 shows a typical cyclic voltammogram obtained using a gold working electrode. The electrolyte contained 1.5 wt.% $AlCl_3$ in the supporting solvent of LiCl-NaCl mixture in the weight ratio of 40:50. The temperature was 700°C. The reference electrode was silver wire immersed in the molten mixture of AgCl-LiCl-NaCl (5:42:53 by weight). Glassy carbon served as the counter electrode. The scan rate was 0.05 V/s and the area of the working electrode was 0.173 cm^2. In Fig. 5.12, the reduction and oxidation processes can clearly be observed. It may also be observed that the cathodic current does not increase sharply, as in the case of magnesium reduction at silver, which suggested the soluble product to the electrode. The rising portion of the cathodic wave was found to obey Heyrovsky-Ilkovic relationship, which confirms the soluble product.(Fig. 5.13)

In Fig. 5.12, the reduction and oxidation peaks are found at -0.545 and -0.489 V with respect to the reference electrode, respectively. In Fig. 5.14, it may be observed that the peak potentials are unchanged with increased scan rates. The difference in the peak potentials was observed to be 56 mV. This value is close to the theoretical value of 62 mV for the simple reversible 3-electron reduction process. However, the ratio of the anodic peak current to the cathodic current is much greater than unity, eliminating the possibility of a simple reversible reaction. With the fact that the peak potentials did not changed with

scan rates, it was concluded that the reduction process at gold electrode was quasi-reversible. Temperature difference was not found to have any appreciable effects on the voltammogram.(Fig. 5.15)

Fig. 5.16 shows a cyclic voltammogram obtained at silver working electrode for the deposition of aluminum from the melt containing 1 wt.% $AlCl_3$ in LiCl-NaCl mixture(40:50 by weight). The temperature was 700°C and the area of the working electrode was 0.097 cm^2. The scan rate was 0.3 V/s. This voltammogram is also characteristic of the formation of soluble product, which may be confirmed by the Heyrovsky-Ilkovic relation.(Fig. 5.17) The difference between the cathodic and anodic peak potentials was 76 mV. Considered that the ratio of anodic peak current to the cathodic peak current is greater than unity for a simple reversible reaction, no information could be obtained about subvalent species. This observation is essentially identical to that of Bouteillon and Marguier.[107] It was concluded that the aluminum reduction from aluminum chloride is a quasi-reversible process over the range of the experiments conducted.

The cathodic peak current was found to be linear in the square root of scan rate, which, within the experimental error, passed through the origin.(Fig. 5.18,19) It may be drawn a conclusion that aluminum reduction from $AlCl_3$-LiCl-NaCl melt is controlled by diffusion in the concentration range studied (1 - 2.2 wt.% $AlCl_3$). This is in good agreement with many reports,[19,109-111] even though some intermediate species have been reported.[42]

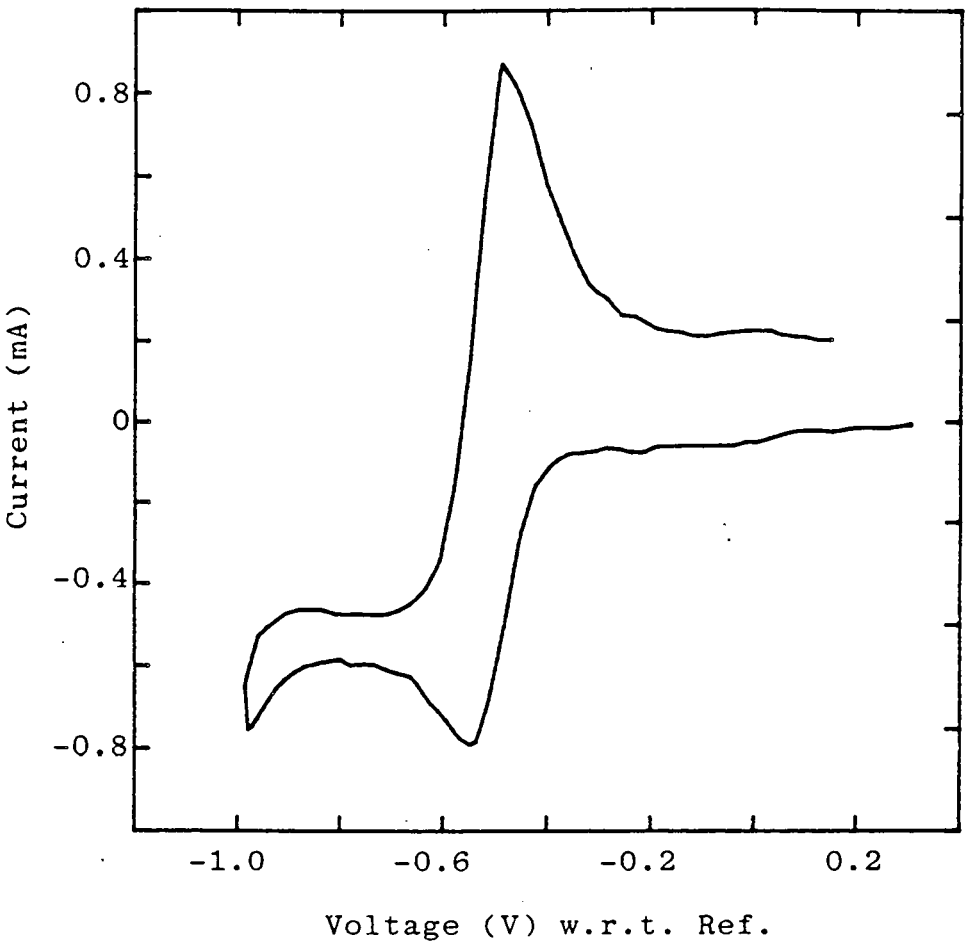

Fig. 5.12 A cyclic voltammogram for 1.5 wt.% $AlCl_3$ in the molten LiCl-NaCl mixture in the weight ratio of 40:50. Working electrode: Gold. Area: 0.173 cm^2 T=700°C. v=0.05 V/s.

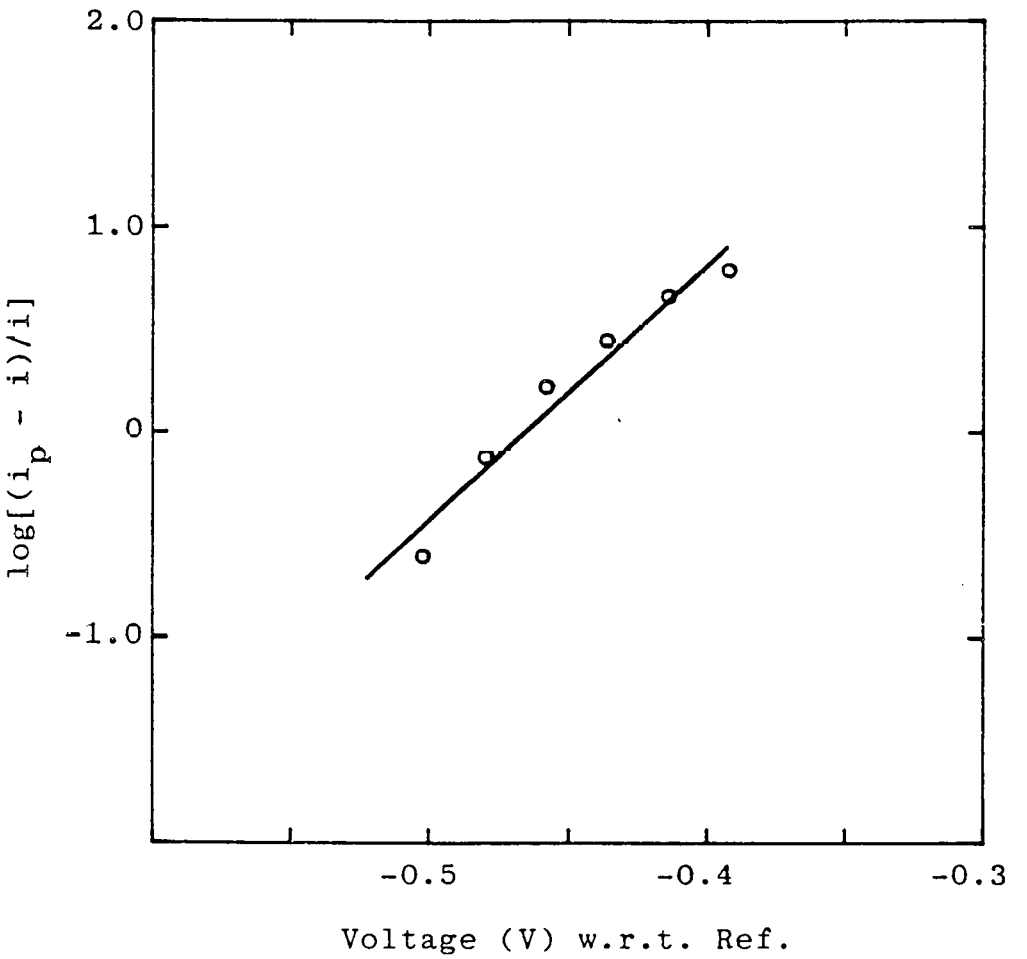

Fig. 5.13 A plot of $\log[(i_p - i)/i]$ vs V on the cathodic wave for Al^{3+} reduction at gold working electrode. $AlCl_3$ content: 1.5 wt.% in the molten LiCl-NaCl mixture in the weight ratio of 40:50. Area: 0.173 cm^2. T=700°C. v=0.05 V/s.

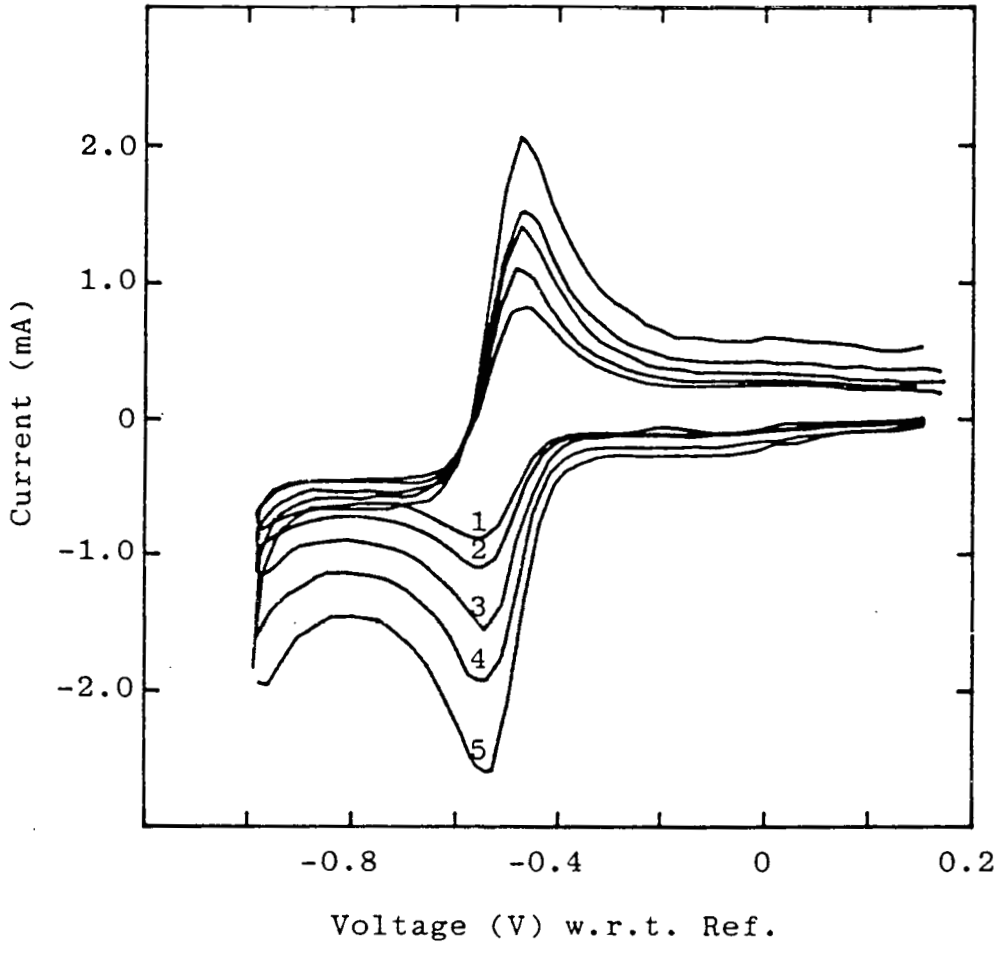

Fig. 5.14 Cyclic voltammograms at different scan rates for 1.5 wt.% $AlCl_3$ in the molten LiCl-NaCl mixture in the weight ratio of 40:50. T=700°C. Working electrode: Gold. Area: 0.173 cm^2.
(1) 0.08 V/s; (2) 0.15 V/s; (3) 0.2 V/s; (4) 0.5 V/s; (5) 1.0 V/s.

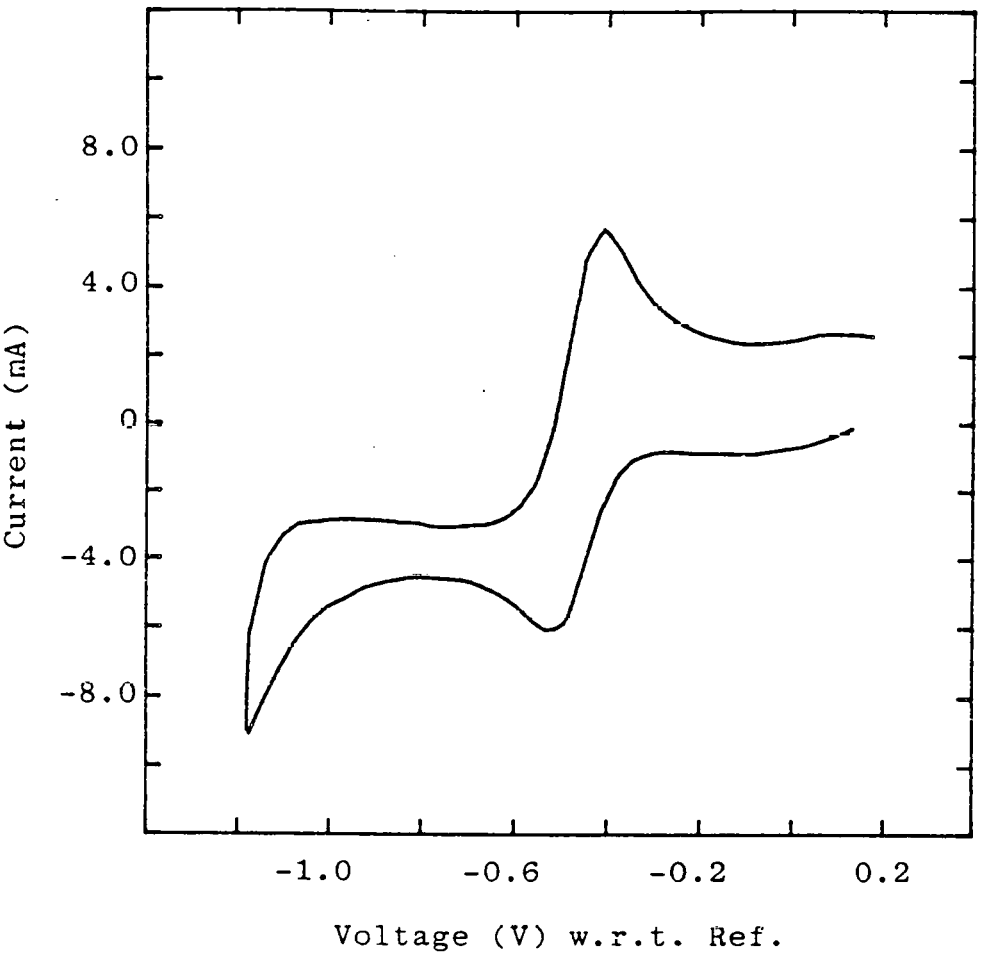

Fig. 5.15 A cyclic voltammogram at 800°C for 1.5 wt.% $AlCl_3$ in the molten LiCl-NaCl mixture in the weight ratio of 40:50. Working electrode: Gold. Area: 0.173 cm^2. v=0.5 V/s.

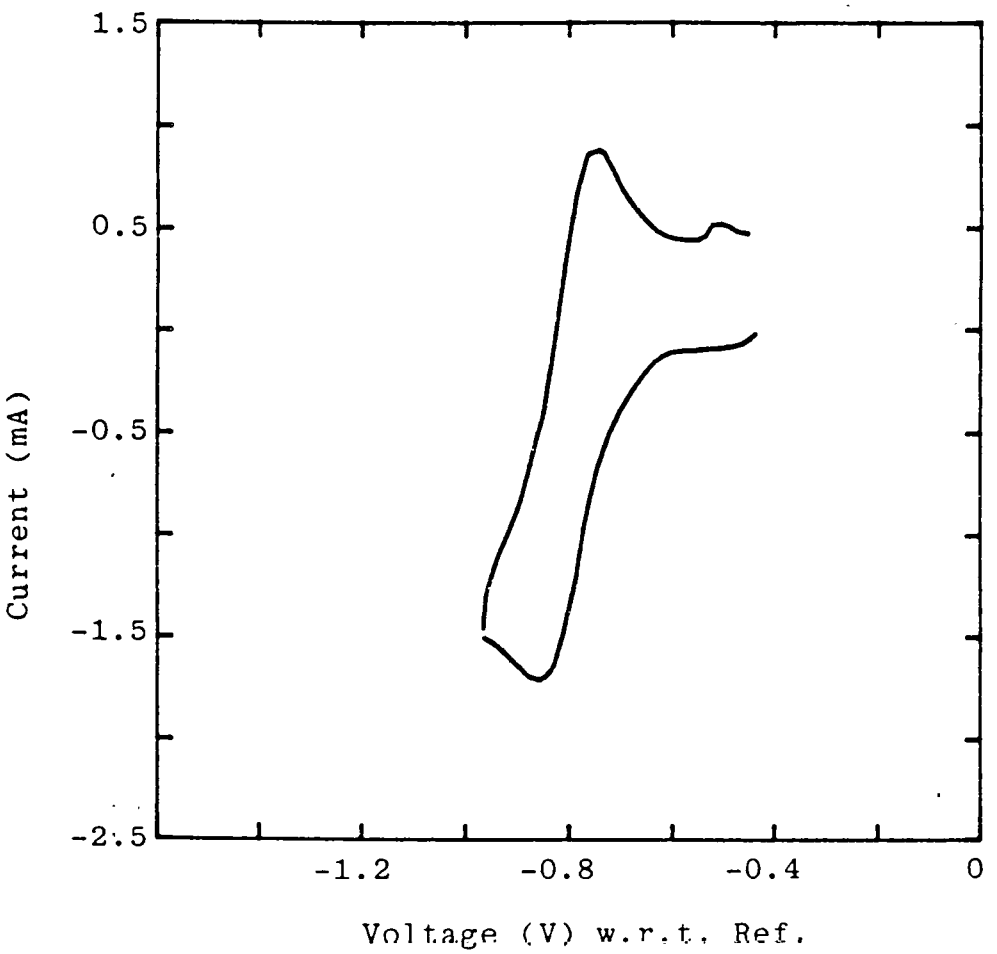

Fig. 5.16 A cyclic voltammogram at silver working electrode for 1 wt.% $AlCl_3$ in the molten LICl-NaCl mixture in the weight ratio of 40:50. T=700°C. Area: 0.097 cm^2. v=0.3 V/s.

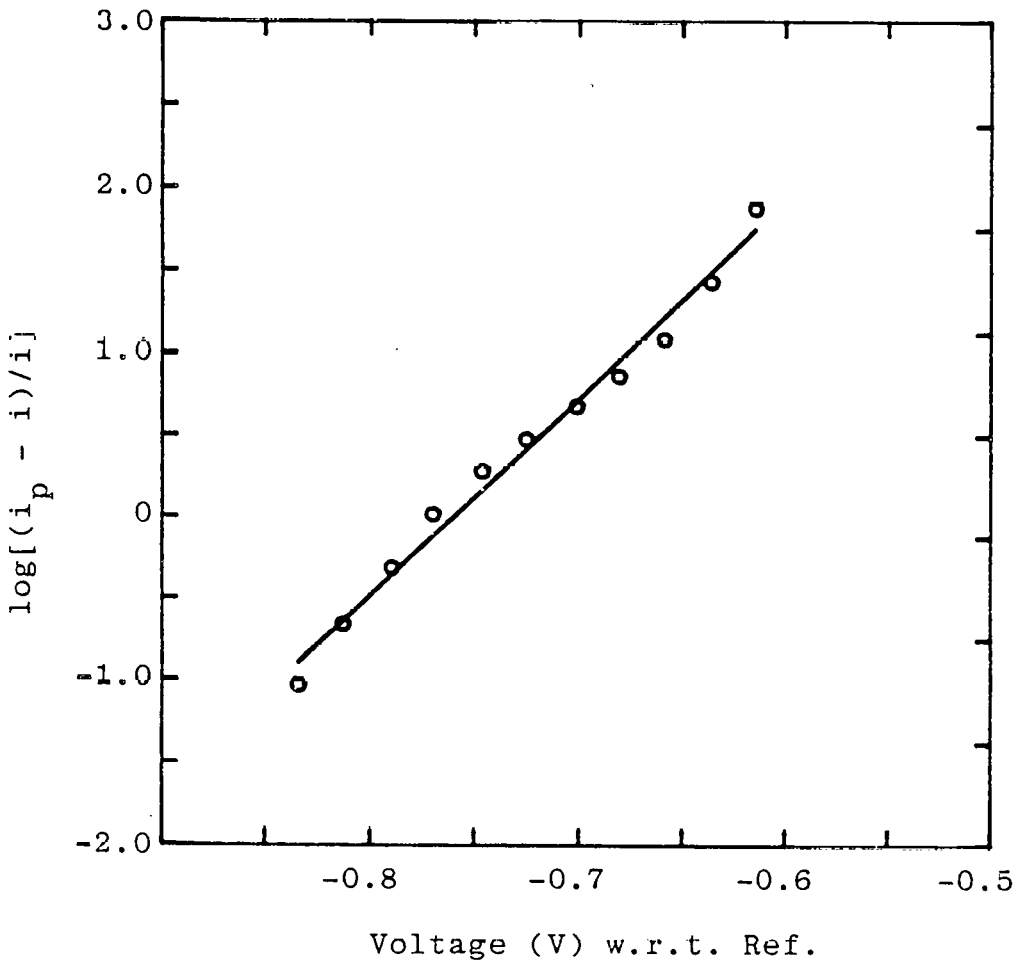

Fig. 5.17 A plot of $\log[(i_p - i)/i]$ vs V on the cathodic wave for Al^{3+} reduction at silver working electrode. $AlCl_3$ content: 1 wt.% in the molten LiCl-NaCl mixture in the weight ratio of 40:50. Area: 0.097 cm^2. T=700°C. v=0.3 V/s.

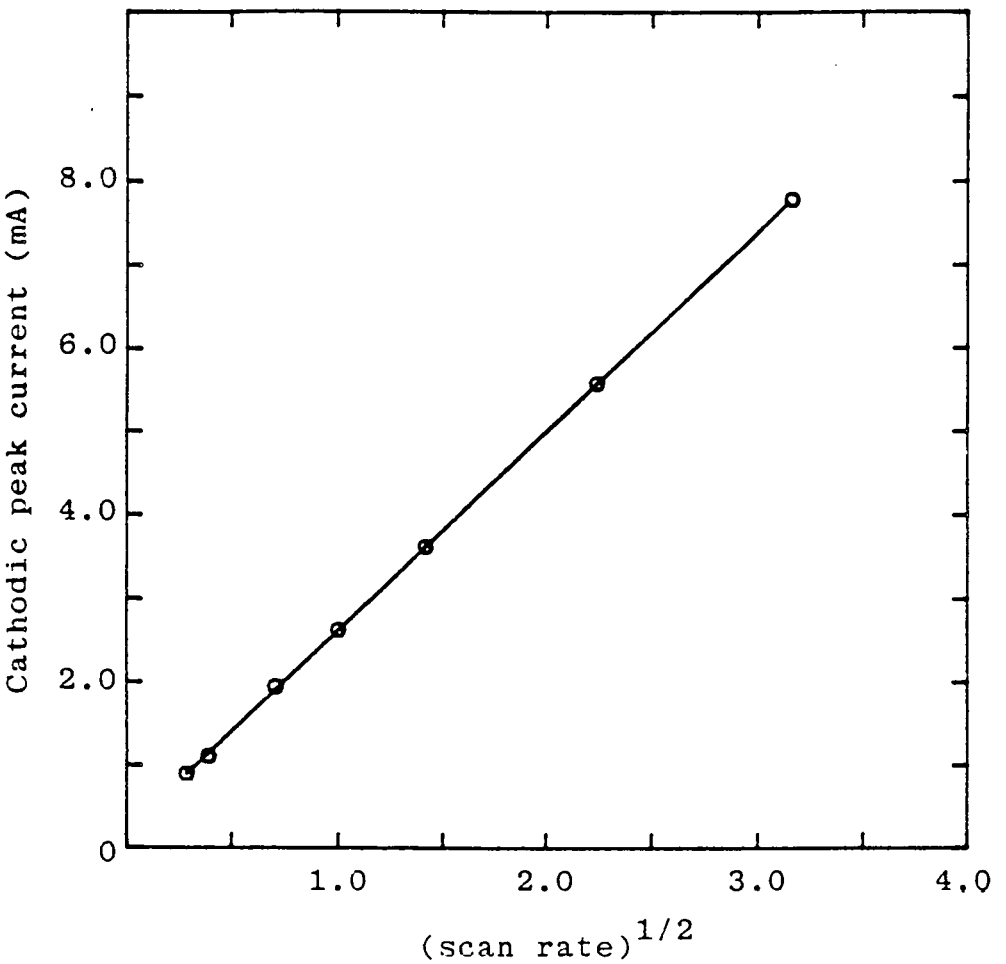

Fig. 5.18 A plot of the cathodic peak current vs (scan rate)$^{1/2}$ for the reduction of Al^{3+} at gold electrode. $AlCl_3$: 1.5 wt.% in the molten LiCl-NaCl mixture in the weight ratio of 40:50. T=700°C A=0.173 cm^2.

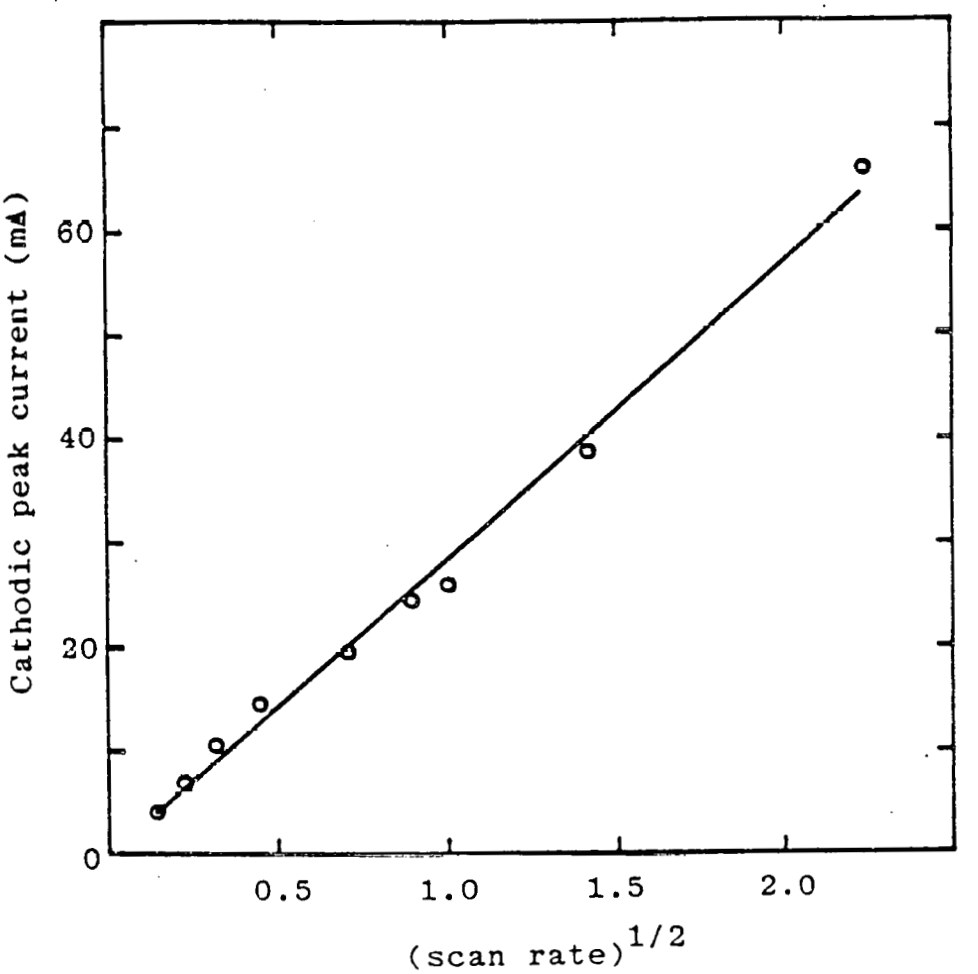

Fig. 5.19 A plot of the cathodic peak current vs (scan rate)$^{1/2}$ for the reduction of Al^{3+} at silver electrode. $AlCl_3$: 1.5 wt.% in the molten LiCl-NaCl mixture in the weight ratio of 40:50. T=700°C A=0.18 cm^2.

6. CONCLUSIONS

From the Raman spectroscopic and electroanalytical studies of aluminum and magnesium electrolysis in chloride melts in laboratory-scale cells which imitated industrial practice, the following is concluded.

1. Magnesium exists in the electrolyte as a tetrahedrally coordinated complex, $MgCl_4^{2-}$. The Raman peaks are located at 107, 142, 249, and 351 cm^{-1}. One of them (249 cm^{-1}) is completely polarized.

2. Aluminum also exists in the alkali chloride melt as the tetrahedrally coordinated $AlCl_4^-$ ion. Other higher complexes such as $Al_2Cl_7^-$ could not be observed in the composition range for the electrolyte representative of industrial practice. The Raman peaks of $AlCl_4^-$ are located at 125, 183, 349, and 483 cm^{-1}. As in the case of magnesium, one of the peaks (349 cm^{-1}) is polarized, and others are not.

3. Calcium appears to coordinate with chlorides in much the same way that magnesium does. Because of the lower charge density of calcium, however, the peaks are not as sharp for $CaCl_4^{2-}$ as they are for $MgCl_4^{2-}$. The principal peak of $CaCl_4^{2-}$ is located at about 180 cm^{-1} and is polarized.

4. It was observed that the stronger Raman peak can be obtained for

the molten mixtures of $MgCl_2$ or $AlCl_3$ with the larger alkali metal chloride. This phenomenon could be explained by the lower charge density of the larger alkali metal cation from which chlorine ion can be drawn more easily to form the chloro complex ion.

5. It was found that Al^{3+} ion can form other complex ion with CsCl at the low concentration of $AlCl_3$. This could be explained by the fact that the possibility for Al^{+3} ion to form higher chlorine complex ion is higher when it is surrounded by more chlorine ions. Chlorine ions can easily be obtained from the lower charge density alkali metal cation.

6. It is possible to identify both the $MgCl_4^{2-}$ and $CaCl_4^{2-}$ peaks when both $MgCl_2$ and $CaCl_2$ are present in the same melt. This is a demonstration of the additivity property of Raman spectroscopy and could serve as the basis for measuring $MgCl_2$ concentration in cell bath on-line in real time basis using the $CaCl_2$ concentration as a standard.

7. The so-called streamers which could be clearly observed during electrolysis were found not to be Raman active. On this basis, it is concluded that the streamers are not covalently bonded compounds such as network oxides. The question of dissolved metal remains unresolved.

8. On silver and platinum electrodes, magnesium deposition reaction from $MgCl_2$-$CaCl_2$-KCl-NaCl melts was found to be quasi-reversible.

Aluminum reduction on gold and silver from $AlCl_3$-LiCl-NaCl melts was also observed to be quasi-reversible.

9. Subvalent species were not identified during aluminum deposition from $AlCl_3$-LiCl-NaCl melt seither by Raman spectroscopy or by cyclic voltammetry in the experiments conducted. If subvalent species exist, they are thought to be undetectable by the instrumentation employed.

10. For the purification of the alkali and alkaline earth chlorides, application of thionyl chloride proved to be the most effective way to eliminate troublesome impurities, especially fine particles which were believed to be undissolved oxides. The use of $SOCl_2$ in this manner has not been reported previously.

All these results are of importance in themselves. Furthermore, the results and experimental techniques developed through this research have established the basis for the study of the more complex, but industrially more significant process, electrolysis of aluminum from molten fluoride media.

* Recommendations for Future Research

In the present research, the streamers were clearly observed during magnesium electrolysis. It would be interesting to relate these phenomena to current efficiency, because they were observed in quantity

during electrolysis, and thus, they were thought to be related to current efficiency. There has been no study on the effect of the streamers on the current efficiency.

The exact base line would be very useful for quantitative Raman measurements, because it would permit the accurate determination of peak area and peak height. Efforts were made to generate the baseline for Raman spectra using the present equipment, but in many systems no consistent results could be obtained. The generation of an exact baseline using more sophisticated data processing software is strongly recommended for future Raman studies.

It was observed that aluminum can form what appears to be an octahedral complex ion in $AlCl_3$ - CsCl melts at great CsCl excess. It would be interesting to study the $AlCl_3$ - CsCl system by a spectro-electrochemical technique because, in the diffusion boundary layer on the cathode, the conditions for the formation of $AlCl_6^{3-}$ are thought to be satisfied. Thus, it should be possible to observe the presence of $AlCl_6^{3-}$ as a kinetic entity.

Appendix 1: Calculation of Diffusion Layer Thickness

$$J = -D \frac{\partial C}{\partial x} = - \frac{D \Delta C}{\delta} = \frac{DC}{\delta}$$

and

$$J = \frac{IAw}{zF}$$

From the above two flux equations, diffusion layer thickness can be calculated.

$$\delta = \frac{zFDC}{IAw}$$

where

$\Delta C = C_{bulk}$
$= 0.10 \times 1.6\ g/cm^3$ at 10 wt.% $AlCl_3$
$D = 5 \times 10^{-6}\ cm^2/s$
$I = 100\ mA = 0.1\ A$
$Aw = 27\ g/mol$
$z = 3$
$F = 96487\ C/mol$

With these values, diffusion layer thickness is calculated.

$$\delta = \frac{0.16\ g/cm^3 \times 3 \times 96487\ C/mol \times 5 \times 10^{-6} cm^2/s}{100\ mA/cm^2 \times 27\ g/mol}$$

$= 0.0857\ cm$
$= 857\ \mu m$

Appendix 2: Fortran Programs for Cyclic Voltammetry

```
C-------------------------------------------------------*
C---FILE NAME: VOLTAM.FOR : MAY 31, 1986-----------------*
C---SAMPLING OF VOLTAGE & CURRENT FROM CYCLIC VOLTAMETRY---*
C---WRITTEN IN DEC MINC23 FORTRAN-------------------------*
C---SUBROUTINE SAMPLE,SAVDAT, AND MINC FORTRAN SYSLIB-*
C-------------------------------------------------------*
      PROGRAM VOLTAM
      DIMENSION IDATA(1600),X(800),Y(800)
      COMMON/DATA/V0,V9,SCR,CRANGE,CTEMP
C---CONTROL DATA INPUT SECTION
C---VOLTAGE IS RELATIVE TO REFERENCE ELECTRODE
C---SCAN RATE = dE/dt , UNIT = VOLT/SEC
      TYPE *,'INITIAL VOLTAGE W.R.T REF = "
      READ(5,*) V0
      TYPE *,'LOWER LIMIT OF SCANNING VOLT W.R.T REF = '
      READ(5,*) V9
      TYPE *,'DATA POINTS PER VOLT (<150) = '
      READ(5,*) DPPV
      TYPE *,'SCAN RATE IN VOLTS = '
      READ(5,*) SCR
C---
           VRANGE=ABS(V9-V0)
           TPT=VRANGE*DPPV+0.5
           TSEC=VRANGE/SCR
           SFREQ=TPT/TSEC
           NPT=INT(TPT+0.5)
C---DATA SAMPLING SECTION
           JSAM=NPT*2
           KSAM=JSAM*2
           ISAM=KSAM
      TYPE *,'TOTAL NO. OF SAMPLES COLLECTED= ',ISAM
           ISMP=IFIX(SFREQ+0.5)
      CALL SAMPLE(IDATA,ISMP,ISAM)
C---CONVERSION OF MACHINE MEASURE UNIT TO ACTUAL FORM
           FACTOR=10.2375/4096.
           X(1)=V0
           Y(1)=0.0
      DO 10 I=1,JSAM
           J=(I-1)*2 +1
           K=I*2
           X(I+1)=(IDATA(J)-2047)*FACTOR
           Y(I+1)=(IDATA(K)-2047)*FACTOR
 10   CONTINUE
```

```
C---MEASURED DATA PREVIEW AND FILE SAVE SECTION
              JSAM=JSAM+1
          WRITE(6,100) (I,X(I),Y(I),I=1,JSAM)
 100      FORMAT(1X,'I= ',I4,2F12.3)
          CALL SAVDAT(X,Y,JSAM)
          STOP
          END
```

```
C-------------------------------------------------------*
C---FILE NAME: SAMPLE.FOR : MAY 31, 1986----------------*
C---DATA SAMPLING ROUTINE BY A/D CONVERTER WITH SPECIFIED--*
C---SAMPLING RATE AND AUTO-GAIN SETTING------------------*
C---SEE RT-11 MANUALS FOR MORE DETAILS ON CAD2FP ROUTINE---*
C-------------------------------------------------------*
      SUBROUTINE SAMPLE(IDATA,ISMP,IPTS)
      DIMENSION INFO(40),IBUF(1000,4),IDATA(2000)
           ISAM=2000
           NSAM=1000
C---SAMPLING PREPARATION SECTION
 10   CONTINUE
      TYPE 100
 100  FORMAT(' CONNECT CHANNEL 0 TO SIGNAL GENRATOR AND'/
     *        ,'          CHANNEL 2 TO CURRENT OUTPUT FROM'/
     *        ,' THE PAR POTENTIOSTAT'/'        ST2 ON'
     *        ,' COMP. TO FRAME SYNC.ON PARC 175 '//)
      TYPE *,' TYPE 1  IF EVERYTHING IS OK '
      READ(5,*) TEST
         IF (TEST.NE.1) GO TO 10
C---HARDWARE CHECK-UP SECTION: TRIGGER  CHECK
           NSWP=1
           PERIOD=(1/FLOAT(ISMP))
           PERIOD=XRATE(PERIOD,IRATE,IPRSET)
           MODE=256
         IF (IPTS.GT.1000) NSWP=2
           ITIMES=0
 20   CALL SETIBF(INFO,IND,,IBUF(1,1),IBUF(1,2),
     *      ,IBUF(1,3),IBUF(1,4))
      TYPE *,'IND = ',IND
      CALL RLSBUF(INFO,IND,0,1,2,3)
      TYPE *,'IND2 = ',IND
         IF (IND.NE.1) PAUSE 'BUFF REL ERROR'
      CALL CLOCKA(IRATE,IPRSET,IND)
         IF (IND.NE.1) STOP 'CLOCK INITI. ERROR'
      CALL ADSWP(INFO,NSAM,0,MODE,IPRSET,,,0,2)
      TYPE *,'INFO = ',INFO(1)
         IF (INFO(1).NE.0) GO TO 20
C---ACTUAL DATA SAMPLING SECTION
C---SAMPLING IS TRIGGERED BY PULSE FROM SIGNAL GENERATOR
 30   CONTINUE
         IF (ITIMES.EQ.NSWP) GO TO 40
      TYPE *,'OK1'
           INO=IWTBUF(INFO,,ID,IND)+1
      DO 32 K=0,1,NSWP-1
      DO 32 I=1,NSAM
           J=I+K*NSAM
           IDATA(J)=IBUF(I,K+1)
 32   CONTINUE
      TYPE *,'SWEEP NO.= ',ITIMES,' INO = ',INO
C     TYPE 200,ID,IBUF,(IBUF(I,INO),I=1,NSAM)
C200  FORMAT(/,' CONVERTED A/D DATA FOR BUFFER #'I1
C    *    ,/(3(I10)))
```

```
          CALL RLSBUF(INFO,IND,ID)
               ITIMES=ITIMES+1
             IF (INFO(1).EQ.0) GO TO 34
 34          IF (NSWP.EQ.1) GO TO 40
          GO TO 30
C---
 40       CONTINUE
          CALL STPSWP(INFO,1,IND)
             IF (IWTBUF(INFO,,ID,IND).GE.0) GO TO 40
          TYPE 300,INFO(1)
 300      FORMAT(/' A/D SWEEP ENDING CODE= 'I3)
          TYPE *,'IND = ',IND
          TYPE *,'NSAM = ',NSAM
C         TYPE 400,ID,IDATA,(IDATA(I),I=1,ISAM)
C400      FORMAT(/,' CONVERTED A/D DATA FOR BUFFER #'I1
C     *        ,/(3(I5)))
          RETURN
          END
```

```
C-------------------------------------------------------*
C---FILE NAME: SAVDAT.FOR : MAY 31,1986-----------------*
C---DATA FILE SAVE ROUTINE------------------------------*
C---X : A REAL ARRAY  FOR INDEPENDENT VARIABLE----------*
C---Y : A REAL ARRAY  FOR DEPENDENT VARIABLE------------*
C---NPTS : TOTAL NUMBER OF POINTS IN X AND Y ARRAY------*
C-------------------------------------------------------*
          SUBROUTINE SAVDAT(X,Y,NPTS)
          DIMENSION X(1),Y(1)
          LOGICAL*1 FILE(15),AFLG,HDR,TEMP(81),FIL2(15)
          COMMON/DATA/V0,V9,SCR,CRANGE,CTEMP
C---FILE NAME INPUT SECTION
               OFFSET=X(1)
               FACTOR=X(2)-X(1)
 10       CALL GTINPT('OUTPUT FILE NAME (<CR> TO QUIT) = '
     *          ,TEMP,NCHR)
             IF (NCHR.EQ.0) GO TO 90
          DECODE(NCHR,100,TEMP,ERR=10) FILE
          CALL GTINPT('PLOTTER FILE NAME = ',TEMP,NCHR)
          DECODE(NCHR,100,TEMP,ERR=10) FIL2
 100      FORMAT (15A1)
C---FILE EXISTENCE CHECK SECTION
               FILE(15)=0
          OPEN(UNIT=1,TYPE='OLD',NAME=FILE,ERR=30)
          CLOSE (UNIT=1)
          TYPE 200
 200      FORMAT ('FILE ALREADY EXISTS: OVERWRITE ? Y/[N] ')
          ACCEPT 210,AFLG
 210      FORMAT (A1)
             IF (AFLG.EQ.'Y') GO TO 30
          GO TO 10
C---FILE FORMAT SELECTION SECTION
 30       CALL GTINPT('FILE FORMAT ([F]/U) = ',TEMP,NCHR)
          DECODE(NCHR,210,TEMP,ERR=30) AFLG
 32       CALL GTINPT('HEADER ON OUTPUT ? ([Y]/N) = '
     *          ,TEMP,NCHR)
          DECODE (NCHR,210,TEMP,ERR=32) HDR
 34       CALL GTINPT('DATA (0:Y ONLY, 1:X-Y PAIR (0/[1]) = '
     *          ,TEMP,NCHR)
               ITYP=1
             IF (NCHR.NE.0) DECODE(NCHR,300,TEMP,ERR=34) ITYP
 300      FORMAT (I2)
C---DATA WRITING SECTION
             IF (AFLG.EQ.'U') GO TO 50
C---FORMATTED DATA FILE
          OPEN (UNIT=1,NAME=FILE,TYPE='NEW',FORM='FORMATTED')
             IF (HDR.EQ.'N') GO TO 42
C---
          TYPE *,'CELL TEMPERATURE = ?'
          READ(5,*) CTEMP
          TYPE *,'CURRENT SCALE = ?'
          READ(5,*) CRANGE
          WRITE(1,400) CTEMP,CRANGE
```

```
 400      FORMAT(1X,'TEMP= ',F8.1,4X,'CURRENT SCALE= ',F8.1)
          WRITE(1,410) NPTS,FACTOR,OFFSET
 410      FORMAT(1X,'NPTS= ',I5,4X,'FACTOR= ',E12.3,4X
     *        ,'OFFSET= ',E12.3)
C---
 42       CONTINUE
             IF (ITYP.EQ.1) GO TO 46
          DO 44 I=1,NPTS
 44       WRITE (1,*,ERR=60) Y(I)
          GO TO 80
C---
 46       CONTINUE
          DO 48 I=1,NPTS
 48       WRITE (1,420) I,X(I),Y(I)
 420      FORMAT(1X,I4,2F12.6)
C---
          OPEN(UNIT=2,NAME=FIL2,TYPE='NEW',FORM='FORMATTED')
          DO 49 I=1,NPTS
 49       WRITE(2,430) X(I),Y(I)
 430      FORMAT(1X,2F12.6)
          GO TO 80
C---UNFORMATTED DATA FILES
 50       CONTINUE
          OPEN (UNIT=1,NAME=FILE,TYPE='NEW',FORM=
     *         'UNFORMATTED')
             IF (HDR.NE.'N') WRITE(1) ITYP,NPTS,FACTOR,OFFSET
             IF (ITYP.EQ.1) GO TO 52
          WRITE (1,ERR=60) (Y(I),I=1,NPTS)
          GO TO 80
 52       WRITE (1,ERR=60) (X(I),Y(I),I=1,NPTS)
          GO TO 80
C---ERROR HANDLING SECTION
 60       CONTINUE
          CALL ERRSNS(IERNO,IUNIT)
          TYPE 600,IERNO
 600      FORMAT (' ERROR ',I4,' : ON WRITING FILE'/)
          GO TO 10
C---
 80       CLOSE (UNIT=1)
 90       RETURN
          END
```

REFERENCES

1. D.E. Hall and E. Spore, "Report of the Electrolytic Industries for the Year 1984," J. Electrochem. Soc., 132(7) (1985) 252C-283C.
2. M.C. Flemings, G.B. Kenney, D.R. Sadoway, J.P. Clark, J. Szekely, An Assessment of Magnesium Production Technology, report to the U.S. Department of Energy, Contract No. EX-76-A-01-02295, Feb. 1, 1981.
3. A.S. Russell, "Pitfalls and Pleasures in new Aluminum Process Development," Metal. Trans.B., 12B, (1981) 203-215.
4. A.S. Russell, "Developments in Aluminium Smelting." Aluminium, 57(6) (1981) 405-409.
5. Kh.L. Strelets, Electrolytic Production of Magnesium, trans. by J. Schmorak, Keter Pubblishing House Jerusalem Ltd, Jerusalem, 1977.
6. Yu.K. Delimarskii and V.F. Makogon, "Peculiarities of the Electroreduction of Aluminum from High-Temperature Aluminum Chloride Melts," Sov. Electrochem., 18(10) (1982) 1232-1236.
7. R.C. Hannah and B.J. Welch, "The Behaviour of Chlorine Bubbles in Aluminium Chloride Reduction Cells," in Light Metals 1978, Vol. 1, J.J. Miller, editor, 107th AIME Annual Meeting, Denver, 1978, pp 165-174.
8. O.A. Lebedev, A.N. Antonov, K.D. Muzhzhavlev, and O.N. Dronyaeva, "Mechanism of Magnesium Losses During Electrolysis," Tsvetn. Met. Sov. J. Non-Ferrous Metals, 11(10) (1970) 55-58.
9. G.J. Kipouros and D.R. Sadoway, "The Chemistry and Electrochemistry of Magnesium Production," in Advances in Molten Salt Chemistry, Vol. 6, G. Mamantov and J. Braunstein, editors, Elsevier, Amsterdam, in press.
10. A. Komura, H. Imanaga and N. Watanabe, "Dispersion of Mg in the Electrolysis of $MgCl_2$-KCl Melts," Denki Kagaku, 41(4) (1973) 281-286.
11. A. Anundskas, K. Grjotheim, A.H. Schultz, H. Svendsen and H.A. Oye, "Benetzungseigenschaften in Systemen von Interesse fur die Magnesium-Elektrolyse (Teil III)," Metall, 29(5) (1975) 493-

496.

12. T. Ostvold and H.A. Oye, "Recombination of Magnesium and Chlorine in the Technical Electrolysis," Light Metals 1980, C.J. McMinn, editor, 109th AIME Annual Meeting, Las Vegas 1980, pp 937-947.
13. T. Ishikawa, "Correlation between Soluble Behavior of Metallic Aluminum and Current Efficiency in the Chloride Melts containing Aluminum Chloride," Yoyuen, 22(2) (1979) 93-113. Chem. Abstr., 91 (1979) 148366g.
14. R.D. Holliday and P. McIntosh, "Laboratory Cell and Hydrodynamic Model Studies of Magnesium Chloride Reduction in Low-Density Electrolytes," J. Electrochem. Soc., 120(7) (1973) 858-866.
15. L.A. Woodward, "General Introduction," pp 1-43, and D.E. Irish, "Raman Spectroscopy of Complex Ions in Solution," pp 240-250, in Raman Spectroscopy, Theory and Practice, H.A. Szymanski, editor, Plenum Press, New York, 1967.
16. N.R. Smyrl, G. Mamantov and L.E. McCurry, "IR Emission Spectra of the $AlCl_4^-$ Ion in $AlCl_3$-MCl (M = Li, Na, K) Melts," J. Inorg. Nucl. Chem., 40 (1978) 1489-1492.
17. Yu.K. Delimarskii, V.F. Makogon, and A.Ya. Zhigailo, "Anodic Behavior of Aluminum in a Fused Chloride Electrolyte," Sov. Electrochem., 5 (1969) 98-100.
18. V.N. Storozhenko, "Solubility of Aluminum in Molten $AlCl_3$ - NaCl in Anodic Polarization," Sov. Electrochem., 8 (1972) 942-945.
19. Yu.K. Delimarskii, V.F. Makogon, G.I. Dybkova and O.P. Gritsenko, "Electrochemical Reduction of Aluminum from Chloroaluminate Melts of Various Cationic Composition," Sov. Prog. Chem., 48(9) (1982) 29-32.
20. G. Torsi, G. Mamantov and G.M. Begun, "Raman Spectra of The $AlCl_3$-NaCl System," Inorg. Nucl. Chem. Letters, 6 (1970) 553-560.
21. G.M. Begun, C.R. Boston, G. Torsi, and G. Mamantov, "The Raman Spectra of Molten Aluminum Trihalide-Alkali Halide Systems," Inorg. Chem., 10(5) (1971) 886-889.
22. E. Rytter, H.A. Oye, S.J. Cyvin, B.N. Cyvin, and P. Klaeboe, "Raman Spectra of $AlCl_3$-AlkCl and Trends in Species Formation," J. Inorg. Nucl. Chem., 35 (1973) 1185-1198.

23. S.J. Cyvin, P.Klaboe, E. Rytter and H.A. Oye, "Spectral Evidence for $Al_2Cl_7^-$ in Chloride Melts," J. Chem. Phys., 52 (1970) 2776-2778.

24. S.-Y. Yoon, Y. Liu, J.H. Flint, G.J. Kipouros, and D.R. Sadoway, "In Situ Raman Spectroscopic Investigation of Melt Chemistry and Electrode Processes in Laboratory-Scale Aluminum Cells," in Light Metals 1986, R.E. Miller, editor, at the 115th Annual TMS-AIME Meeting, New Orleans, 1986, pp 479-482.

25. S.-Y. Yoon, J.H. Flint, G.J. Kipouros, and D.R. Sadoway, "Raman Scattering Studies of Molten Salt Electrolysis of Light Metals," in Energy Reduction Techniques in Metal Electrochemical Processes, R.G. Bautista and R. Wesely, editors, TMS-AIME, Warrendale PA, 1985, 479-490.

26. W.E. Haupin, R.S. Danchik and J.W. Luffy, "Identification of Metal Fog in Electrolysis of Aluminum Chloride," in Light Metals 1976, 105th AIME Annual Meeting, Las Vegas, 1976, pp 159-169.

27. W.R. Heineman, "Spectroelectrochemistry, Combination of Optical and Electrochemical Techniques for Studies of Redox Chemistry," Anal. Chem., 50(3) (1978) 390A-402A.

28. M.H. Brooker and G.N. Papatheodorou, "Vibrational Spectroscopy of Molten Salts and Related Glasses and Vapors," in Advances in Molten Salt Chemistry 5, G. Mamantov, editor, Elsevier, New York, 1983, pp 26-184.

29. K. Balasubrahmanyam, "Raman Spectra of Liquid $MgCl_2$-KCl System," J. Chem. Phys., 44(9) (1966) 3270-3273.

30. R.J. Capwell, "Raman Spectra of Crystalline and Molten $MgCl_2$," Chem. Phys. Letters, 12(3) (1972) 443-446.

31. C.-H. Huang and M.H. Brooker, "Raman Spectrum of Molten $MgCl_2$," Chem. Phys. Letters, 43(1) (1976) 180-182.

32. M.H. Brooker and C.-H. Huang, "Raman Spectroscopic Studies of Structural Properties of Solid and Molten States of the Magnesium Chroride - Alkali Metal Chloride System," Can. J. Chem., 58 (1980) 168-179.

33. H. Gerding and H. Houtgraaf, "The Raman Spectra of the Compounds $NaCl.AlCl_3$ and $NOCl.AlCl_3$," Rec. Trav. Chem., 72 (1953) 21-38.

34. K. Balasubrahmanyam and L. Nanis, "Raman Spectra of Liquid $AlCl_3$.KCl and $AlCl_3$.NaCl," J. Chem. Phys., 42(2) (1965) 676-680.

35. H.A. Oye, E. Rytter, P. Klaeboe, and S.J. Cyvin, "Raman Spectra of KCl-$AlCl_3$ Melts and Normal Coordinate Analysis of $Al_2Cl_7^-$," Acta Chem. Scand., 25 (1971) 559-576.

36. R. Fehrmann, J.H. von Barner, N.J. Bjerrum, and O.F. Nielsen, "Chloro Complexes in Molten Salts. 8. Potentiometric and Raman Spectroscopic Study of the Systems NaCl-$AlCl_3$, NaCl-$AlCl_3$-Na_2O, NaCl-$AlCl_3$-$SeCl_4$, and NaCl-$AlCl_3$-$SeCl_4$-Na_2O at 175°C," Inorg. Chem., 20 (1981) 1712-1718.

37. S. Duan, P.G. Dudley, and D. Inman, "Voltammetric Studies of Magnesium in Chloride Melts.," in Molten Salts, Proceedings of the Fifth International Symposium, M.-L. Saboungi, D.S. Newman, K. Johnson, and D. Inman, editors, (The Electrochemical Society, Inc., Pennington, NJ) Vol. 86-1, pp 248-261.

38. V.F. Makogon, G.I. Dybkova and T.A. Tishura, "Volt-Ampere Investigation of Magnesium Chloride in a NaCl-KCl Supporting Electrolyte," Sov. Progress Chem., 46(11) (1980) 108-109.

39. R. Tunold, "The Cathode Reaction in Magnesium Electrolysis," in Light Metals 1980, C.J. McMinn, editor, 109th AIME Annual Meeting, Las Vegas, 1980, pp 949-957.

40. K. Akashi, S. Furihata, and S. Kurosawa, "The Polarographic Reduction Wave of Magnesium Ion(II) in a Molten LiCl-KCl Eutectic Mixture," Electrochim. Acta, 24(5) (1979) 581-583.

41. V.Ya. Kudyakov and M.V. Smirnov, "Solubility of Aluminum in Molten Mixture of its Trichloride with Chlorides of Alkali Metals," J. Appl. Chem. USSR, 53(5) (1980) 741-744.

42. S. Takahashi and N. Koura, "Electrode kinetic Studies on Al in Molten $AlCl_3$-NaCl-KCl Electrolyte by Rotating Ring-Disk Electrode," Denki Kagaku, 50(10) (1982) 852-853.

43. Yu.K. Delimarskii, V.F. Makogon and O.P. Gritsenko, "The Investigation of Discharge of Aluminum Ions from a High Temperature Chloroaluminate Melt," Sov. Progress in Chemistry, 46(2) (1980) 1-4.

44. S. Fougner, "New Directions in Electrolytic Production of

Magnesium," in Light Metals 1974, Vol.2, H. Forberg, editor, 103rd AIME Annual Meeting, Dallas, 1974, pp 515-533.

45. N. Jarrett, "Advances in the Smelting of Magnesium," in Metallurgical Treatises, J.K. Tien and J.F. Elliott, editors, AIME, 1981, pp 159-169.

46. R. Neelameggham and J.C. Priscu, "Energy Reduction Approaches in Magnesium Production," presented at the 114th Annual AIME Meeting, New York, 1985.

47. N. Hoy-Peterson, "Some Aspects of the Electrolytic Production of Magnesium in IG Cells," J. Metals, 21(4) (1969) 43-49.

48. K. Grotheim, C. Krohn, M. Malinovsky and J. Thonstad, Aluminum Electrolysis, Fundamentals of the Hall-Heroult Process, Aluminium-Verlag, Dusseldorf, 1982, pp 3-23.

49. D. Pletcher, Industrial Electrochemistry, Chapman and Hall, London, 1982.

50. J.G. Peacey and W.G. Davenport, "Evaluation of Alternative Methods of Aluminum Production," J. Metals, 26(7) (1974) 25-28.

51. Von H. Flood and S. Urnes, "Die Berechnung der Aktivitaten in Magnesiumchlorid-Alkalichlorid-Schenekz aus Strukturmodellen," Z. Elektrochem., 59 (1955) 834-839.

52. V.A. Maroni, E.J. Hathaway, and E.J. Cairns, "Structural Studies of Magnesium Halide-Potassium Halide Melts by Raman Spectroscopy," J. Phys. Chem., 75(1) (1971) 155-159.

53. V.A. Maroni, "Vibrational Frequencies and Force Constants for Tetrahedral $MgX_4^{=}$ (X = Cl,Br, and I) in MgX_2-KX Melts," J. Chem. Phys., 55(10) (1971) 4789-4792.

54. M.H. Brooker, "A Raman Spectroscopic Study of the Structural Aspects of K_2MgCl_4 and Cs_2MgCl_4 as Solid Single Crystals and Molten Salts," J. Chem. Phys., 63(7) (1975) 3054-3061.

55. J.H.B. George, J.A. Rolfe, and L.A. Woodward, "Raman Effect and the Nature of the Undissociated Part of Thallous Hydroxide in Solution," Trans. Faraday Soc., 49, (1953) 375-382.

56. E.W. Dewing, "Thermodynamics of the System NaCl-$AlCl_3$," Metal. Trans. B, 12B (1981) 705-719.

57. E.A. Ukshe and E.B. Kachina-Pullo, "Electrical Conductivity in the

$KCl-MgCl_2$ System," Russ. J. Inorg. Chem., 11(5) (1966) 638-642.

58. L.E. Topol, "Thermodynamic Considerations in Molten Metal-Metal Salt Solutions," J. Phys. Chem., 69(1) (1965) 11-17.

59. O.J. Kleppa and F.G. McCarty, "Thermochemistry of Charge-Unsymmetrical Binary Fused Halide Systems. II. Mixture of Magnesium Chloride with the Alkali Chlorides and with Silver Chloride," J. Phys. Chem., 70(4) (1966) 1249-1255.

60. E.E. Schrier and H.M. Clark, "Interaction in Salt Vapors and Activity Coefficients in the Potassium Chloride - Magnesium Chloride System," J. Phys. Chem., 67 (1963) 1259-1263.

61. C.R. Boston, "Molten Salt Chemistry of the Haloalumintes," in Advances in Molten Salt Chemistry, J. Braunstein, G. Mamantov, and G.P. Smith, editors, Plenum Press, 1971, pp 129-163.

62. P.A. Casabella and N.C. Miller, "Al^{27} Quadrupole Coupling in Solid $AlCl_3$," J. Chem. Phys., 40(5) (1964) 1363-1368.

63. L.G. Boxall, H.L. Jones, and R.A. Osteryoung, "Solvent Equilibria of $AlCl_3$-NaCl Melts," J. Electrochem. Soc., 120(2) (1973) 223-231.

64. H. Linga, K. Motzfeldt and H.A. Oye, "Vapor Pressures of Molten Alkali Chloride - Aluminum Chloride Mixtures," Ber. Bunsenges. Phys. Chem., 82 (1978) 568-576.

65. V.Ya. Kudyakov and M.V. Smirnov, "Dependence of the Activity Coefficient of Auminum Trichloride on its Concentration in Alkali-Metal Chlorides," J. Appl. Chem. USSR, 53(1) (1980) 32-34.

66. S. Takahashi, T. Muneta and N. Koura, "X-ray Diffraction of the Molten Salt 50 mol.% $AlCl_3$ - 50 mol.% LiCl," J. Chem. Soc., Faraday Trans. 2, 81(2) (1985) 319-326.

67. S. Biggin, S. Cummings, J.E. Enderby and M. Blander, "The Structure of Equimolar LiCl-$AlCl_3$ Melt by Neutron Scattering,"in Molten Salts, Proceedings of the Fifth International Symposium, M.-L. Saboungi, D.S. Newman, K. Johnson, and D. Inman, editors, (The Electrochemical Society, Inc., Pennington, NJ) Vol. 86-1, pp 81-96.

68. P. Klaeboe, E. Rytter and C.E. Sjogren, "Infared High Temperature Spectra of Aluminium Chloride and Related Species," J. Mol.

Structure, 113 (1984) 213-226.

69. J. Hvistendahl, P. Klaeboe, E. Rytter and H.A. Oye, "Infrared Emission Spectra of Alkali Chloroaluminates and Related Melts," Inorg. Chem., 23(6) (1984) 706-715.

70. N.E. Colthup, L.H. Daly and S.E. Wiberley, Introduction to Infrared and Raman Spectroscopy, Academic Press, 1975, pp 1-68.

71. D.A. Long, Raman Spectroscopy, McGraw-Hill Co., New York, 1977

72. J. Giergiel, K.R. Subbaswamy, and P.C. Eklund, "Light Scattering from Molten Alkali Halides," Phys. Rev. B: Condens. Matter, 29(6) (1984) 3490-3499.

73. A. Savitzky and M.J.E. Golay, "Smoothing and Differentiation of Data by Simplified Least Squares Procedures," Anal. Chem., 36(8) (1964) 1627-1639.

74. C.G. Enke and T.A. Nieman, "Signal-to-Noise Ratio Enhancement by Least-Squares Polynomial Smoothing," Anal. Chem., 48(8) (1976) 705A-712A.

75. T.R. Griffiths, "Molten Salt Spectroscopy," in Molten Salt Techniques, R.J. Gale and D.G. Lovering, editors, Vol. 2, Plenum Press, New York, 1984, pp 79-135.

76. C. Raptis, "A Reliable, Versatile Optical Furnace for Raman Spectroscopy of Molten Salts and Hot Solids," J. Phys. E: Sci. Instrum., 16(8) (1983) 749-752.

77. I. Barin and O.Knacke, Thermochemical properties of inorganic substances, Springer-Verlag, Berlin, 1973.

78. I. Barin, O. Knacke, and O. Kubaschewski, Thermochemical properties of inorganic substances, supplement, Springer-Verlag, Berlin, 1977.

79. W.K. Behl and H.C. Gaur, "Preparation of Pure Anhydrous Magnesium Chloride - A Re-examination of the Ammonium Carnallite Method," J. Sci. Industr. Res., 20B(1961) 231-232.

80. H.J. Gardner, C.T. Brown and G.J. Janz, "The Preparation of Dry Alkali Chlorides for Solutes and Solvents in Conductance Studies," J. Phys. Chem., 60 (1956) 1458-1460.

81. S.-Y. Yoon, J.H. Flint, G.J. Kipouros, and D.R. Sadoway, "Raman Scattering Studies of Magnesium Electrolysis," in Light Metals

1986, R.E. Miller, editor, 115th Annual TMS-AIME Meeting, New Orleans, 1986, pp 1009-1012.

82. J.H.R. Clarke and L.V. Woodcock, "Light Scattering from Ionic Liquids," J. Chem. Phys., 57(2) (1972) 1006-1007.

83. R.C. Evance, An Introduction to Crystal Chemistry, 2nd edition, Cambridge University Press, Cambridge, Great Britain, 1964, pp 31-54.

84. D.P. Strommen and K. Nakamoto, Laboratory Raman Spectroscopy, John Wiley & Sons, New York, 1984, pp 76-92.

85. S.-Y. Yoon and D.R. Sadoway, "Spectroelectrochemical Study of Magnesium electrolysis," Light Metals 1987, R.D. Zabreznik, editor, 116th TMS Annual Meeting, TMS, Warrendale, 1987, pp 851-859.

86. K. Sakai, T.Nakamura, N. Umesaki and N. Iwamoto, "Bounds of Complex Formation for Alkali-Earth Cation in Molten Alkali Chlorides," Phys. Chem. Liq., 14(1) (1984) 67-78.

87. V.N. Storozhenko, "Thermodynamics of the Interaction of Aluminum Chloride with Sodium Chloride in an Equimolar Melt," Russ. J. Phys. Chem., 48(7) (1974) 1010-1012.

88. Yu.V. Borisoglebskii, M.M. Vetyukov, and Z.Yu. Shatova, "Thermodynamic Characteristics of Aluminum Chloride in Melts of the Ternary System NaCl-KCl-$AlCl_3$," J. Appl. Chem. USSR, 51(5) (1978) 1143-1145.

89. B. Gilbert, G. Mamantov, and G.M. Begun, "Raman spectrum of the AlF_4^- ion in molten fluorides," Inorg. Nucl. Chem. Letters, 10 (1974) 1123-1129.

90. B. Gilbert, G. Mamantov, and G.M. Begun, "Raman spectra of aluminum fluoride containing melts and the ionic equilibrium in molten cryolite type mixtures," J. Chem. Phys., 62(3) (1975) 950-955.

91. A.P. Ratvik, T. Ostvold and H.A. Oye, "Solution of Chlorine in NaCl-$AlCl_3$ and CsCl-$AlCl_3$ Melts," Acta Chem. Scand., A39 (1985) 623-638.

92. O.Waenes and T. Ostvold, "Solutions of Chlorine in Molten Chlorides. 2. Solubility and Diffusivity of Chlorine in

Chloroaluminate Melts," Acta Chem. Scand., A37(4) (1983) 293-306.

93. N.G. Bukun and E.A. Ukshe, "The Reaction of Metallic Magnesium with Fused Chlorides," Russ. J. Inorg. Chem., 6(4) (1961) 465-468.

94. M. Krumpelt, J. Fischer, and I. Johnson, "The Reaction of Magnesium Metal with Magnesium Chloride," J. Phys. Chem., 72(2) (1968) 506-511.

95. J. D. Van Norman and J.J. Egan, "The Magnesium-Magnesium Chloride System. A Chronopotentiometric Study," J. Phys. Chem., 67 (1963) 2460-2462.

96. H. Wendt and K. Reuhl, "Performance of Aluminum Deposition from Chloride Melts," in Molten Salts, Proceedings of the Fourth International Symposium, M. Blander, D.S. Newman, M.-L. Saboungi, G. Mamantov, and K. Johnson, editors, (The Electrochemical Society, Inc., Pennington, NJ) Vol. 84-2, pp 418-429.

97. K. Matiasovsky, P. Fellner, M. Chrenkova-Paucirova, G. Brautigam, and H.-H. Emons, "Density and Electrical Conductivity of Molten NaCl-KCl-$AlCl_3$ Mixtures," Electrochim. Acta, 25 (1980) 195-200.

98. Yu.V. Borisoglebskii, M.M. Vetyukov, and Nguyen Van Thy, "Investigation of the Density of Melts in the Ternary System NaCl-KCl-$AlCl_3$," J. Appl. Chem. USSR, 50(1) (1977) 39-41.

99. L.V. Krylov, Yu.V. Borisoglebskii, and M.M. Vetyukov, "Cathode Polarization in the Electrolysis of Melts Containing Aluminum Chloride," Tsvetn. Met. Sov. J. Non-Ferrous Metals, 25(1) 39-41.

100. Yu.V. Borisoglebskii, M.M. Vetyukov, L.V. Krylov and Yu.V. Biryukov, "Coefficients of Diffusion of Aluminum Ions in Melts Containing Aluminum Chloride," J. Appl. Chem. USSR 58(7) (1985) 1327-1330.

101. B.S. Del Duca, "Electrochemical Behavior of the Aluminum Electrode in Molten Salt Electrolysis," J. Electrochem. Soc., 118(3) (1971) 443-446.

102. G. Torsi and G. Mamantov, "Potentiometric Study of the Dissociation of the Tetrachloroaluminate Ion in Molten Sodium Chloroaluminates at 175 - 400°C," Inorg. Chem., 10(9) (1971) 1900-1902.

103. K. Schulze and H. Hoff, "Electrode Kinetics of Aluminium in Chloride Melts with respect to Electrocrystallization," Electrochim. Acta, 17 (1972) 119-133.

104. T. Sato, T. Ishikawa, and R. Midorikawa, "Studies on the Electrochemical Deposition and Dissolution of Aluminum Electrodes and the Codeposition of Alkali Metals with Aluminum in Molten Aluminum Chloride - Alkali Chloride Mixtures," Denki Kagaku, 41(6) (1973) 446-451.

105. P. Rolland and G. Mamantov, "Electrochemical Reduction of $Al_2Cl_7^-$ Ions in Chloroaluminate Melts," J. Electrochem. Soc., 123(9) (1976) 1299-1303.

106. R.A. Carpio and L.A. King, "Deposition and Dissolution of Lithium-Aluminum Alloy and Aluminum from Chloride-Saturated LiCl-$AlCl_3$ and NaCl-$AlCl_3$ Melts," J. Electrochem. Soc., 128(7) (1981) 1510-1517.

107. V.I. Sal'nikov, V.P. Butorov, B.V. Mel'nikov, V.A. Lebedev, and I.F. Nichkov, "Diffusion Coefficient of Aluminum Ions in an Equimolar Mixture of Sodium and Potassium Chlorides," Sov. Electrochem., 10 (1974) 1142-1143.

108. S.L. Gol'dshtein, S.P. Raspopin, and V.A. Fedorov, "Kinetics of K^+(Na^+) and Al^{3+} Ion Discharge at Liquid Aluminum," Sov. Electrochem., 13(12) (1977) 1545-1550.

109. J. Bouteillon and A. Marguier, "A Study of the Electrochemical Reduction of $AlCl_3$ in an NaCl-KCl Equimolar Mixture," Surf. Tech., 22 (1984) 205-217.

110. Y.J. Zhang, A. Bjorgum, U. Erikson, R. Tunold, and R. Odegard, "On the Kinetics of the Cathodic Deposition of Aluminum on Glassy Carbon and Tungsten Electrodes from $AlCl_3$ + NaCl + KCl Melts," J. Electroanal. Chem., 210 (1986) 127-136.

111. R. Tunold, Y.J. Zhang and R. Odegard, "Kinetics of the Deposition of Aluminium from Chloride Melts," in Molten Salts, Proceedings of the Fifth International Symposium, M.-L. Saboungi, D.S. Newman, K. Johnson, and D. Inman, editors, (The Electrochemical Society, Inc., Pennington, NJ) Vol. 86-1, pp 408-424.

112. E.R. Brown and R.F. Large, "Cyclic Voltammetry, AC Polarography and Related Techniques," in Electrochemical Methods, Physical Methods

of Chemistry, Part IIA, Techniques of Chemistry, Vol. 1, A. Weissberger and B.W. Rossiter, editors, Wiley-Interscience, 1971, pp 423-530.

113. A.D. Pelton and S.N. Flengas, "Thermodynamics of Molten Silver Chloride - Alkali Chloride Solutions by Electromotive Force Measurements," J. Electrochem. Soc., 117(9) (1970) 1130-1140.

114. JANAF Thermochemical Tables, 1965.

115. J.A. Plambeck, Electroanalytical Chemistry, Basic Principles and Applications, John Wiley & Sons, New York, 1982, pp 256-281.

116. R.S. Nicholson and I. Shain, "Theory of Stationary Electrode Polarography," Anal. Chem., 36(4) (1964) 706-723.

117. G. Mamantov, Department of Chemistry, University of Tennessee, Knoxville TN, private communication, 25 August 1986.

118. R.H. Wopschall and I. Shain, "Effects of Adsorption of Electroactive Species in Stationary Electrode Polarography," Anal. Chem., 39(13) (1967) 1514-1527.

119. D.D. MacDonald, Transient Techniques in Electrochemistry, Plenum Press, New York, 1977, pp 185-228.